METEOROLOGICAL OFFICE
27 SEP 1984
LIBRARY
144215

METEOROLOGICAL OFFICE
London Road, Bracknell, Berks.

MET.O.15 INTERNAL REPORT

No. 57

REVIEW OF FOG MODEL DEVELOPMENT AND RESULTS 1980-1984

by

J D Turton and R Brown

September 1984

Cloud Physics Branch (Met.O.15)

REVIEW OF FOG MODEL DEVELOPMENT AND RESULTS 1980-1984

1. INTRODUCTION

This report reviews the development of and results from a numerical model of radiation fog. The report consists mainly of a series of notes which were written between 1981 and 1983 describing developments of and experiments with the model. These notes are included in this report as a series of Annexes to the main review. The model is based on that described by Brown and Roach (1976) but includes the 1-D momentum equations with exchange coefficients made functions of the local Richardson number (Ri) following the level 2 formulation of Mellor and Yamada (1974). The original model of Brown and Roach was extended to aid the interpretation of measurements made through deep fogs during the 1975-1977 field project at Cardington, Bedford, UK. The initial version of the extended model (Brown 1980a) was used to simulate the temperature and wind structure associated with mature fogs. In particular it was able to reproduce the large windshear associated with the fog top. This is a consequence of the destabilisation of the boundary layer by radiative cooling at the fog top and warming at the surface by the soil heat flux, which leads to enhanced momentum transfer to the surface from upper levels. The original model could not simulate this process because besides having no momentum equations, the exchange coefficients were fixed at values appropriate to the pre-fog stable boundary layer.

2. RATIONALE OF MODEL DEVELOPMENT

The long term aim of the Meteorological Office studies is to aid the forecasting of the formation, growth and dissipation of radiation fog. The initial version of the extended model (Brown 1980a) was further developed in order to examine the formation stage of radiation fog, since this is perhaps the most important and difficult problem. Such a model could either be used operationally or in a research context to devise new forecasting rules and give advice to forecasters in problem areas such as the effect of frost.

Before the model can be used to aid forecasting it is necessary to examine the realism of the model. This was to be done in two ways. One, the model would be compared in detail with observations from the Cardington field project. Besides indicating the realism of the model it was hoped that this would allow the reasons for serious discrepancies to be identified. The problems anticipated with this approach were that only a limited number (3) of case studies could be performed because of their complexity and that it would be difficult to identify the effects of advection. Therefore, two, the model would also be compared with a selection of forecasting rules, essentially looking at how fog formation is related to the initial humidity, temperature and wind fields. In essence the rules represent a statistical summary of many observations and so should minimise the effects of advection. However it was realised that it would be difficult to explain the physical reasons for discrepancies between the model predictions and the rules.

Once the realism of the model could be established it was proposed to use the model to investigate the sensitivity of fog formation to various factors including the properties of the soil, wind lulls, deposition of frost etc. Although such models are being developed by other workers for operational use this is believed to be somewhat optimistic because of the subtle balances involved in fog formation. In addition it was hoped to use the model to investigate the development of the mature fog and also, more importantly, fog clearance processes, eg by advection of a cloud sheet or by solar radiation.

3. REALISATION OF MODEL DEVELOPMENT

The initial version of the extended model (Brown 1980a) required significant development, which included both improvement of the numerical methods and inclusion of more physical processes, before it was sufficiently realistic to allow comparisons with observations. Many of the technical details of the improvements made up to 1982 are described in Annex 1. Some of the modifications and proposals given in Annex 1 have since been modified. A brief discussion of the developments described in Annex 1 are given below.

The initial version of the extended model (Brown 1980a) became unstable if the momentum equations were integrated at grid points closer to the surface than 1 m, a log-linear wind profile was assumed beneath this. The instability was cured by changing to a staggered, much less non-linear grid and not differentiating terms like $\partial/\partial z\,(K\,\partial\Psi/\partial z)$ before expressing them in the numerical algorithm for solving the diffusion equation. The method of calculating the surface temperature was changed to a simpler

direct method, the algorithm used in 1980 having been discovered to be inaccurate under some circumstances. In order to allow the diurnal cycle to be represented the downward solar flux at the earth's surface was parametrized as a function of time of year and day (via the zenith angle). Heating of the boundary layer by direct solar absorption was neglected. The 1980 model did not allow evaporation unless fog was present. Evaporation was introduced, being driven by the difference between the saturation mixing ratio at the surface and the mixing ratio at the first grid point above the surface. It was soon discovered that allowing the full (ie potential evaporation) produced a very low Bowen ratio and the boundary layer became very humid. Thus only a fraction of the potential evaporation was allowed, the fraction being calculated from an assumed surface resistance to evaporation, following the analysis of Monteith (1981). Even then plausible values of resistance seemed to still allow an unrealistic amount of evaporation during the day.

When the developments described above were completed the model was compared with two different forecasting rules with encouraging results. An obvious discrepancy was that the model did not produce a low enough minimum temperature and the minimum temperature was not sensitive enough to the afternoon relative humidity. The former problem was caused by an isothermal soil being specified at the start of the integration. When a realistic soil temperature profile was specified lower minima were produced. It was more difficult to explain the second problem but the simple longwave radiation scheme was identified as a potential cause. This was only valid for a constant water vapour mixing ratio of 5g kg-1. These results are described in more detail in Annex 2.

Following the results of the comparisons with the forecasting rules further development of the model took place in order to incorporate the rest of the processes believed necessary to realistically simulate the field data. The model radiation scheme was replaced by the 5 band scheme of Roach and Slingo (1979). In the original version of the model the longwave transmissivity due to the droplets and gravitational settling velocity were parametrized as a function of liquid water content. The Roach and Slingo scheme required the drop-size distribution to be specified and a distribution shape based on a gamma function was assumed. The distribution was completely determined from the specified drop concentration, ratio of volume to linear mean radius and the model predicted liquid water content. These modifications are described in detail in Annex 3.

As noted previously the calculation of the surface temperature in the model had been changed to a simpler direct method although the soil properties remained constant with depth. Full details of the revised method of calculation of the surface temperature are given in Annex 4. The initial comparisons with the Cardington field project observations revealed several problems with the model. These included the necessity to allow the thermal properties of the soil to vary with depth in order to represent the insulating character of the surface layer at Cardington. The soil heat diffusion scheme was then made implicit and the soil properties (thermal conductivity and thermal capacity) were allowed to vary with depth. This was necessary to simulate realistically the variation with time of both the temperature and soil heat flux at 5 cm depth. Details of these modifications to the soil scheme are described in Annex 5.

The other main problem uncovered through the initial comparisons was the continued overestimation of evaporation during the day, despite following the formulation given by Monteith (1981) proposed in Annex 1. This formulation expresses the fraction of potential evaporation in terms of a surface resistance to evaporation. However as soon as the evaporation was reduced the surface temperature increased thus increasing the potential evaporation. The net result was that the evaporation was extremely insensitive to the value of surface resistance. A new formula was introduced relating the evaporation to a surface resistance but not as a fraction of the potential value. This followed the approach in the Met O 11 mesoscale model and succeeded in reducing the evaporation. Further details of these changes to the model evaporation scheme are described in Annex 6.

Although the model was essentially complete following the modifications described above one doubt remained. This was in the radiation scheme because the analytic functions used by Roach and Slingo to fit the gaseous transmissivities were only valid down to a path length of 1 mb. Even over this path length significant deviations from their 'best estimate' of transmissivity were apparent in some bands. New fits to the transmissivities were constructed from a series of decaying exponentials, using the exponential sum fitting of transmissivity (ESFT) technique. Pathlengths in the range 10^{-7} g cm^{-2} to 10^{2} g cm^{-2} were fitted with an accuracy of at least 1% and typically 0.01%. Using a typical nocturnal temperature and humidity profile from the model, the radiative cooling below 3 m was reduced by up to a factor of 5 using the more accurate fits. At greater heights the differences were negligible. The exponential sum fits were too computationally expensive to use in the model, instead they

are used once at the start of an integration to construct a look up table of transmissivity against absorber path length. Thereafter the transmissivity is calculated by interpolation using values from the table. The radiative heating rates obtained by this method show no significant differences to those calculated directly using the ESFT technique. Annex 7 describes in detail these changes to the radiation scheme and gives all the terms required for the ESFT fits.

Tests were then carried out to examine the sensitivity of the results to the structure of the model. The properties studied were the model grid spacing at the surface, the empirical constants in the turbulence scheme which have been revised by Mellor and Yamada several times and the specification of the initial conditions. The model results were found to be insensitive to changing the height of the bottom grid point from 0.03 m to 1 m. This is because the model only produces a small surface to screen temperature difference and hence underestimates the radiative cooling near the surface. Greater sensitivity was found if a lower geostrophic windspeed was used or the surface radiative temperature was specified to be several degrees lower than the model predicted surface temperature. Therefore the grid spacing of 0.03 m was retained for the study of fog formation but a spacing of 1 m should suffice for simulating a mature fog. The model was also found to be insensitive to the changes in constants in the turbulence scheme and the latest constants given by Mellor and Yamada (1982) were chosen for further work. The sensitivity to the initial windfield (which may not be in balance with the model equations) was examined by integrating the model with a neutral temperature profile until the windfield came into balance. Although the surface winds were still turning slightly after 15 hours, the windspeed changed little after 5

hours. In fact even using the unbalanced initial wind only made a small difference to the subsequent development of the nocturnal boundary layer and the formation of fog.

Tests were also carried out to examine the effect of the surface adjustment to the exchange coefficients, this is described in Annex 8. However the surface layer profiles were found to be fairly insensitive to any changes in this adjustment.

The model in all the tests described above in this report had turbulent exchange coefficients which were functions of the local Ri following the level 2 formulation of Mellor and Yamada (1974). Using their revised empirical constants this formulation predicts a critical value of Ri = 0.19 at which turbulence ceases. In a recent publication by Yamada (1983), in which he describes a simplified version of their level 2.5 (exchange coefficient a function of turbulent kinetic energy) turbulence scheme, he uses part of the level 2 stability functions. He points out that for agreement with their more sophisticated level 4 model that he could not allow turbulence to be extinguished when Ri exceeds the critical value. Instead when Ri exceeds 0.16 the stability functions retain a value appropriate to this Ri. This modification to the level 2 formulation was tested in the model, however a second term within the level 2 formulation causes turbulence to cease at Ri = 0.89. The modification increased the nocturnal boundary layer depth by a factor of two to three and produced profiles of temperature, humidity and wind which were much closer to the observed profiles. However the near surface windspeed was increased slightly on account of the extra momentum generated in the deeper boundary layer. Some results from the comparisons with the Cardington observations using the version of the model with the modified stability

functions (Ri_c = 0.89) are described by Turton and Brown (1984). Two versions of the model currently exist, one uses the basic level 2 turbulence formulation for which Ri_c = 0.19 and the other uses the modifications to the stability functions which give Ri_c = 0.89.

4. REFERENCES

Brown R 1980a, Some field observations of radiation fog and their interpretation, Proc Int Conf Cloud Physics, Clermont-Ferrand, France, 309-312.

Brown R 1980b, A numerical study of radiation fog with an explicit formulation of the microphysics, Quart J R Met Soc, 106, 781-802.

Brown R and Roach W T 1976, The physics of radiation fog: II - A numerical study, Ibid, 102, 335-354.

Carpenter K M 1977, Surface exchanges in a mesoscale model of the atmosphere, Met O 11 Tech Note 96, Meteorological Office, Bracknell.

Corradini C and Torra G 1980, The parametrization of the gravitational water flux in fog models, J Atmos Sci, 37, 2535-2539.

Craddock J M and Pritchard D 1951, Forecasting the formation of radiation fog - a preliminary approach, Met Res Paper No. 624.

Deardorff J W 1976, On the entrainment rate of a stratocumulus-topped mixed layer, Quart J R Met Soc, 102, 563-582.

Deardorff J W 1978, Efficient prediction of ground surface temperature and moisture, with inclusion of a layer of vegetation, J Geophys Res, 83, 1889-1903.

Frost R 1948, Calculation of night minimum temperatures, Prof Notes No. 95, Meteorological Office, Bracknell.

Hoffert M I and Storch J 1979, A scheme for computing surface fluxes from mean flow observations, Bound-Layer Met, 17, 429-442.

Hunt G E and Mattingly S R 1976, Infrared radiative transfer in planetary atmospheres - I. Effects of computational and spectroscopic economies on thermal heating/cooling rates, J Quant Spectrosc Radiat Transfer, 16, 505-520.

Levin L M 1958, Functions to represent drop size distributions in clouds. The optical density of clouds, Bull Acad Sci USSR Geophys Ser, 10, 698-702.

McClatchey R A, Benedict W S, Clough S A, Burch D E, Calfee R F, Fox K, Rothman I S and Garing J S 1973, AFCRL Atmospheric absorption line parameters compilation, Env Res Paper No. 434.

Mellor G L and Yamada T 1974, A hierarchy of turbulence closure models for planetary boundary layers, J Atmos Sci, 31, 1791-1806.

Mellor G L and Yamada T 1982, Development of a turbulence closure model for geophysical fluid problems, Rev Geophys Space Phys, 20, 851-875.

Monteith J L 1957, Dew, Quart J R Met Soc, 83, 322-341.

Monteith J L 1981, Evaporation and surface temperature, Ibid, 107, 1-27.

Richtmeyer R D and Morton K W 1967, Different methods for initial value problems, 2nd Edition, John Wiley and Sons.

Rider N E and Robinson G D 1957, A study of the transfer of heat and water vapour above a surface of short grass, Quart J R Met Soc, 77, 375-401.

Roach W T and Slingo A 1979, A high resolution infrared radiative transfer scheme to study the interaction of radiation with cloud, Ibid, 105, 603-614.

Slingo A and Schrecker H M 1982, On the shortwave radiative properties of stratiform water clouds, Ibid, 108, 407-426.

Swinbank W C 1949, Prediction diagrams for radiation fog, Prof Notes No 100, Meteorological Office, Bracknell.

Thom A S 1975, Momentum, mass and heat exchange in plant communities, in Vegetation and the Atmosphere, Vol I (Ed Monteith J L), Academic Press.

Turton J D and Brown R 1984, Interpretation of observations of radiation fog using a numerical model, Proc Int Conf Cloud Physics, Tallinn, Estonia, USSR to appear.

Yamada T 1983, Simulations of nocturnal drainage flows by a q21 turbulence closure model, J Atmos Sci, 40, 91-106.

Zdunkowski W G and Nielsen B C 1969, A preliminary prediction analysis of radiation fog, Pure Appl Geophys, 75, 278-299.

ANNEX 1

THE REVISED MODEL OF RADIATION FOG CONTAINING THE SOLUTION OF THE 1-D MOMENTUM EQUATIONS

Introduction

This note describes the numerical model of radiation fog at its present (March 1982) stage of development. This seems appropriate because the development has reached a plateau. All important physical processes are now believed to be well represented in the model apart from the effect of surface vegetation and the fact that the radiation scheme assumes a constant water vapour mixing ratio of 5g/kg. However before making a significant effort to remedy the latter deficiency it is proposed to undertake a series of integrations with the present model in order to evaluate its realism.

Model equations

The model is based on that of Brown and Roach (1976) but with the addition of the 1-D momentum equations. Thus the equations for the basic model variables become:-

$$\frac{\partial \theta}{\partial t} = -\frac{1}{\rho C_p}\frac{\partial F_N}{\partial z} + \frac{\partial}{\partial z}\left(K_H \frac{\partial \theta}{\partial z}\right) + \frac{L}{C_p} C \qquad (1)$$

$$\frac{\partial q}{\partial t} = \frac{\partial}{\partial z}\left(K_H \frac{\partial q}{\partial z}\right) - C \qquad (2)$$

$$\frac{\partial w}{\partial t} = \frac{\partial}{\partial z}\left(K_H \frac{\partial w}{\partial z}\right) + \frac{\partial}{\partial z}(V_s w) + C \qquad (3)$$

$$\frac{\partial u}{\partial t} = f v + \frac{\partial}{\partial z}\left(K_M \frac{\partial u}{\partial z}\right) \qquad (4)$$

$$\frac{\partial v}{\partial t} = f(u_g - u) + \frac{\partial}{\partial z}\left(K_M \frac{\partial v}{\partial z}\right) \qquad (5)$$

where θ is potential temperature, F_N net longwave flux, q , w water vapour and liquid water mixing ratios, C rate of condensation, V_s mean droplet settling velocity, u , v , orthogonal wind components. u_g is the geostrophic wind, assumed constant with height. The model axes are taken to be orientated so that $v_g = 0$. f is the coriolis parameter, set equal to $1.1 \times 10^{-4}\ s^{-1}$.

The exchange coefficients for heat, water vapour and liquid water (K_H) are set equal but the exchange coefficient for momentum (K_M) is allowed to differ. The exchange coefficients are made functions of the local gradient Richardson number (Ri) using the formulation of Mellor and Yamada (1974).

$$K_M = l^2 \frac{\partial \bar{V}}{\partial z} S_M \quad (6)$$

$$K_H = l^2 \frac{\partial \bar{V}}{\partial z} S_H \quad (7)$$

Where l is a neutral mixing length which remains to be defined and $\bar{V} = (u^2 + v^2)^{1/2}$. S_M , S_H are complicated stablity functions derived by Mellors and Yamada from a second order closure model of turbulence by neglecting the smaller terms. This formulation was found to be in good agreement with the full second order closure model during an integration simulating the diurnal cycle of surface heating and cooling. The functions S_M , S_H are described in Appendix 1. Their form implies a critical gradient Ri of 0.22 at which turbulence ceases. The model exchange ceofficients are then set equal to 2.2×10^{-5} m^2 s^{-1}. The mixing length is given by

$$\frac{1}{l} = \frac{1}{kz} + \frac{1}{l_0} \quad (8)$$

i.e. l approaches kz as $z \rightarrow 0$ but is limited to a value l_0 as $z \rightarrow \infty$. A value of l_0 of 40 m well simulates the atmospheric boundary layer, (P Mason personal communication). It is proposed to experiment with the value of l_0 , for example Mellor and Yamada suggest making l_0 proportional to the depth of the turbulent layer. In the case of a mature deep fog with a strong capping inversion it may be desirable to add a third term to (8) to allow for the reduction in mixing length as the inversion is approached from beneath.

Numerical solution of the diffusion and momentum equations

Boundary layer models generally terminate the integration of these equations at a grid point several metres from the surface. Fluxes from the surface are either imposed or calculated from drag coefficients. However in the case of radiation fog important interactions are occurring below a metre prior to fog formation and it is necessary to model these explicitly.

The original fog model placed the first grid point in air at 0.03 m above the surface and this specification is retained. Later on it is intended to examine the sensitivity of the results to the surface grid spacing. Use of a small grid spacing imposes severe numerical problems in solving the diffusion equation. For example using an explicit scheme, as in the original model, there is no stability for time steps $t \geq (\Delta z)^2 / 2K$. This limited the time step in the original model to 1 s. A much smaller time step would have been required had the model allowed K to increase with the development of a mature fog. Thus in the current model a fully implicit diffusion scheme is used. The equation to be solved is first transformed to the form -

$$B\,T_{L+1}^{t+1} + A\,T_{L}^{t+1} + C\,T_{L-1}^{t+1} = -T_{L}^{t} - D \qquad (9)$$

Where L represents the spatial co-ordinate, t is the current time and A to D are constants (or pseudo-constants for K a function of Ri) which depend upon the time step, exchange coefficients and type of grid. The series of equations represented by (9) are solved by an efficient matrix inversion technique described by Richtmeyer and Morton (1967).

In a version of the model described by Brown (1980b) a non-linear (cubic) grid was used together with centred space differencing. Corrections were applied for the highly non-linear grid. Before applying a finite difference scheme the spatial differentiation was performed i.e. the numerical algorithm was based on

$$\frac{\partial K}{\partial z}\frac{\partial T}{\partial z} + K\frac{\partial^2 T}{\partial z^2} \qquad (10)$$

Unfortunately to achieve stability it was necessary to apply spatial smoothing to the K profile and to terminate the integration of the momentum equations at 1 m. Beneath this a neutral wind profile was imposed based on u_* calculated from the 1 m wind.

The current scheme is based upon that used in a model of the stable boundary layer by P Mason (personal communication). The differentiation is not performed mathematically and the rate of change of a variable is determined by the difference of two fluxes e.g. in the explicit scheme used by Mason.

$$\frac{T_L^{t+1} - T_L^{t}}{\tau} = \left(K_{L+1/2}\frac{(T_{L+1}^{t+1} - T_L^{t+1})}{(z_{L+1} - z_L)} - K_{L-1/2}\frac{(T_L^{t+1} - T_{L-1}^{t+1})}{(z_L - z_{L-1})} \right) \Big/ (z_{L+1/2} - z_{L-1/2}) \qquad (11)$$

The $L+1/2$ indicates that a staggered grid is used, K is defined on a grid intermediate between the main grid points at which θ , u , v are defined. For use in the fog model equations of the form of (11) are transformed to equation (9) and solved implicitly. The cubic grid has been replaced by a grid which is much less non-linear close to the surface. The grid spacing increases from the surface upwards in an ad hoc but regular manner. No correction is applied for the grid non-linearity.

Equations (1) to (8) lead to logarithmic (neutral) profiles of $\bar{V}$ and θ as $z \to 0$. This implies that $\partial\bar{V}/\partial z$, $\partial\theta/\partial z \to \infty$ as $z \to 0$. Even the use of a grid spacing as small as 0.03 m cannot resolve the surface gradients properly. The problem has been largely overcome by adjusting K_1 in a manner similar to Mason (personal communication). If K_{1m} is the exchange coefficient

midway between the surface ($z_1 = 0$) and the first grid point above the surface (z_2) then for an accurate solution

$$K_{1M}\left(\frac{\partial \bar{V}}{\partial z}\right)_1 = K_{1M}\frac{\bar{V}_2}{z_2} = u_*^2 \qquad (12)$$

where $u_1 = 0$ at $z_1 = 0$. The equilibrium solution for neutral conditions is then

$$\bar{V}_2 = \frac{u_*}{k}\ln\left(\frac{z_2 + z_0}{z_0}\right) \qquad (13)$$

For a logarithmic wind profile $\bar{V}_2 / z_2$ is a poor approximation to $(\partial \bar{V}/\partial z)_1$ as $z \to 0$. Thus K_{1M} is adjusted so that $K_{1M}\,\bar{V}_2/z_2$ gives a value of u_* consistent with that calculated from (13) i.e. u_* is assumed to be constant from z_2 to the surface. Substituting for u_* in (13) from (12) yields:-

$$K_{1M} = \frac{z_2 k^2 \bar{V}_2}{\left(\ln\left[\frac{z_2 + z_0}{z_0}\right]\right)^2} \qquad (14)$$

It can be shown that for a neutral temperature profile the adjusted value of K_{1H} is also given by equation (14).

This scheme has shown good agreement with the original explicit scheme when applied to a neutral and stable boundary layer. The original scheme uses $z_2 =$ 2.7 m whilst the implicit scheme was tested both for this value and $z_2 =$ 0.03 m. Since it was desired to test the numerical scheme only, all stable integrations used a simple stability factor $(1 - 3Ri)^2$. It is encouraging that it proved possible to produce a constant flux layer down to 0.03 m. The comparison has been described in a separate note.

Stability is now achieved for time steps of 1 s or less without recourse to spatial smoothing of the K profile. However the integration time can be reduced by introducing time smoothing for K .

$$K_S^{t+1} = \beta K_S^t + (1-\beta) K^{t+1} \qquad (15)$$

A time step of 5 or 10 s can be used with β set to 0.5. Careful comparisons with unsmoothed runs are envisaged before final values of time step and β are chosen.

Droplet settling

The mean droplet fall speed (V_s) required for equation (3) is still parametrized in terms of liquid water mixing ratio

$$V_s = 6.25\, w \qquad (16)$$

where V_s is in cm s^{-1}, w in g Kg^{-1}. Centred differences are used to evaluate $\partial/\partial z\,(V_s w)$ since V_s is only defined at the same grid point as w.

Radiative transfer equations

The scheme described by Brown and Roach (1976) is still incorporated into the model. This lacks flexibility because it assumes a constant water vapour mixing ratio of 5 g/Kg in order to specify the gaseous transmissivity as a function of distance. The transmissivity in the atmospheric window is also assumed to be unity. This approximation will become poorer as the model depth is increased in order to solve the momentum equations.

The model scheme has recently been compared with the five band scheme of Roach and Slingo (1979), for a clear air case with water vapour mixing ratios around 4 g/Kg. Surprisingly good agreement was found so that the present scheme may be used with confidence so long as the mixing ratios are kept around this value.

In the longer term it will be necessary to update or replace the model radiation scheme. One possibility is to incorporate the Roach and Slingo scheme directly into the model. This will require the specification of a drop-size distribution. The present scheme makes the liquid water transmissivity a function of liquid water path which is equivalent to assuming that the droplet absorption efficiency factor is proportional to droplet radius. Corradini and Torra (1980) have reported that the proportionality constant used by Brown and Roach gives excellent agreement with more exact calculations. However they also report that the parametrization of droplet settling velocity is very poor. If the Roach-Slingo scheme is used the model will have to produce a drop-size distribution as a function of liquid water content using one of the many formulations reported in the literature. The opportunity could then be taken to calculate the mean settling velocity from the drop-size distribution.

Surface temperature and soil heat flux

The original model used an algorithm due to Zdunkowski and Neilsen (1969) to calculate the surface temperature as a function of time. Unfortunately this was found to be in error when significant gradients of exchange coefficient were encountered at the surface. This has been abandoned in favour of a more

direct approach described for example by Deardorff (1978). Whilst Zdunkowski and Neilsen produced an expression for the instantaneous time rate of change of surface temperature the direct method assumes that the surface temperature responds with zero time constant so as to maintain continuity of fluxes at the air-surface interface. The method reduces to the following steps:-

(i) Calculate the surface soil heat flux as a residue of the other surface fluxes predicted by the model

$$F_G = -(F_N + F_H + F_L) \qquad (17)$$

where F_G, F_N, F_H, F_L are the soil heat flux, net radiative flux, sensible and latent fluxes respectively.

(ii) Approximate the surface temperature gradient by the value over the first grid interval and set the surface temperature T_s to give the value of F_G from (17) i.e.

$$T_s = T_{s-1} + \frac{\Delta z_s F_G}{\rho C K_s} \qquad (18)$$

Where ρ, C are the density and thermal capacity of the soil, K_s is an exchange coefficient for soil ($\rho C K_s = k$ thermal conductivity), $\Delta z_s = z_s - z_{s-1}$ where $s-1$ represents the first grid point beneath the surface.

(iii) Solve the heat diffusion equation for soil

$$\frac{\partial T}{\partial t} = K_s \frac{\partial^2 T}{\partial z^2} \qquad (20)$$

subject to boundary conditions $T = T_s$ at $z = z_s$ and T = constant T_d say at $z = z_d$.

Equation (20) is solved on a non-linear grid using 15 grid points to a depth of 2 m. An explicit method is used with correction for grid non-linearity. Δz_s has been reduced from the original model value of 0.03 m to 0.0039 m in order to better approximate the surface temperature gradient. With the current value of K_s, 3.7×10^{-7} m^2 s^{-1}, the explicit scheme is stable for $\tau < 40$ s. Satisfactory agreement has been found with analytic solutions for a constant and sinusoidally varying soil heat flux. The scheme does not allow for variations of K_s with depth. This may require modification in the near future since K_s may often decrease towards the soil surface in reality.

Evaporation and surface mixing ratio

It is only possible to explicitly calculate the surface mixing ratio by use of sophisticated models of the transfer of water through soil as referenced for example by Monteith (1981). This is clearly beyond the scope of

the present work. However some improvement of the original treatment of q_{v0} is required, especially since it is proposed to integrate the revised model through a diurnal cycle. In the original model $q_{v0} = RH_0 \cdot q_{vs}(T_s)$ at the start of the integration, where RH_0 , T_s are specified externally. Since solar radiation was not incorporated all integrations commenced by cooling. q_{v0} remained unaltered and the latent heat flux made no contribution to the surface energy balance until $q_{v0} > q_{vs}(T_s)$. Thereafter $q_{v0} = q_{vs}(T_s)$ as the surface temperature fell and the latent heat flux contributed to the surface energy balance. As the surface temperature commenced to rise in response to radiative shielding by the fog, q_{v0} was maintained at the appropriate $q_{vs}(T_s)$. However once the fog had cleared q_{v0} was no longer adjusted and the latent heat flux ceased to contribute to the surface energy balance. If this scheme were to be used for a diurnal cycle the important contribution of evaporation to the daytime surface energy balance would be neglected and the relative humidity would be underestimated.

In the new scheme evaporation or condensation is driven by the difference between the saturated mixing ratio at the surface $q_{vs}(T_s)$ and the mixing ratio at the first grid point above the surface q_{v2} .

$$F_L = f_p \cdot \rho L K_1 \frac{(q_{vs}(T_s) - q_{v2})}{z_2} \qquad (21)$$

For dew deposition i.e. $q_{vs}(T_s) < q_{v2}$, the factor f_p is set at unity. If the surface remained covered with a copious supply of water during the day then f_p should be set to unity for evaporation also. However as described by Monteith (1981), evaporation is normally less than this because of drying of the upper soil layer in the case of bare soil or in the case of a plant canopy because evaporation is mainly taking place by the mechanism of evapotranspiration. It is common in general circulation models to describe evaporation by equation (21) with f_p set a value between 0.6 and 0.8. Deardorff (1978) has suggested making f_p a function of the soil moisture content at the surface with the latter quantity made a function of the diffusion of water from deeper layers and evaporation. This seems too elaborate for the present model. Therefore f_p is set at a constant less than unity if $q_{vs}(T_s) > q_{v2}$ unless fog is present. It is then assumed that the ground is still thoroughly wetted by the dew and fog deposited overnight and f_p is retained at unity.

Monteith (1981) has criticised the use of a constant f_p even when the surface properties are constant and it is proposed to try a simple variable formulation of f_p following Monteith's analysis. He writes equation (21) in the form of an analogue of Ohms Law.

$$F_L = \rho L \frac{(q_{z0} - q_{z2})}{r_v} \qquad (22)$$

Where r_v is a resistance to evaporation given by

$$r = \int K_D(z)^{-1} \, dz \qquad (23)$$

He proceeds to show that if the surface is well wetted so that $q_{z0} = q_{rs}(T_s)$ then $r_v = r_H$ where r_H is the resistance for heat transfer (defined in a similar manner to (23)) and $f_p = 1$. However if because of a drying soil or a surface vegetation canopy r_v exceeds r_H by an amount r_s then

$$f_p = \frac{(\Delta + \gamma)}{\Delta + \gamma(1 + r_s/r_H)} \qquad (24)$$

Where $\Delta = \frac{\partial q_{rs}(T)}{\partial T}$ and $\gamma = \frac{c_p}{L}$

f_p is seen to be a function of temperature and r_H even if r_s is constant. One advantage of this formulation is that it allows access to the literature on evaporation which is generally formulated in terms of r_s.

Solar radiation absorbed at the surface

The solar radiation absorbed at the surface is parametrized using a modified form of the equation of Hoffert and Storch (1979)

$$S = (1 - \alpha) S_0 \tau^{\sqrt{\sec \Xi}} \cos \Xi \qquad (25)$$

where α is the surface albedo, S_0 the solar constant and Ξ the zenith angle which is calculated using a standard trigonometrical formula as a function of time of year and time of day. τ is a constant which is adjusted for agreement with a 24 band solar radiative transfer scheme. Hoffert and Storch used $\tau^{\sec \Xi}$ but equation (25) gives a better fit around sunset when compared to the radiation scheme. In principal τ could also be adjusted for attenuation by cloud or fog. Direct atmospheric heating by solar absorption is omitted. Whilst this can be significant it is hoped that the present simulation will be sufficiently accurate for comparisons with forecasting rules and to provide realistic initial conditions for the development of the nocturnal boundary layer.

Remaining boundary conditions

At the top boundary $u = u_g$, $v = 0$, $w = 0$, q is constant and $\bar{\theta}$ changes by radiative cooling only. The downward longwave fluxes inside and outside the atmospheric window are specified with reference to the atmospheric profile being simulated.

At the air-surface interface $u = v = 0$, $w = 0$, roughness length $z_0 = 0.02$ m.

Release of latent heat after condensation

It is believed that the model as described thus far will adequately simulate the development of the nocturnal boundary layer and the initial stage of fog formation. However the exchange coefficient formulation of Mellor and Yamada is based on a 'dry' model. No allowance is made for the generation of buoyancy by the latent heat released by condensation. This section describes tentative proposals to remedy this deficiency.

In a 'dry' model θ is a conservative property and also describes the buoyancy. If water vapour is introduced but condensation does not occur θ is still conserved but virtual potential temperature θ_v describes the buoyancy where

$$\left.\begin{aligned} \theta_v &= \theta [1 + 0.61 q] \quad \text{in clear air} \\ &= \theta [1 + 0.61 q - w] \quad \text{in cloudy air} \end{aligned}\right\} \qquad (26)$$

θ_v is also conserved in this case. When condensation occurs neither θ nor θ_v are conserved although θ_v (with allowance for the drag of the liquid water) still describes the buoyancy. The conservative thermodynamic variables are wet bulb and equivalent potential temperatures. The latter (θ_e) is convenient for model use

$$\theta_e = \theta + \frac{L}{c_p} q \qquad (27)$$

Preliminary runs of the fog model have led to the development of a lapse rate approaching the wet adiabatic value in the mature fog, due to the release of latent heat. $\partial\theta/\partial z$ then tends to a positive value leading to an unrealistic sensible heat flux. Even more seriously Ri becomes positive so that the release of latent heat stabilises the atmosphere. In a region of low windshear this could lead to Ri exceeding Ri_c and the cessation of turbulence. It is clearly important to prevent this occurrence.

Consider first the correction to the value of the sensible heat flux. When θ is not conserved it is not permissible to write $\overline{w'\theta'} = -K \partial\theta/\partial z$

Assuming that the cloudy air remains saturated Deardorff (1976) has shown that

$$\overline{w'\theta'} = \frac{\overline{w'\theta_e'}}{\left[1 + \frac{\epsilon L^2 q_s}{R_d c_p T^2}\right]} \qquad (28)$$

where $\epsilon = 0.622$ and R_d is the gas constant for dry air. Since θ_e is conserved it is possible to transform (28) using a flux gradient relationship

$$\overline{w'\theta'} = \frac{-K \frac{\partial\theta_e}{\partial z}}{\left[1 - \frac{\epsilon L^2 q_s}{R_d c_p T^2}\right]} \qquad (29)$$

It is proposed to use (29) to evaluate the sensible heat flux at grid points where liquid water is present.

The appropriate adjustment to Ri is less certain. Recognising that $\partial\theta/\partial z$ occurs in the numerator of Ri by the appreciation of the flux gradient relationship to the expression for the flux Richardson number, it may be sufficient to replace $\partial\theta/\partial z$ by $\partial\theta_e/\partial z\left[1 + \epsilon L^2 q_s/R_d c_p T^2\right]^{-1}$. This would at least ensure that Ri approached zero in a well mixed cloudy boundary layer.

Since buoyancy production of turbulent KE is proportional to $\overline{w'\theta_v'}$ in a moist atmosphere it may be more realistic to express Ri in terms of θ_v. Using equation (26) for clear air one may write

$$\overline{w'\theta_v'} = (1 + 0.61 q_\ell)\,\overline{w'\theta'} + 0.61\,\theta\,\overline{w'q'} \qquad (30)$$

Application of the flux-gradient relationship to (30) would suggest that $\partial\theta/\partial z$ should be replaced by $(1 + 0.61\, q_\ell)\,\partial\theta/\partial z + 0.61\,\theta\,\partial q_\ell/\partial z$. In cloudy air $\overline{w'\theta'}$ may be expressed in terms of the conservative variables θ_e and $q_{\ell w}$ ($= q_\ell + w$) following Deardorff (1976).

$$\overline{w\theta_v'} = \Xi_4\,\overline{w'\theta_e'} - \theta\,\overline{w'q_{\ell w}'} \qquad (31)$$

Where Ξ_4 is a function of temperature and saturated humidity mixing ratio. $\partial\theta/\partial z$ is then replaced by $\Xi_4 \partial\theta_e/\partial z - \theta\,\partial q_{\ell w}/\partial z$. Whilst this approach is attractive it must be born in mind that it has not been demonstrated that it is compatible with the extension of the Mellor and Yamada second order closure scheme to a moist atmosphere.

APPENDIX I THE STABILITY FUNCTIONS OF MELLOR AND YAMADA (1974)

$$S_M = B_1^{1/2} (1 - R_f)^{1/2} \tilde{S}_m^{3/2} \quad (1A)$$

$$S_H = B_1^{1/2} (1 - R_f)^{1/2} \tilde{S}_m^{1/2} \tilde{S}_H \quad (2A)$$

R_f is the flux Richardson number. Their theoretical model predicts the following relationship between R_f and gradient Richardson number Ri .

$$R_f = 0.725 \left[Ri + 0.186 - \left(Ri^2 - 0.316 Ri + 0.0346 \right)^{1/2} \right] \quad (3A)$$

$$\tilde{S}_m = 3A_1 \left[\frac{Y_1 - C_1 - (6A_1 + 3A_2)\Gamma/B_1}{Y_1 - Y_2\Gamma + 3A_1\Gamma/B_1} \right] (Y_1 - Y_2\Gamma) \quad (4A)$$

$$\tilde{S}_H = 3A_2 (Y_1 - Y_2\Gamma) \quad (5A)$$

Where $Y_1 = 1/3 - 2A_1/B_1 \qquad Y_2 = B_2/B_1 + 6A_1/B_1$

$$\Gamma = R_f/(1 - R_f)$$

The constants A_1 to C_1 have been evaluated by comparing the model with neutral data assuming $l = kz$. They take the following values

$$A_1 = A_2 = 0.78 \qquad B_1 = 15.0, \; B_2 = 8.0 \qquad C_1 = 0.056$$

ANNEX 2

RESULTS FROM A SERIES OF INTEGRATIONS TO COMPARE THE MACROPHYSICAL FOG MODEL WITH EMPIRICAL FORECASTING RULES

Introduction

A series of integrations using a numerical model of radiation fog based on that of Brown and Roach (1976) (described here in Annex 1) were undertaken. The basic objective was to assess the realism of the model by comparison with the empirical forecasting rules used operationally, and to identify any particular defects in the model as it stands at present.

The empirical rules

A number of empirical methods for forecasting fog formation exist, these are listed below.

1. Fog-point (Briggs)
2. Fog-point (Saunders)
3. Fog-point (Craddock and Pritchard 1951)
4. Fog forecast (Swinbank 1949)

Of these rules Craddock and Pritchard (henceforth referred to in the text as C+P) and Swinbank are the most amenable for comparison with the fog model as the input to the rules are model parameters. These two methods are described in Appendix 1, together with their interpretation.

Initial conditions

Each integration was started at midday (model time) and then integrated over a diurnal cycle to investigate nocturnal radiation fog formation. Temperature, humidity and wind profiles were the required input conditions. The temperature and wind profiles used were taken from previous integrations made to generate such profiles which would be in balance with the model equation set. Wind profiles with geostrophic wind speeds of 2 ms^{-1}, 4 ms^{-1}, 6 ms^{-1} and 8 ms^{-1} were used throughout the experiments. The initial humidity profiles allowed the specification of another variable, dewpoint for C+P and hydrolapse for Swinbank. Realistic humidity profiles with screen height (1.49 m in the model) humidities of 40%, 60% and 80% were used to provide a range of initial conditions. It is essential to specify a realistic hydrolapse near the ground to avoid the model producing very large latent heat fluxes, which affect the surface energy balance and cause the integration to subsequently fail.

Results

a. Craddock and Pritchard

The details of the comparisons are summarized in Table 1 and Fig. 1. A quick look at the formulae of C+P reveal the observations inherrent in their method. An increase in windspeed inhibits fog formation, an increase in temperature (dewpoint constant therefore a decrease in humidity) also inhibits fog formation whilst an increase in dewpoint (temperature constant therefore an increase in humidity) encourages fog formation. Fog formation prediction then essentially depends upon humidity and windspeed, although it has some dependence upon temperature.

The model results clearly show an increase in fog probability for higher humidities at a given windspeed and an increase in fog probability for lower windspeeds; in accordance with C+P. The model fog points at 4 ms^{-1} show agreement with those from C+P, but at 2 ms^{-1} are somewhat higher (this is not unexpected since C+P treat windspeeds of 0-6 ms^{-1} identically). The spread of model fog points at different humidities was found to be less than that from C+P.

Important also is the forecast of minimum temperature; the model succeeded in producing lower minimum temperatures at lower humidities (lower dew point), but they showed considerably less spread. At lower windspeeds the model produced lower minimum temperatures although again C+P treat windspeeds of 0-6 ms^{-1} identically. The model minimum temperatures were consistently higher than those forecast by C+P, the sensitivity of model minimum temperature to various parameters is described later in this note.

In summary the model behaviour generally agreed with C+P and appears sensitive to the same conditions. Two cases were found when the model disagreed with the forecast; case (i) with $Ug = 2\ ms^{-1}$, R.H. = 40% where C+P lack of resolution at lowwindspeeds may be in part responsible and case (ii) with $Ug = 8\ ms^{-1}$, R.H. = 80% where the C+P forecast is somewhat subjective due to the interpretation of $T_f - T_{min}$.

b. Swinbank

The same model integrations as used for the C+P comparisons were used with the necessary parameters being extracted. In some cases values for the hydrolapse ($\Delta\alpha/\Delta p$) were beyond the scale of the nomogram and so the forecast was extrapolated where possible. In the integrations the hydrolapse was taken from screen level to the capping inversion of the daytime boundary layer. The growth of the model boundary layer depends strongly upon the initial stability of the atmosphere, but the model is capable of simulating realistic daytime boundary layer development.

The details of the comparisons are summarized in Table 2 and Fig. 2. The behaviour forecast by the method is that fog is more likely with a weaker afternoon hydrolapse, with a lower 1800 dewpoint depression (higher humidity) and with less windshear (lower windspeeds).

Forecasts by this method, where possible gave agreement with the fog model and the model showed the same behaviour as forecast by this method.

Examining the results from both sets of comparisons it appears that the model is capable of realistic behaviour and gives good agreement with the two forecasting rules used in these comparisons. However some important discrepancies have been noted particularly in the model minimum temperatures and this is discussed in the following section.

Model minimum temperatures

a. Empirical forecasts

As noted previously the model minimum temperatures are consistently higher and show much less variation with dewpoint than those predicted by C+P. To check the C+P minimum temperatures, forecasts of minimum temperature using a method due to McKenzie were made. Forecasts by this method produced an almost identical spread of minimum temperatures for different dew points as C+P although the minima were consistently higher than those of C+P. This indicates that the spread of temperatures obtained by these two rules is likely to be realistic as both rules are based upon observational data.

b. Sensitivity tests

The version of the model used in the integrations fixes an isothermal soil temperature profile at the surface temperature at the start of the integration, clearly this is unrealistic. To examine the effect of soil temperatures on the minimum screen height temperature several integrations were made with different initial soil temperature profiles. A reference integration with U_g = 6 ms^{-1} and RH = 40% was chosen for comparison. Profile (a) in Fig. 3 is the reference isothermal profile, profile (b) is for the soil temperatures taken from the integration to generate the initial conditions for the reference case, and profile (c) is taken from a climatic average for November. The effect of the changed soil temperature profiles on the model cooling is shown in Fig. 4. The deepsoil temperatures (greater than 0.5 m depth) show no response to a diurnal cycle and have a negligible effect on the cooling, but the temperature of the upper soil layers does respond to a diurnal cycle and consequently affects the cooling. Clearly the colder upper

soil produces the lower minimum temperatures with slightly stronger cooling, but principally due to cooling commencing earlier during the afternoon. This effect is clearly important and the latest version of the model now incorporates a specified initial soil temperature profile.

The forecast minimum temperatures show a strong dependence upon dewpoint and one reason for this is that the latent heat released in dew formation can reduce the total cooling by several degrees (Frost 1948, Monteith 1957). A simple test was performed in which the latent heat released by dew formation was removed and curve (d) in Fig. 4 shows the resultant cooling; the effect is to increase the cooling by $\sim 0.5^{\circ}C$ which is small compared to the variations in the forecast minima.

The other main effect on the cooling is radiation. The present radiation scheme as described by Brown and Roach (1976) assumes a constant water vapour mixing ratio of 5 gkg^{-1} and although this gives good agreement with the five band scheme of Roach and Slingo (1979) at vapour mixing ratios around 4 gkg^{-1} in clear air, it will become poorer as the vapour mixing ratio decreases and at lower temperatures. Clearly the present radiation scheme is insensitive to different humidities and so this is potentially a major source of the discrepancies noted. Tests to examine the effect of the radiation scheme are beyond the scope of this note, but the scheme of Roach and Slingo (1979) is being incorporated into the model and will be reported on in due course.

Appendix 1

a. Fog-point (Craddock and Pritchard)

The method predicts a fog point T_f (i.e. the screen temperature at which fog is likely to form), where T_f is given by

$$T_f = 0.044\ T_{12} + 0.844\ T_{d12} - 0.55 + A$$

where T_{12}, T_{d12} are the midday temperature and dewpoint, A is a constant depending upon cloud cover and windspeed. C+P suggest that in forecasting fog likelyhood the difference between the forecast T_f and the forecast T_{min} (given by their method below) might be interpreted as follows:

$T_f - T_{min}$	Forecast
$+1^{\circ}C$ or higher	fog
$+0.5^{\circ}C$ to $-1.5^{\circ}C$	more or less serious risk of fog
$-2^{\circ}C$ or lower	negligible risk of fog

where T_{min} is given by

$$T_{min} = 0.316\ T_{12} + 0.548\ T_{d12} - 1.24 + K$$

where T_{12}, T_{d12} are as defined above.

K is a constant depending upon cloud cover and windspeed, $K \neq A$ and values of each are tabulated in HWF. Clearly all the input variables are model values and are well defined. However the suggested interpretation of $T_f - T_{min}$ when $0.5^{\circ}C > T_f - T_{min} > -1.5^{\circ}C$ is somewhat grey and the interpretation in these comparisons has been modified as follows:

$T_f - T_{min}$	Forecast
$> 0.5^{\circ}C$ to $< 1^{\circ}C$	very high risk of fog
$> -0.5^{\circ}C$ to $\leqslant 0.5^{\circ}C$	high risk of fog
$\geqslant -1.5^{\circ}C$ to $\leqslant -0.5^{\circ}C$	low risk of fog
$> -2^{\circ}C$ to $< -1.5^{\circ}C$	very low risk of fog

b. Swinbank

This method is applicable to England, south east of a line Wash-Birmingham-Southampton. The method requires as input the following information.

$\Delta x / \Delta p$	afternoon hydrolapse to inversion (or 800 mb if no inversion lower) ($mgkg^{-1}\ mb^{-1}$)
T-D	dew point depression at 1800 ($^{\circ}C$)
G	forecast gradient wind speed for 1800-0700 (kts)
V	forecast windspeed at anenometer height for 1800-0700 (kts)

Then the forecast is made using the nomogram reproduced in Fig. 5, where there are five forecast categories A, B, C, X and Y, which are as follows:

C and Y	Fog will not develop
B and Y	Fog is improbable, even locally
A and Y C and X	Fog may or may not develop, if it does it will be patchy
B and X	As above but higher probability of local fog
A and X	Fog will develop, 50% chance of being widespread

The afternoon hydrolapse was calculated from the model output for 1500, G was taken to be the specified geostrophic wind speed (which is fixed for each integration) and V was taken to be the hourly average of the model 9.9 m windspeed over the period whilst fog-free.

Table 1

a.	$Ug = 2\ ms^{-1}$	$T_{12} = 6.5^{o}C$		
	RH_{12} %	40	60	80
	T_{d12} ^{o}C	-6.1	-0.8	3.5
	T_f (C+P) ^{o}C	-5.4	-0.9	2.7
	T_{min} (C+P) ^{o}C	-4.7	-1.8	0.5
	$T_f - T_{min}$ (C+P) ^{o}C	-0.7	0.9	2.2
	Forecast (C+P)	low risk	very high risk	fog
	Model	fog by 0600	fog by 0200	fog by 1900
	T_{min} (model) ^{o}C	-	-	-
	T_f (model)	$-0.1 > T_f > -0.3$	$1.3 > T_f > 1.0$	$4.9 > T_f > 4.1$
b.	$Ug = 4\ ms^{-1}$	$T_{12} = 6.6^{o}C$		
	RH_{12} %	40	60	80
	T_{d12} ^{o}C	-6.0	-0.7	3.5
	T_f (C+P) ^{o}C	-5.3	-0.9	2.7
	T_{min} (C+P) ^{o}C	-4.6	-1.7	0.6
	$T_f - T_{min}$ (C+P) ^{o}C	-0.7	0.8	2.1
	Forecast (C+P)	low risk	very high risk	fog
	Model	no fog	fog by 0700	fog by 2300
	T_{min} (model) ^{o}C	-0.8	-	-
	T_f (model) ^{o}C	-	$T_f < -0.1$	$2.8 > T_f > 2.5$
c.	$Ug = 6\ ms^{-1}$	$T_{12} = 6.6^{o}C$		
	RH_{12}%	40	60	80
	T_{d12} ^{o}C	-6.1	-0.8	3.4
	T_f (C+P) ^{o}C	-5.4	-0.9	2.6
	T_{min} (C+P) ^{o}C	-4.7	-1.8	0.5
	$T_f - T_{min}$ (C+P) ^{o}C	-0.7	0.9	2.1
	Forecast (C+P)	low risk	very high risk	fog
	Model	no fog	fog by 1000	fog by 2300
	T_{min} (model) ^{o}C	-0.6	-0.3	-
	T_f (model) ^{o}C	-	no fog at screen	$T_f < 3.2$

d. $Ug = 8\ ms^{-1}$ $T_{12} = 6.4^{o}C$

RH_{12}%	40	60	80
T_{d12} ^{o}C	-6.2	-0.9	3.3
T_f (C+P) ^{o}C	-7.0	-2.5	1.0
T_{min} (C+P) ^{o}C	-3.7	-0.8	1.5
$T_f - T_{min}$ (C+P) ^{o}C	-3.3	-1.7	-0.5
Forecast (C+P)	negligible risk	very low risk	low risk
Model	no fog	*stratus by 0500	fog by 2300 (formed by lowering of stratus)
T_{min} (model) ^{o}C	-0.4	-0.6 (at 0600)	-
T_f (model) ^{o}C	-	-	$T_f < 3.4$

(* lowered to 13.5 m by 06Z, integration then failed).

Table 2

a.	$Ug = 2\ ms^{-1}$ (4 kts)			
	RH_{12} %	40	60	80
	$(\Delta x/\Delta p)_{15}$ $mgkg^{-1}mb^{-1}$	84	74	17
	$(T-D)_{18}$ °C	0.19	0.03	0.00
	V kts	4.13	4.24	4.31
	$(G-V)^2$ kts^2	0.0	0.1	0.1
	Forecast areas	A,X	A,X	A,X
	Forecast	fog	fog	fog
	Model	fog	fog	fog
b.	$Ug = 4\ ms^{-1}$ (8 kts)			
	RH_{12} %	40	60	80
	$(\Delta x/\Delta P)_{15}$ $mgkg^{-1}mb^{-1}$	113	69	34
	$(T-D)_{18}$ °C	0.29	0.04	0.00
	V kts	4.34	4.36	4.57
	$(G-V)^2$ kts^2	13.4	13.2	11.8
	Forecast areas	not known	A or B, X	A,X
	Forecast	-	fog or fog probable	fog
	Model	no fog	fog	fog
c.	$Ug = 6\ ms^{-1}$ (12 kts)			
	RH_{12} %	40	60	80
	$(\Delta x/\Delta p)_{15}$ $mgkg^{-1}mb^{-1}$	105	67	36
	$(T-D)_{18}$ °C	0.55	0.27	0.05
	V kts	5.59	5.58	5.86
	$(G-V)^2$ kts^2	41.1	41.2	37.7
	Forecast areas	not known	B,X	B,X
	Forecast	-	fog probable	fog probable
	Model	no fog	fog	fog
d.	$Ug = 8\ ms^{-1}$ (16 kts)			
	RH_{12} %	40	60	80
	$(\Delta x/\Delta p)_{15}$ $mgkg^{-1}mb^{-1}$	90	60	33
	$(T-D)_{18}$ °C	0.76	0.37	0.24
	V kts	7.27	7.32	7.66
	$(G-V)^2$ kts^2	76.2	75.3	69.6
	Forecast areas	C,Y	C,X	B,X
	Forecast	no fog	fog possible	fog probable
	Model	no fog	low stratus	fog formed by lowering of stratus

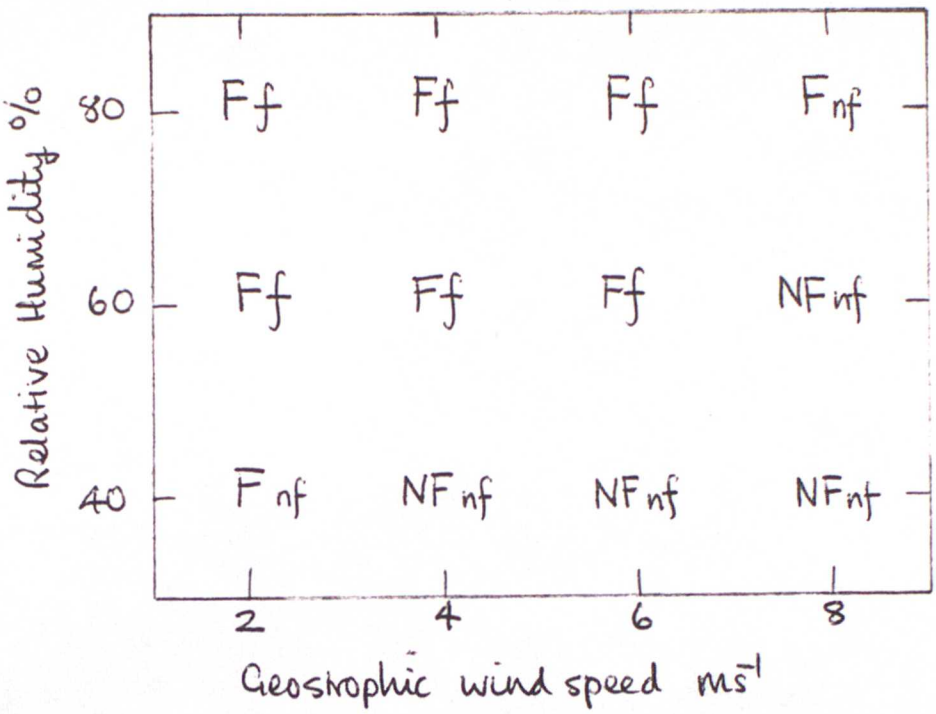

Fig. 1 Comparison of model and C+P forecast, where F, NF are model fog and no fog respectively and f, nf are forecast fog and no fog respectively

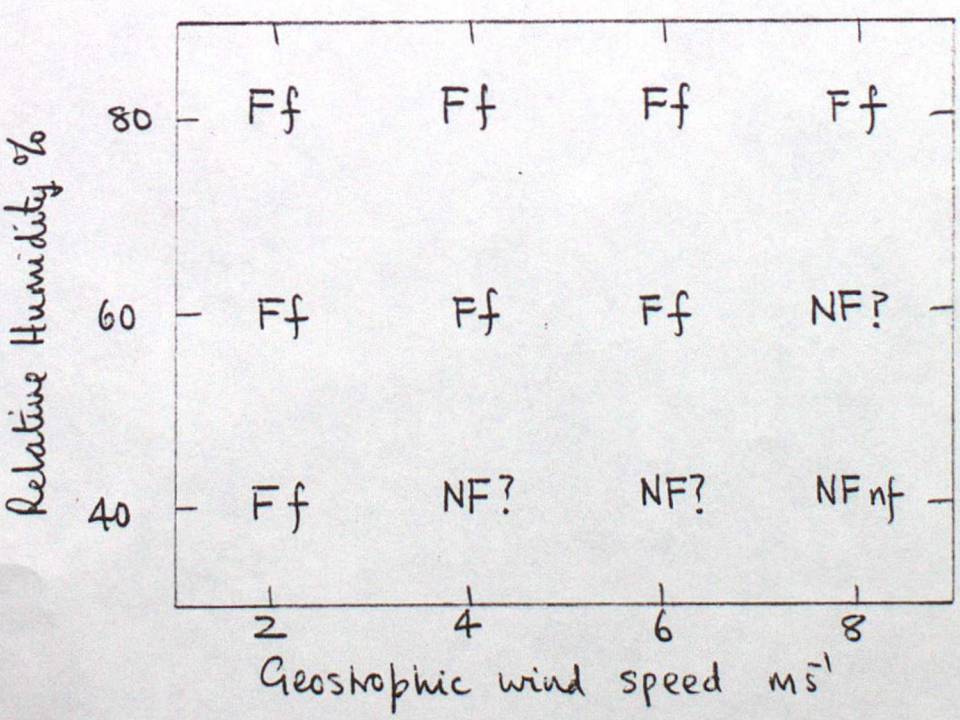

Fig 2 Comparison of model and Swinbank forecast, where F, NF, f, nf are as above and ? when no forecast possible

E.R.

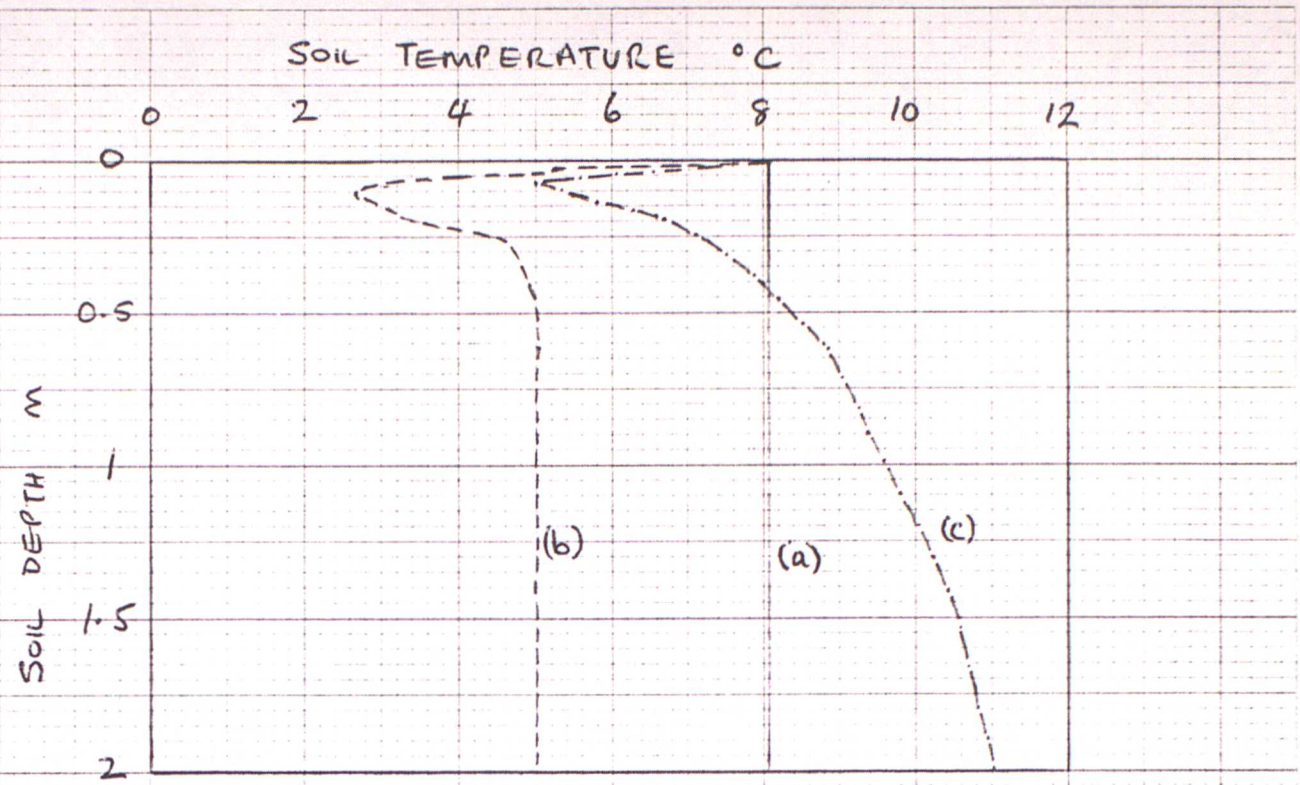

Fig 3. Soil temperature profiles (a) reference profile (b) generated profile (c) climatic profile

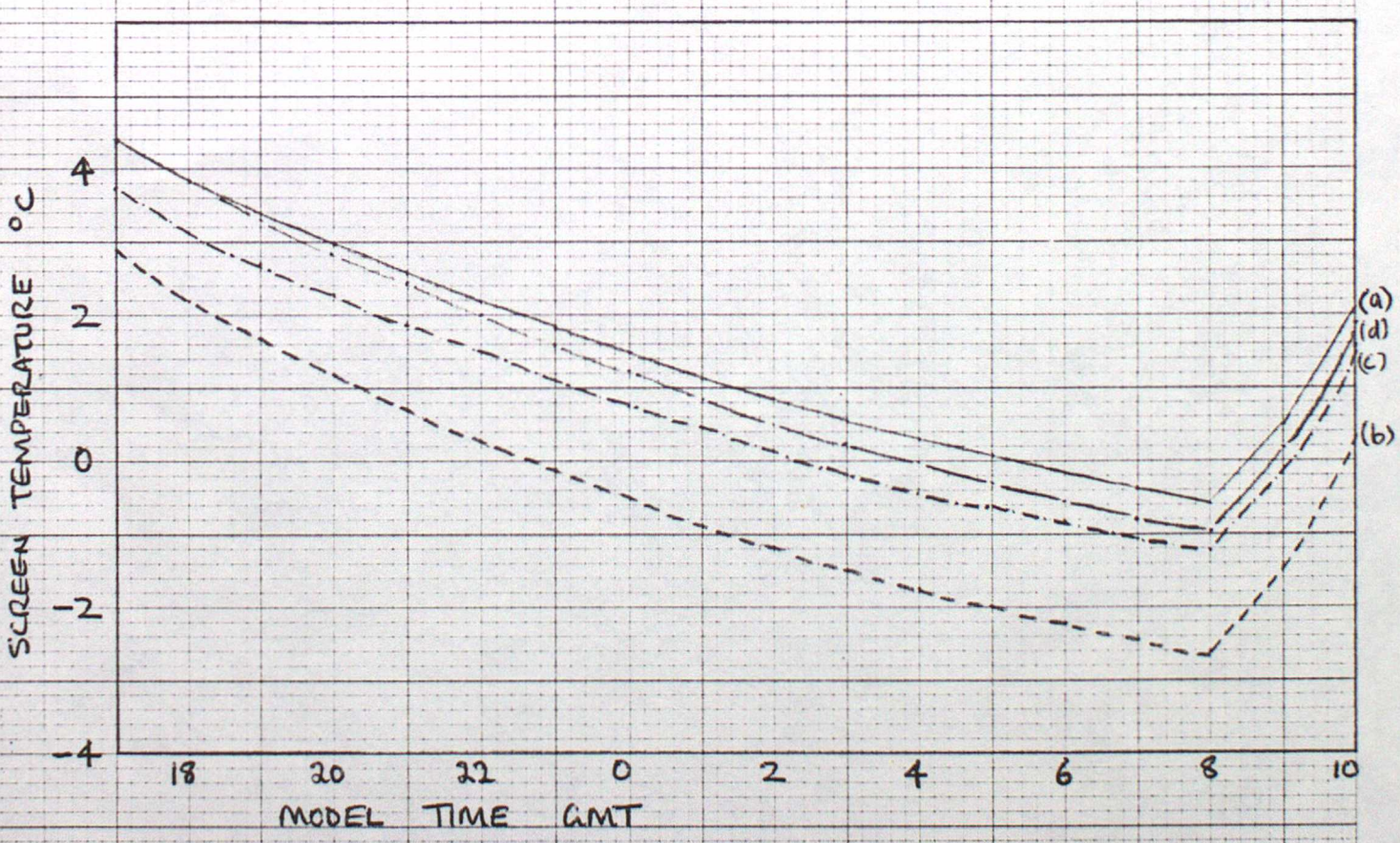

Fig 4. Nocturnal cooling (a) reference integration (b) generated profile (c) climatic profile (d) latent heat removed integration

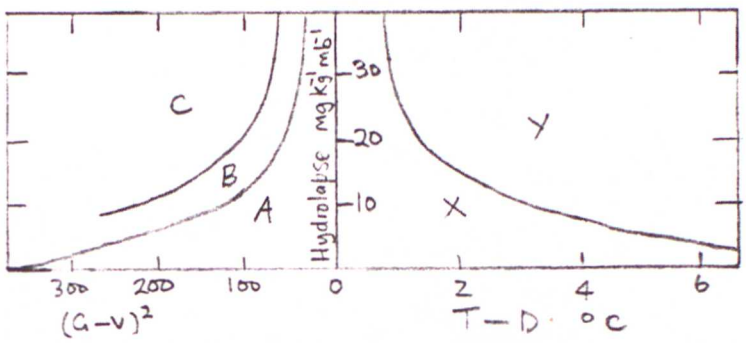

Fig 5 Fog prediction diagram (Swinbank)

ANNEX 3

THE REVISED MODEL OF RADIATION FOG CONTAINING A FIVE BAND HIGH RESOLUTION INFRA-RED TRANSER SCHEME

Introduction

Recent integrations of the macrophysical fog model to assess its realism by comparison with the empirical forecasting rules used operationally (Annex 2) identified some defects in the model as described in Annex 1. One of the principal discrepancies identified from the comparisons was the low spread in model night minimum temperatures. The minima obtained showed little dependence on humidity (dewpoint) in contrast to the wide spread suggested by the empirical rules. It was suggested that the radiation scheme used in the model was potentially a major source of this discrepancy. To remedy this a more realistic radiation scheme (Roach and Slingo 1979) has been included in the fog model and this note describes the modified model and tests to examine the effect of this and other associated modifications.

Radiation Scheme

The radiation scheme in the model used for the comparisons with the forecasting rules was that described by Brown and Roach (1976) in the original fog model paper; this scheme is henceforth referred to as the BR

scheme. The BR scheme is a two band scheme with radiative properties evaluated inside and outside the atmospheric window. Inside the window the water vapour transmissivity is unity, outside the window absorption due to atmospheric constituents is averaged. The downward fluxes at the model top are calculated from the Aughton ascent for 0000 on 7 December 1971 and give boundary conditions for the radiative calculations. The BR scheme assumes a constant water vapour mixing ratio of 5 gkg^{-1} and so is insensitive to the model humidity profile.

The scheme due to Roach and Slingo (1979), henceforth referred to as the RS scheme, is a five band scheme in which the atmospheric window has an ozone absorption band and a background water vapour continuum. Elsewhere absorption due to water vapour, carbon dioxide and water droplets are considered individually in each band. The absorption due to water vapour depends upon the specified water vapour mixing ratio and so the scheme is sensitive to the model humidity profile.

Implementation of the RS scheme in the model

The RS scheme uses pressure as its vertical coordinate so this requires the specification of a previously undefined pressure grid in the model. This grid can be defined through the hydrostatic relationship by

$$\ln p_{i+1} = \ln p_i - 2g(h_{i+1} - h_i) / R(T_{i+1} + T_i)$$

where p_0 is the surface pressure. The RS scheme requires profile data for levels above the model top (1377 m). Additional data cards are used to specify the upper air sounding which together with the model profile provides the input to the scheme.

The present version of the RS scheme has been slightly modified so that multiple cloud/fog layers can be handled since the model can produce more than one layer of cloud/fog. This should allow more realistic experiments to be done to simulate fog clearance by the advection of cloud.

The RS scheme also requires the specification of a droplet size distribution where cloud/fog exists in order to calculate the liquid water transmissivity. It is convenient to use a gamma distribution (Levin, 1958) to specify the droplet spectrum as the distribution parameters required can be specified in the model. The gamma distribution is described in detail in Appendix 1.

The RS scheme produces radiative cooling rates (rcr's) which are for layers between the specified grid levels such that each rcr is approximately representative for a point midway between grid levels. In the fog model rcr's are required at each grid level and the simplest method of achieving this is by averaging adjacent rcr's. It is worth noting the effect of this averaging at cloud/fog top, where the top is characterized by a region of marked radiative cooling. Averaging with the (above) adjacent estimate will underestimate this radiative cooling, however the uppermost grid level in the cloud/fog does not represent the actual cloud/fog top as the top may be somewhere between that grid level and the level above so that such an estimate is not inconsistent.

Droplet settling

The liquid water gravitational flux is defined by

$$G = \int v_s(r)\, dW = \bar{v}_s W$$

where $\bar{V}_S$ is the mean droplet settling velocity, this has been parametrized previously in terms of the liquid water mixing ratio by

$$\bar{V}_S = 6.25\, W$$

where $\bar{V}_S$ is in cms^{-1}, W in gkg^{-1}. Corradini and Torra (1980) have reported that $\bar{V}_S$ and W show no significant correlation, hence this parametrization is poor. The specification of a dropsize distribution allows the mean droplet settling velocity to be calculated, this is particularly simple for a gamma distribution. Corradini and Torra (1980) show that

$$\bar{V}_S = \frac{G}{W} = \frac{(4\pi\rho k_S N/3) \int r^5 f(r)\, dr}{(4\pi\rho N/3) \int r^3 f(r)\, dr}$$

which is identical to

$$\bar{V}_S = k_S \mu_5 / \mu_3$$

where k_S is a constant from Stokes law ($k_S = 1.26\ 10^8\ m^{-1}s^{-1}$) and μ_3, μ_5 are moments of the droplet distribution. The mean droplet settling velocity from the gamma distribution is given by

$$\bar{V}_S = k_S \beta^2 (\alpha+4)(\alpha+5)$$

where α, β are the distribution parameters. The mean droplet settling velocity depends upon the specified droplet concentration so the difference in settling between continental and maritime fogs could be characterised.

It was noticed that the present version of the fog model only allowed gravitational settling in ground based fogs, this is unrealistic and the model has been modified to allow settling in any cloud/fog layer. This may have some consequence during the formation of a fog in the model if it forms initially away from the surface, and may partially explain the persistence of stratus noted in earlier integrations.

Potential temperature

The model variable for temperature is θ , this has been calculated previously by

$$\theta_i = T_i + 0.0098\ h_i$$

which assumes constant pressure at all heights i.e. neglects the θ/T term. Since the model top is now at 1377 m the assumption of constant pressure is less tenable. The problem has been overcome because a pressure grid has been defined for the radiation scheme and so this can also be used to calculate θ. θ is calculated using Poissons equation for moist air where

$$\theta_i = T_i\ (1000/P_i)^{k_i'}$$

and

$$k_i = 0.236(1 - 0.29q_i)$$

Investigation into the effects of the modifications to the fog model

All of the modifications discussed have been incorporated into the fog model and it is important to identify the effect of each modification. For this purpose a series of test integrations were performed. Table 1 summarizes these test integrations.

a. Radiation scheme

Two integrations of the unmodified model were made with specified geostrophic windspeeds of 2 ms^{-1} and 8 ms^{-1} (referred to as A2 and A8 in Table 1) to provide reference cases that did and did not form fog respectively. Isothermal air and soil temperature profiles at 5C were specified together with a humidity profile which ranged from 90% at the surface to 75% at the model top. Integrations were started at 1800 (model time) and were for 7 hours to 0100.

Comparisons of the integrations for clear conditions show that the cooling was increased when the RS scheme was introduced. This is shown by Fig. 1 which shows the fall of screen temperature during the period. After 5 hours integration the screen temperature is over 1C lower and fog formed by 2315 in integration B8 which includes the RS scheme. This is encouraging because the model previously underestimated the night minimum

temperature. Fig. 2 shows the temperature profiles after 5 hours integration, the main features being the colder temperatures below ~75 m height and colder temperatures aloft in integration B8. This cooling aloft was due to cooling in the atmospheric window which the BR scheme ignores. The enhanced cooling at the model top was due to the very dry air aloft specified from the Aughton ascent; in future integrations radiative cooling at the model top could be set to zero to prevent the model top temperature from falling in this way. Such a boundary condition is unlikely to have any significant effect on the model boundary layer. The effect of averaging the rcr's was only to cause a screen temperature difference of ~0.1C after 5 hours integration in the clear air case.

A similar comparison was also made with integration A2 when fog formed. In A2 fog initially formed by 2100 at ~6 m height and lowered to the ground by 2130 and grew to 25 m by 0100. In comparison in integration B2 fog formed at ~2 m by 1930, lowered to the ground by 2000 and grew to 35 m by 0100. Fog formed earlier during integration B2 because of the greater fall in temperature with the fog point being reached earlier. The rate of growth of the fog in both integrations is similar. When cloud/fog top rcr's are extrapolated to produce an estimate of the cloud/fog top cooling (integration E2), this cooling is increased. This has the effect of increasing the liquid water content of the model fog with peak liquid water mixing ratios of over 0.6 gkg^{-1} being produced, these peak values are excessive even though the settling removes over twice as much liquid water from the fog. By 0100 the fog in integration E2 has grown to 45 m the same as in integration D2 but the fog liquid water content is much higher. This suggests that simply averaging the rcr's through cloud/fog top should be adequate.

b. Droplet settling

Droplet settling calculated from the gamma distribution as described previously was also included in the model, an integration was made to compare the calculated settling (integration C2) with the parametrized settling (integration B2). Both integrations were identical until fog formed by 1930 after which the development of the fog was influenced by the settling. Figs. 3 and 4 show liquid water profiles after 5 and 7 hours integration respectively (i.e. at 2300 and 0100). After 5 hours both fogs have the same vertical extent and the liquid water profiles are similar. After 7 hours the fog liquid water contents are significantly different with higher liquid water contents for the fog in integration B2 (with the parametrized settling). The amounts of water deposited on the ground by settling at this time were 19.47 gm^{-2} and 10.03 gm^{-2} for integrations C2 and B2 respectively, suggesting that the calculated settling is more efficient. Droplet settling is linked to the radiative cooling of the fog because the removal of drops through settling reduces the liquid water content which then causes less radiative cooling, so less condensation occurs such that an equilibrium state may result. This is apparent in integration E2 where the radiative cooling at fog top is greater, so that the fog liquid water content is higher, so more fog liquid water is removed by droplet settling. The amount of water deposited on the ground by settling after 7 hours is 19.89 gm^{-2} and 51.35 gm^{-2} in integrations D2 and E2 respectively. The liquid water content profiles in integration C2 are similar to those for integration A2 for fogs which have had a similar lifetime and are fairly representative of profiles in radiation fog.

c. Potential temperature

Integrations were performed to examine the effect of the θ formulation. In the model θ is used as the temperature variable and the values of θ are used to calculate the exchange coefficients so the formulation of θ may have some effect on the diffusion of momentum, water vapour and liquid water as well as on temperature and subsequently on condensation and evaporation.

Comparison of integrations B8 and D8 before fog formed showed negligible difference, even after 5 hours integration. Similar comparisons of integrations C2 and D2 which formed fog earlier also showed negligible differences in the temperature, humidity, liquid water and wind profiles even after 7 hours integration. This is not too surprising since any errors in $d\theta$ due to the original calculation (neglecting the θ/T term) are only likely to be significant towards the model top. In this region the stratification is stable with $Ri > Ri_c$ (where $Ri_c = 0.22$) so $K_M = K_H =$ $2.2\ 10^{-5}\ m^2s^{-1}$ which is a consequence of the formulation of Mellor and Yamada (1974) for the exchange coefficients. The more accurate calculation of θ may have some slight influence when integrating during the day when a convective boundary layer exists. The basic difference between the two ways of calculating θ is that the original calculation produces a very slightly stabler stratification away from the surface.

Comparison of the revised model with previous integrations

One of the principal defects in the previous model version as described in Annex 1 , identified from comparisons with the empirical forecasting rules was the low variation in night minimum temperature with dewpoint (humidity) and the consistently high minima. Tests described previously have indicated that the revised model is capable of producing lower minimum temperatures than before. To examine if the minimum temperatures were sensitive to the humidity profile four integrations were performed, integrations M1 to M4 which are summarized in Table 1. These integrations were started at 1800 (model time) and then integrated for 15 hours, the initial humidity profiles specified were those used for previous comparisons with the forecasting rules. Fig. 5 shows the fall in screen height temperature for these integrations. The previous model version produced a difference in minima of only 0.7C between the integrations for the dry (40%) and humid (80%) initial humidity profiles. The revised model produced a difference of 2.2C for these initial profiles, this is more realistic. The net flux at the surface (R_N) shows some interesting behaviour. In the previous model version R_N is slightly less for the 40% humidity profile, this is due to the colder ground emitting slightly less longwave radiation and the absorption due to water vapour in the air column being the same as for the 80% humidity profile since it assumes a constant water vapour mixing ratio. In contrast the revised model produces a higher net flux at the surface for the 40% humidity profile as the absorption due to water vapour is less than that for the 80% humidity profile, the difference in ground emission being much smaller.

Some of the previous comparisons with the empirical forecasting rules were re-run using the revised model and the integrations compared. Fig. 6 shows the nocturnal cooling for four such integrations. In some of these cases formation of fog or stratus inhibited the fall of temperature and so the temperature was extrapolated when this occurred, extrapolated temperatures are shown by the dashed curves in the Figure. In each case the cooling is increased in the revised model because of the RS scheme, it is evident that the minimum temperatures were lower for lower windspeeds and for lower humidities, as predicted by the empirical rules. However the temperature difference due to the different initial humidity profiles was only 1C whilst the empirically predicted difference was about 3C, this was probably due to the choice of humidity profiles which only differed up to the model top (1377 m), above this identical profile data from the Aughton ascent was specified. The empirical method of Craddock and Pritchard (1951) was derived from data in which no airmass change occurred so the hydrolapse changed little overnight, and they suggest that their empirical formulae are representative of a situation with an 'average' hydrolapse, 'average' soil conductivity and 'average' air pollution. They give the mean square error in minimum temperature due to the method as about 2C and the model values are within this, given the simplicity of the model this is in reasonable agreement.

Table 1 - Test Integrations

Integration No.	Description	Initial conditions
A2	BR radiation scheme parametrized settling approximate θ formulation.	Ug = 2 ms^{-1} RH 90% to 75% T_{air}=T_{soil}=5C
B2	RS radiation scheme parametrized settling approximate θ formulation.	as A2
C2	RS radiation scheme calculated settling approximate θ formulation.	as A2
D2	RS radiation scheme calculated settling θ from Poissons eqn.	as A2
E2	RS radiation scheme (rcr extrapolated at fog top) calculated settling θ from Poissons eqn.	as A2
A8	BR radiation scheme parametrized settling approximate θ formulation.	Ug=8 ms^{-1} RH 90% to 75% T_{air}=T_{soil}=5C
B8	RS radiation scheme parametrized settling approximate θ formulation.	as A8
D8	RS radiation scheme calculated settling θ from Poissons eqn.	as A8
M1	BR radiation scheme parametrized settling approximate θ formulation.	Ug = 6 ms^{-1} RHscreen = 40% T_{air}=T_{soil} = 5C
M2	BR radiation scheme parametrized settling approximate θ formulation.	Ug = 6 ms^{-1} RHscreen = 80% T_{air}=T_{soil}= 5C
M3	RS radiation scheme calculated settling θ from Poissons eqn.	as M1
M4	RS radiation scheme calculated settling θ from Poissons eqn.	as M2

Appendix 1

The gamma distribution after Levin (1958).

The probability density function of the gamma distribution is given by:

$$f(r) = r^{\alpha} \exp(-r/\beta) / (\alpha!\, \beta^{(\alpha+1)})$$

where f(r) is the frequency of occurrence of radius r from $r-\Delta r/2$ to $r+\Delta r/2$ and α and β are the distribution parameters with $\alpha > -1$ and $\beta > 0$.

The principal moments of the distribution are:

$$\mu_1 = \beta(\alpha+1)$$

$$\mu_2 = \beta^2(\alpha+1)(\alpha+2)$$

$$\mu_3 = \beta^3(\alpha+1)(\alpha+2)(\alpha+3)$$

where the nth moment is given by:

$$\mu_n = \beta^n [(\alpha+1)(\alpha+2)\ldots.(\alpha+n)]$$

the mean radius r_m, mean areal radius r_a and mean volume radius r_v are given by:

$$r_M = \mu_1$$

$$r_a = (\mu_2)^{1/2}$$

$$r_v = (\mu_3)^{1/3}$$

Given the mean radius r_m and the liquid water content $W = 4\rho_L \pi r_v^3 N/3$ the distribution parameters α and β can be found.

In the model liquid water mixing ratio is known at each grid level in cloud/fog and by specifying the concentration N and distribution shape through the ratio r_v/rm then r_m is determined, hence α and β are found. r_v/r_m is taken to be equal to 1.1 in the tests described in this note.

E.R.

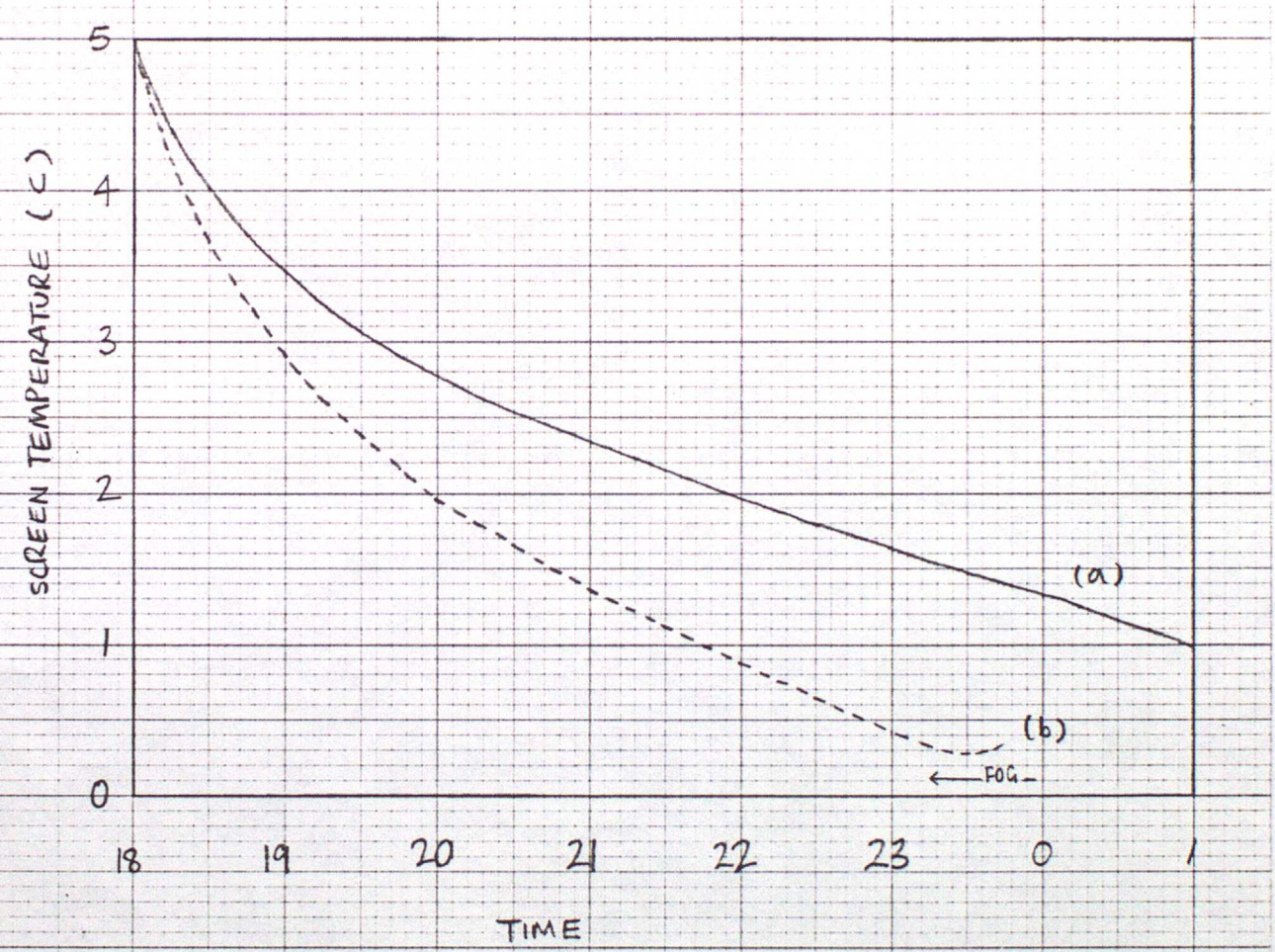

FIG.1 Nocturnal cooling (a) integration A8 BR scheme (b) integration B8 RS scheme, $U_g = 8\ ms^{-1}$.

AIR TEMPERATURE PROFILES AFTER 5 HOURS INTEGRATION

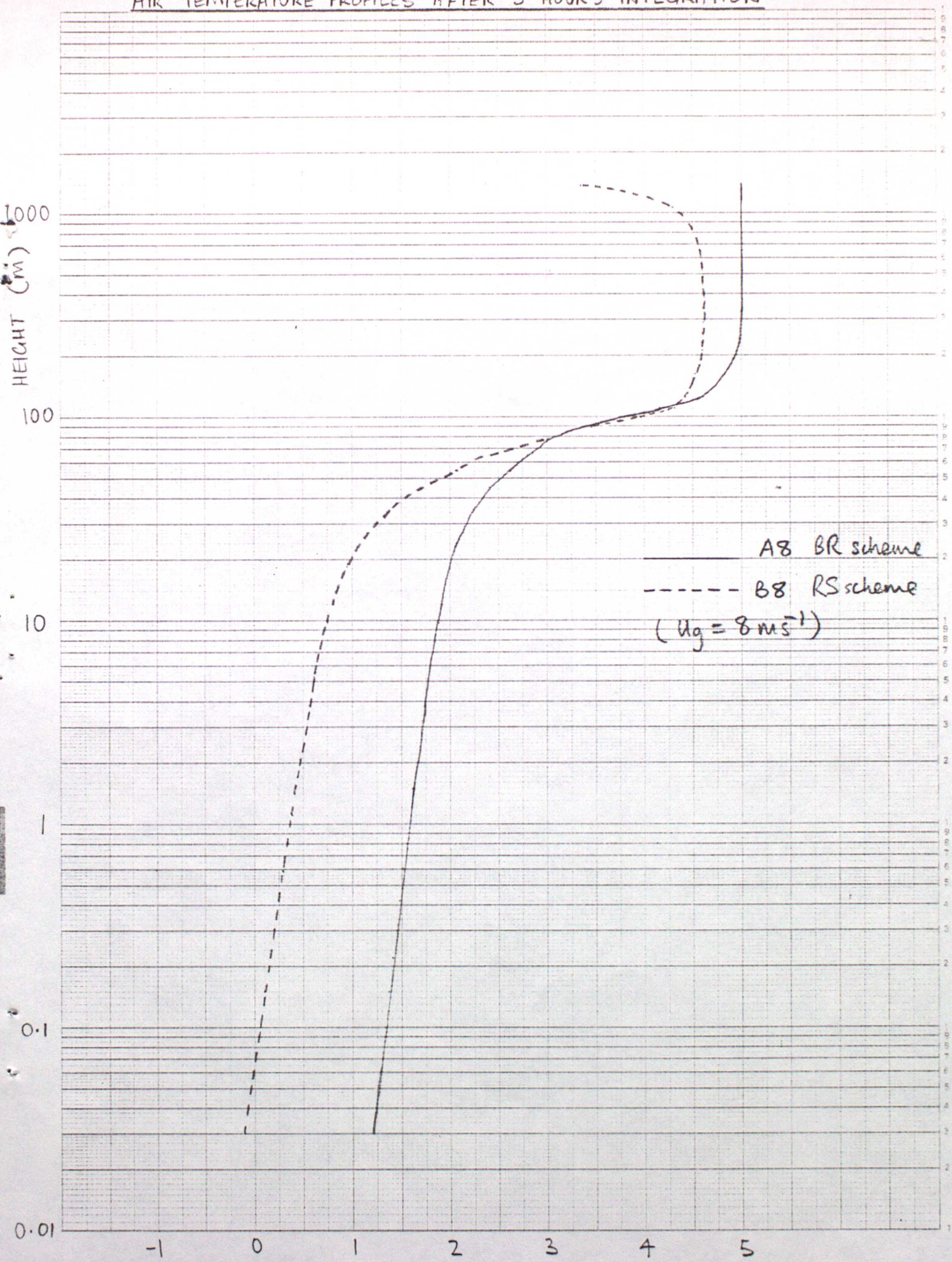

FIG. 2

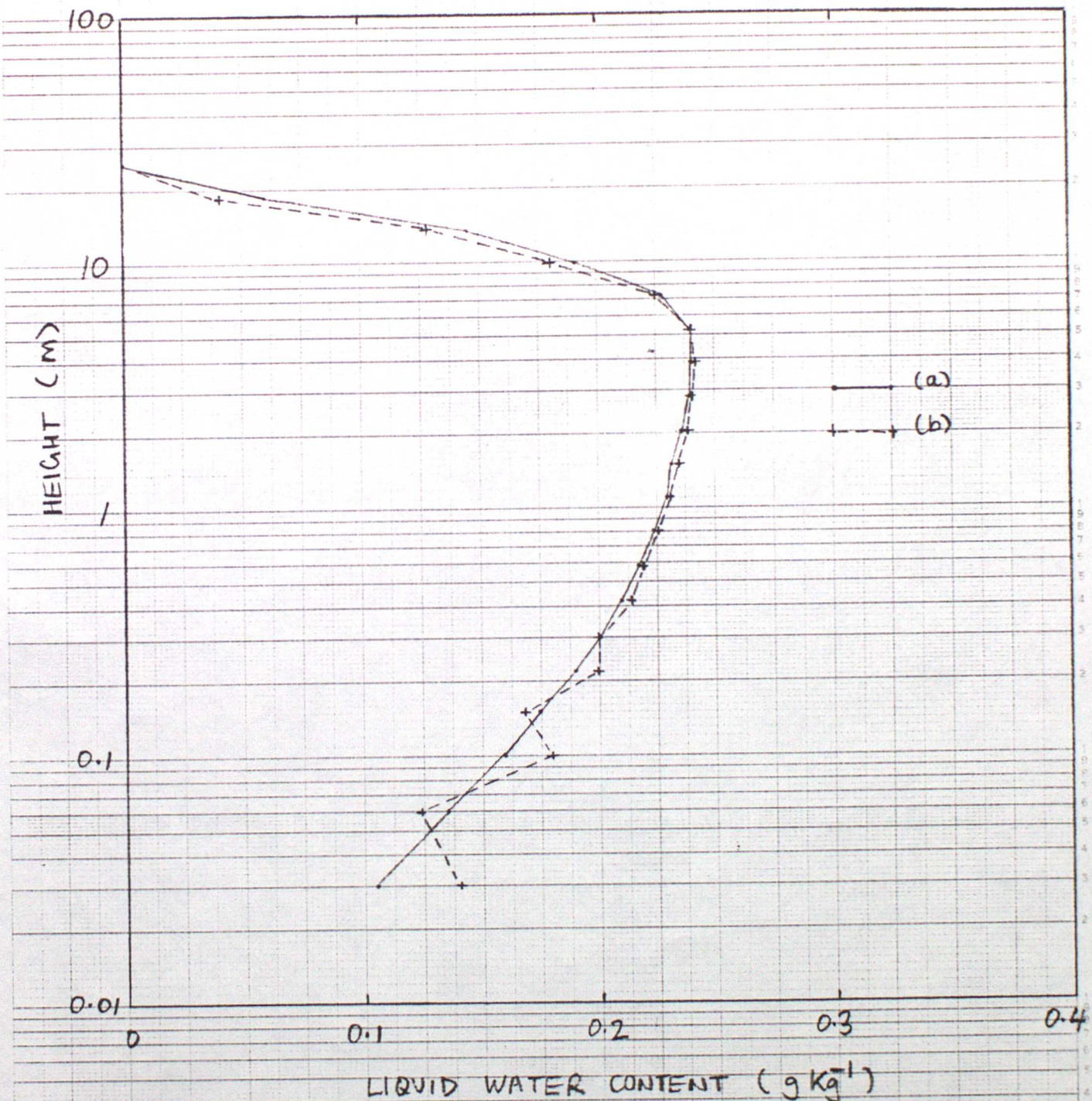

FIG. 3 Liquid water profiles after 5 hours (a) integration B2 parametrized settling (b) integration C2 settling from γ distribution. $u_g = 2\,ms^{-1}$, RS scheme.

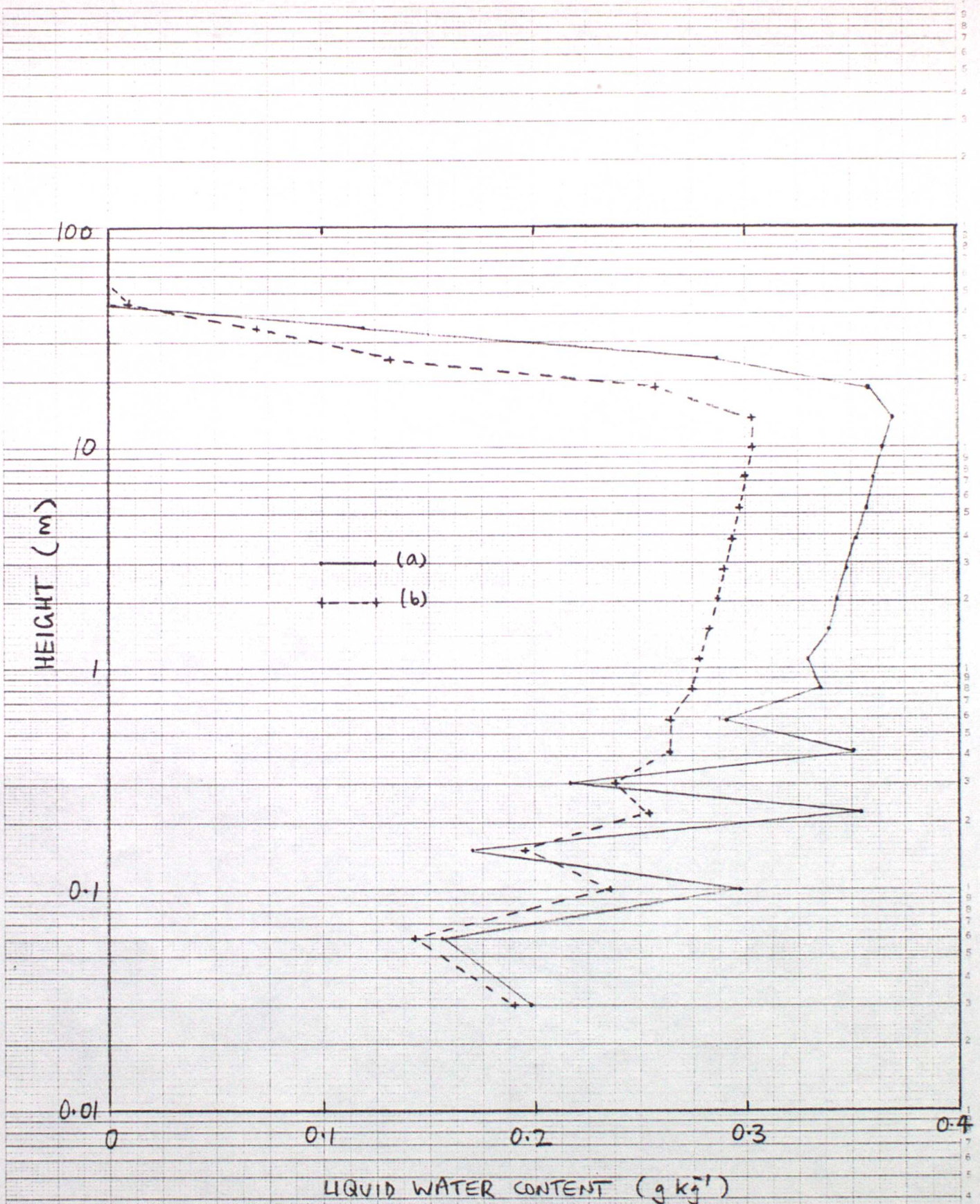

FIG. 4 Liquid water profiles after 7 hours (a) integration B2 parametrized settling (b) integration C2 settling from δ distribution. $U_g = 2\ ms^{-1}$, RS scheme.

E.R.

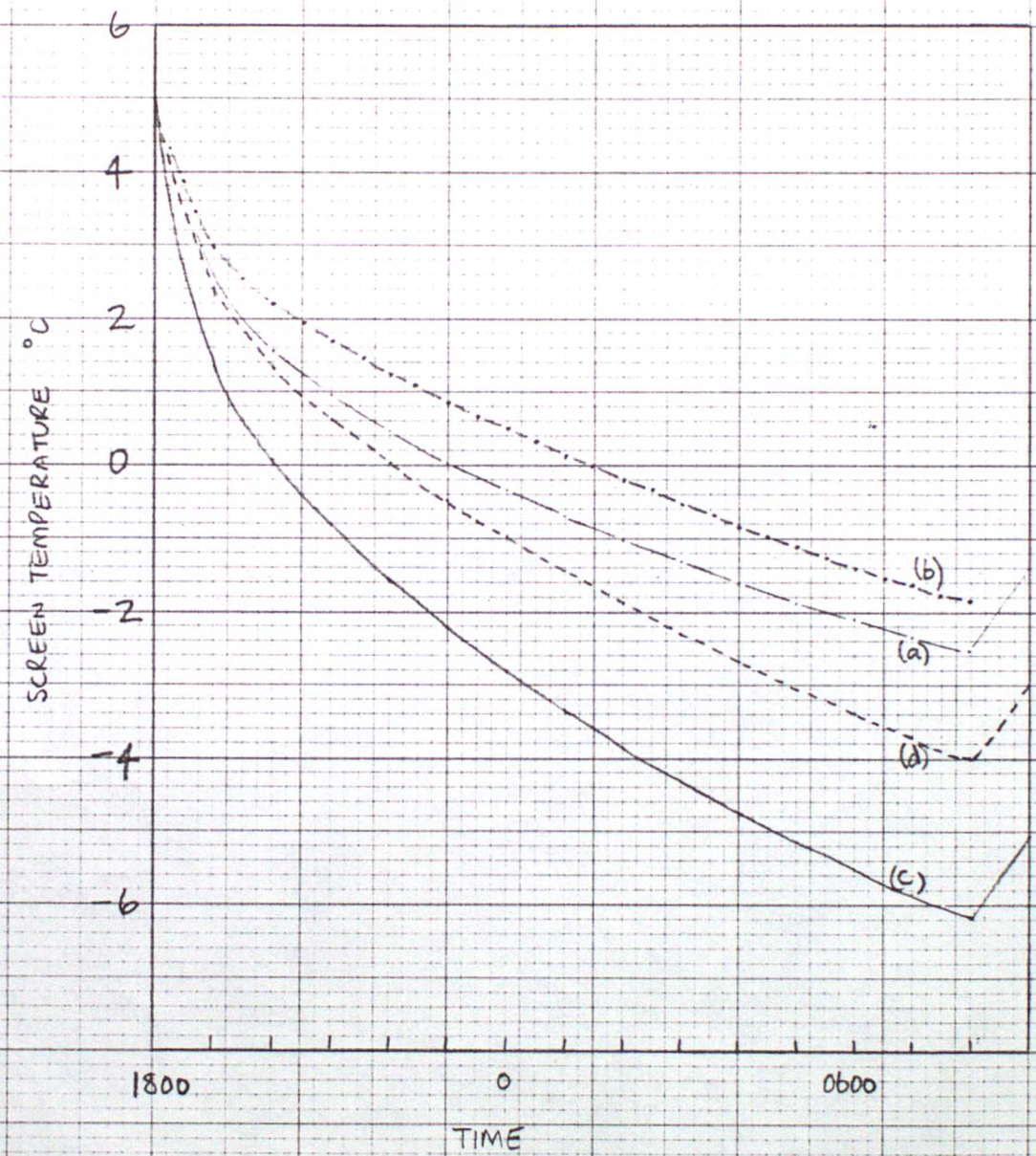

FIG. 5 Nocturnal cooling (a) integration M1 RH_{screen} = 40% BR scheme, (b) integration M2 RH_{screen} = 80% BR scheme, (c) integration M3 RH_{screen} = 40% RS scheme, (d) integration M4 RH_{screen} = 80% RS scheme. $U_g = 6\ ms^{-1}$.

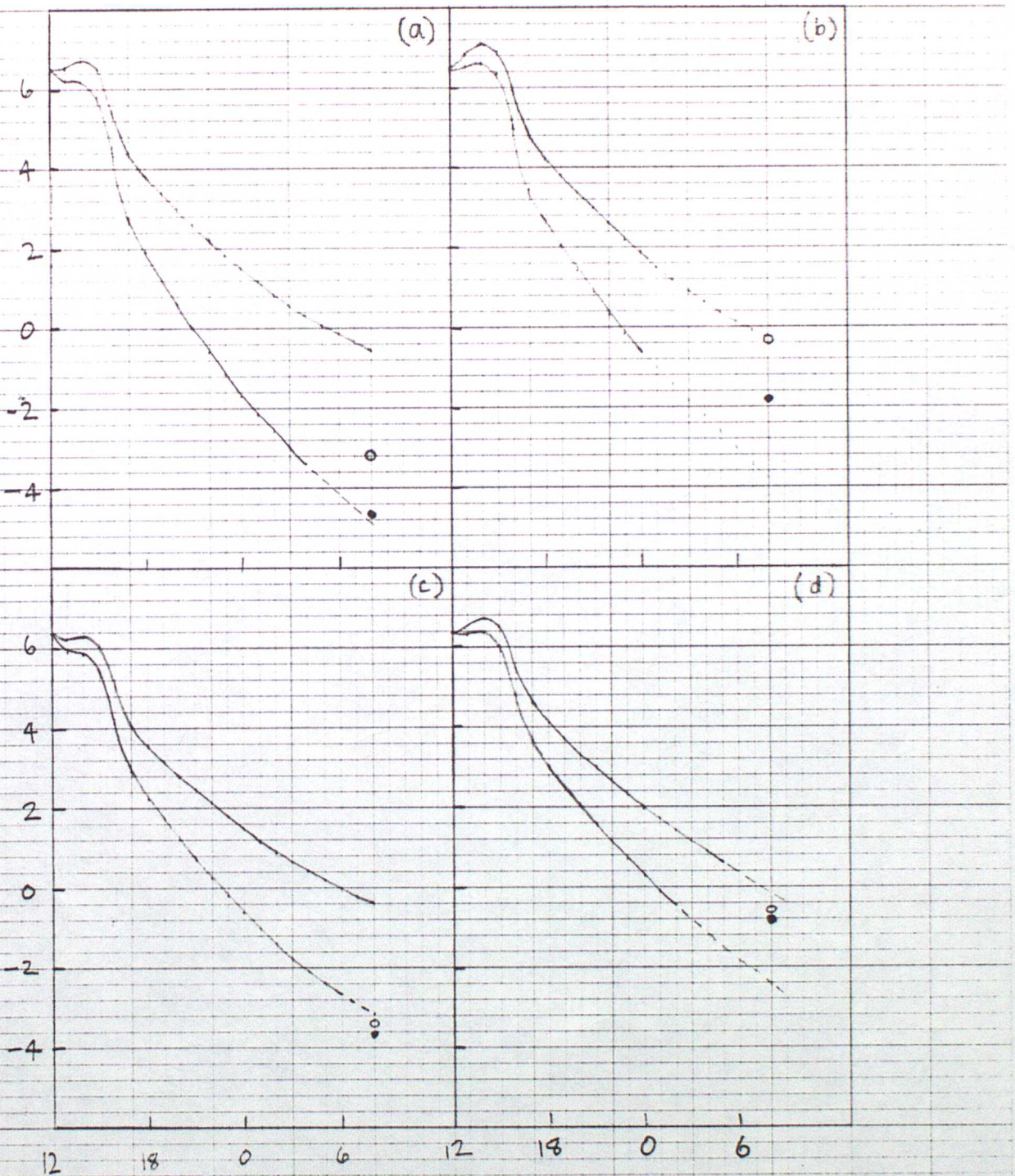

FIG. 6 Nocturnal cooling (a) $U_g = 6\,ms^{-1}$ RH = 40%, (b) $U_g = 6\,ms^{-1}$ RH = 60%, (c) $U_g = 8\,ms^{-1}$ RH = 40% and (d) $U_g = 8\,ms^{-1}$ RH = 60%. The upper curves are for the previous model version, the lower curves for the revised model, the dashed lines are where the temperatures are extrapolated. • and ○ represent predicted minimum temperatures by Craddock and Pritchard and M'Kenzie respectively.

ANNEX 4

Calculation of the Surface Temperature as a Function of Time in the Radiation Fog Model

Introduction

Recent experiments using the version of the macrophysical fog model with specified exchange coefficients constant in time have revealed an error in the routine to calculate the surface temperature. The original algorithm for surface temperature was copied from Zdunkowski and Nielsen (1971). This was tested with zero values of exchange coefficient in air and gave results in reasonable agreement with the classical solution due to Brunt. However, in the latest series of experiments with specified K profiles, the method has been found to be unrealiable when K varied significantly with height. In fact if $K_{s+1} > 3 K_s$ (where s represents the surface grid point and $s+1$ the first grid point above the surface) then a downward directed heat flux enhances surface cooling. Such positive feedback eventually causes the model to blow up. If the K values are so low that the sensible heat flux only makes a small contribution to the surface energy balance then the error remains small even if K varies with height. This was the case for the original model runs reported in the 1976 Quarterly Journal. There would also have been a serious error if the soil exchange coefficient had varied with depth since the soil heat flux was a dominant factor. Luckily K_{soil} has always been taken as constant.

The original method has been replaced with a more straightforward approach as described for example by Deardorff (1978). The theory and tests of this method are described below. A theoretical treatment of the error in the Zdunkowski and Neilsen method is given in Appendix 1.

Theory

The course of the soil temperature T with time at any depth is given by

$$\frac{\partial T}{\partial t} = \frac{\partial}{\partial z}\left(K \frac{\partial T}{\partial z}\right) \qquad (1)$$

with boundary conditions

$$\left.\begin{aligned} F_N + F_H + F_L + F_G &= 0 \qquad z = 0 \\ T &= \text{constant}, \; T_d \text{ say} \qquad z = z_d \end{aligned}\right\} \qquad (2)$$

where z_d is a depth which is not reached by the diurnal temperature cycle over the course of the integration. F_N, F_H, F_L, F_G are the net radiation, sensible heat flux, latent heat flux and soil heat flux.

In order to calculate the surface temperature T_s it is necessary to solve (1) as z approaches zero which is impossible numerically. However analytic solutions to equations (1) and (2) are possible in certain idealised cases and these are described later. Deardorff's method essentially involves using a high resolution grid close to the surface in order to obtain a close numerical approximation to the temperature gradient and soil heat flux there. At present K is assumed to be constant in depth as in all previous integrations. Deardorff's method then reduces to the following steps

(i) Calculate the surface soil heat flux as the residue of the other surface fluxes ie $F_G = -(F_N + F_H + F_L)$

(ii) Approximate the surface temperature gradient by the value over the first grid interval and set the surface temperature to give the value of F_G from (i) ie

$$F_G = \rho C K \left(\frac{\partial T}{\partial z}\right)_{z=0}$$

$$\simeq \rho C K \frac{T_s - T_{s-1}}{\Delta z_s}$$

$$\therefore \quad T_s = T_{s-1} + \frac{\Delta z_s F_G}{\rho C K} \qquad (3)$$

where ρ, C are the density and thermal capacity of the soil and $\Delta z_s = z_s - z_{s-1}$

(iii) Solve equation (i) numerically with T_s and T_d as boundary conditions.

(iv) Re-evaluate the surface fluxes and repeat steps (i)-(iii).

The main constraint on this method is the jump in T_s at the first time predicted by equation (3) if the soil is initially isothermal. This obviously depends upon the soil properties and the choice of Δz_s

Choice of Grid

The soil grid used in later versions of the model was defined by

$$z = A e^{\beta I} \qquad (4)$$

where I is the grid point number and A and β were chosen to give $\Delta z_s = 0.03$m. This is too large for our use of Deardorff's method since $\Delta T_s = 3^\circ$C at the surface initially with our usual soil constants and $F_N \simeq 70 \, W m^{-2}$ Thus a new grid has been defined by

$$z = A e^{\beta I} - \delta \qquad (5)$$

where $A = 5.39273 \times 10^{-3}$m, $\beta = 0.39439$, $\delta = 0.008$m. Then $\Delta z_s = 0.0039$m and $\Delta T_s = 0.3^\circ$C initially. The number of grid points to 2m has been increased from seven to fifteen. The numerical algorithm for equation (1) is identical to that used previously except that $(z+\delta)$ replaces z ie

$$T_I^{t+\tau} = T_I^t + \frac{K\tau}{\beta(z+\delta)^2}\left[\frac{1}{\beta}\left(T_{I+1}^t + T_{I-1}^t - 2T_I^t\right) - \frac{\left(T_{I+1}^t - T_{I-1}^t\right)}{2}\right] \qquad (6)$$

The numerical stability of this scheme is limited to time steps $\tau < \frac{(\Delta z)^2}{K}$ With the current K value of $3.7 \times 10^{-7} m^2 s^{-1}$, $\tau < 40$ s for stability. At present $\tau = 10$ s and so there is some margin to increase τ or increase K_s.

Analytic Solutions

Analytic solutions for equations (1) and (2) are necessary to check the numerical scheme. They are only available with simple boundary conditions.

(i) F_G = Constant

This is Brunt's well known solution which approximates to conditions on a clear night with low windspeed when $F_G \simeq -F_N$. With an isothermal temperature profile initially

$$T(z,t) = T(z,0) - \frac{F_G}{\rho C K}\left[2\left(\frac{Kt}{\pi}\right)^{\frac{1}{2}} e^{-\frac{z^2}{4Kt}} - \frac{2}{\pi^{\frac{1}{2}}} z \int_{\frac{z}{2\sqrt{Kt}}}^{\infty} e^{-u^2}\,du\right] \quad (7)$$

$$T(0,t) = T(0,0) - \frac{2}{\sqrt{\pi}} \frac{F_G}{\rho C \sqrt{K}} \sqrt{t} \quad (8)$$

(ii) $F_G = A \sin\left(\omega t + \frac{\pi}{4}\right)$

This can be used to simulate the diurnal cycle.

$$T(z,t) = \bar{T} + \frac{A}{(\omega \rho C k)^{\frac{1}{2}}} \cdot \exp -z\left(\frac{\omega}{2K}\right)^{\frac{1}{2}} \cdot \sin\left(\omega t - \left(\frac{\omega}{2K}\right)^{\frac{1}{2}} z\right) \quad (9)$$

$$T(0,t) = \bar{T} + \frac{A}{(\omega \rho C k)^{\frac{1}{2}}} \sin \omega t \quad (10)$$

Hence A is identified with the amplitude of the surface temperature wave

$$\Delta T_0 = \frac{A}{(\omega \rho C k)^{\frac{1}{2}}} \quad (11)$$

Results

A test program has been written to compare the numerical method with the exact solutions noted above. Figures (1) to (3) show the difference between the numerical and exact solutions as a function of time. Figure (1) is for constant F_G . The initial 0.3°C error is due to the surface temperature drop required at the first time step to produce the specified soil heat flux of 70 wm^{-2} . The error falls rapidly to -0.15°C at fifteen minutes and then increases slowly to -0.27°C at 7 hours. Since the surface temperature has fallen about 8.4°C at this time this represents an error of 3.2% in the temperature drop. In fact the percentage error expressed in terms of the temperature drop decreases monotonically with time from 5% at 1 hour to 3.2% at 6 hours and is then constant to 7 hours. The 3 cm percentage error decreases from 5.9% at 1 hour to 3.7% at 6 hours and then increases slightly to 3.8% at 7 hours.

Figure (2) shows the results for a heat flux varying sinusoidally with a period of 24 hours. The peak error is again around 0.27°C, at 4 to 5 hours. Note that since the analytic solution for $t = 0$ was used as a starting condition there is

zero error at this time. The percentage error expressed as

$$\frac{(T_{\text{numerical}} - T_{\text{exact}})}{T_{\text{mean}} - T_{\text{exact}}} \times 100$$

is 7.9% at the surface after 1 hour and decreases to 0 by 11 hours. It then changes sign and starts to increase again. This integration has not completed a cycle but the results shown in Figure 3 suggest the error will rise again to around 8%. The percentage errors at 3 cm are generally larger especially initially. They decrease from 28% at 1 hour to 1.7% at 12 hours. However when the percentage error is large the actual departure from the mean is small (eg only 0.2°C at 1 hour) so the physical consequences will be negligible.

Similar results are obtained using a 1 hour period, Figure 3. This probably exceeds the highest frequency with which the soil heat flux will change in the case of a rapidly deepening fog. The absolute error in the surface temperature peaks at 0.2°C and is in phase with the peak of the soil heat flux. This represents a percentage error of about 17% which is the maximum error. The absolute and percentage error decrease to zero in phase with the soil heat flux. At 0.03 m the percentage error peaks at 67% but since this represents only 0.02°C it is unlikely to degrade the accuracy of the fog model.

Inclusion in the Fog Model

The new method has been included in the macrophysical fog model. At the same time a correction for the non-linearity of the grid has been included in the calculation of the fluxes of sensible and latent heat. This increased the surface values by about 30%. The net effect is that the latent heat flux, which contributes to the surface energy balance once the surface is saturated, slows down the cooling more noticeably than in the original method and fog fails to form. In fact when the latent flux is first introduced, because it suddenly appears at one time-step, the surface temperature rises, the surface desaturates and the latent heat flux at the surface is set to zero again. The temperature then falls, the surface saturates, F_L is reintroduced, etc. This leads to an oscillation with a period of two time-steps which persists with decreasing amplitude for at least several hours. It is not clear yet whether this is responsible in any way for the failure of fog to form.

Appendix I Analysis of the Error in the Zdunkowski and Neilsen Method

Zdunkowski and Neilsen have produced an algorithm to predict the surface temperature as a function of time. This is based on equation (2) plus equation (1) and its analogue in air applied to thin layers either side of the soil-air interface. They attempt to solve the latter equations at the surface by using Taylor's expansion to derive the surface gradients from values at the first grid point ie equation (1) becomes

$$\frac{T_s - T_{s-1}}{\tau} = \left[\frac{K_s - K_{s-1}}{\Delta z_s}\right]\left|\frac{\partial T}{\partial z}\right|_- + K_s\left|\frac{\partial^2 T}{\partial z^2}\right|_- \qquad (1A)$$

where $-$ represents a value at the surface on the soil side. Also

$$T_{s-1} = T_s - \Delta z_s\left|\frac{\partial T_s}{\partial z}\right|_- + \frac{(\Delta z_s)^2}{2}\left|\frac{\partial^2 T_s}{\partial z^2}\right|_- \qquad (2A)$$

Using equations (1A), (2A) plus the analogous equations for air and equation (2) written in the form:-

$$-F_N + C_p \rho_a K_s'\left|\frac{\partial T}{\partial z}\right|_+ - C\rho K_s\left|\frac{\partial T}{\partial z}\right|_- \qquad (3A)$$

they eliminate $\left|\frac{\partial T}{\partial z}\right|_\pm$ $\left|\frac{\partial^2 T}{\partial z^2}\right|_\pm$ and hence produce an expression for $\frac{T_s - T_{s-1}}{\tau}$ which depends only on the values at the grid points either side of the surface and at the surface.

Unfortunately their algorithm produces unrealistic results if K varies significantly with height, as noted in the introduction. This is because the surface gradients are often indeterminate from grid-point values remote from the surface. The added information provided by Taylor's expansion only produces reasonable results so long as the higher derivative terms can be ignored. This can be illustrated by considering a simple steady state problem for which an analytic solution exists.

If $\left.\begin{aligned} T = T_0 &, \quad z = 0 \\ T = T_H &, \quad z = z_H \end{aligned}\right\}$ constant in time

and $K = A(z+h)$

then the equilibrium solution for $T(z)$ is

$$T(z) = T_0 + B \ln\left(\frac{z+h}{h}\right) \qquad (4A)$$

where $B = (T_H - T_0)\ln^{-1}\left(\frac{z_H + h}{h}\right)$

Note that low h values are associated with a large gradient of K in the vertical. If $h \gg z$, K is nearly constant. From (4A) the derivatives

for use in the Taylor expansion are:-

$$\frac{\partial T}{\partial z} = \frac{B}{z+h} \qquad \left(\frac{\partial T}{\partial z}\right)_{z=0} = \frac{B}{h}$$

$$\frac{\partial^2 T}{\partial z^2} = \frac{-B}{(z+h)^2} \qquad \left(\frac{\partial^2 T}{\partial z^2}\right)_{z\to 0} = -\frac{B}{h^2}$$

$$\frac{\partial^3 T}{\partial z^3} = \frac{+2B}{(z+h)^3} \qquad \left(\frac{\partial^3 T}{\partial z^3}\right)_{z\to 0} = \frac{2B}{h^3}$$

If $Z = 0.03$ m the terms in the Taylor expansion become

		$\Delta z\left(\frac{\partial T}{\partial z}\right)_{z=0}$		$\frac{(\Delta z)^2}{2}\left(\frac{\partial^2 T}{\partial z^2}\right)_{z=0}$		$\frac{(\Delta z)^3}{6}\left(\frac{\partial^3 T}{\partial z^3}\right)_{z=0}$
$h = 1$	$T_{s+1} = T_s +$	$0.03B$	$-$	$4.5\times10^{-4}B$	$+$	$9\times10^{-6}B$
$h = 0.1$	$T_{s+1} = T_s +$	$0.3B$	$-$	$0.045B$	$+$	$0.009B$
$h = 0.01$	$T_{s+1} = T_s +$	$3B$	$-$	$4.5B$	$+$	$9B$

If $K = 3K_s$ then $3Ah = A(0.03 + h)$ and $h = 0.015$. Thus the alogorithm breaks down when the slope of the K profile implies an h value such that $\frac{(\Delta z)^3}{6}\left(\frac{\partial^3 T}{\partial z^3}\right)_{z=0}$ becomes comparable with the other terms.

Appendix 2

Soil Constants

k	Thermal conductivity	$WM^{-1}\ {}^{o}K^{-1}$
C	Thermal capacity	$J\ Kg^{-1}\ {}^{o}K^{-1}$
ρ	Density	$Kg\ m^{-3}$
K	Exchange coefficient	$m^2 s^{-1}$

	k	ρC ($J\ m^{-3}\ {}^{o}K^{-1}$)	K
Sandy clay, 15% water (model values)	0.91	2.46×10^{6}	3.7×10^{-7}
O'Neil Expt Site	0.62	2.81×10^{6}	4×10^{-7}
Clay	2.81	2.34×10^{6}	1.2×10^{-6}
Sand	0.25	1.26×10^{6}	2×10^{-7}
Still Water	0.63	4.16×10^{6}	1.5×10^{-7}

Values above are taken from Deardorff (1978), except the model value which is taken from the Smithsonian Tables.

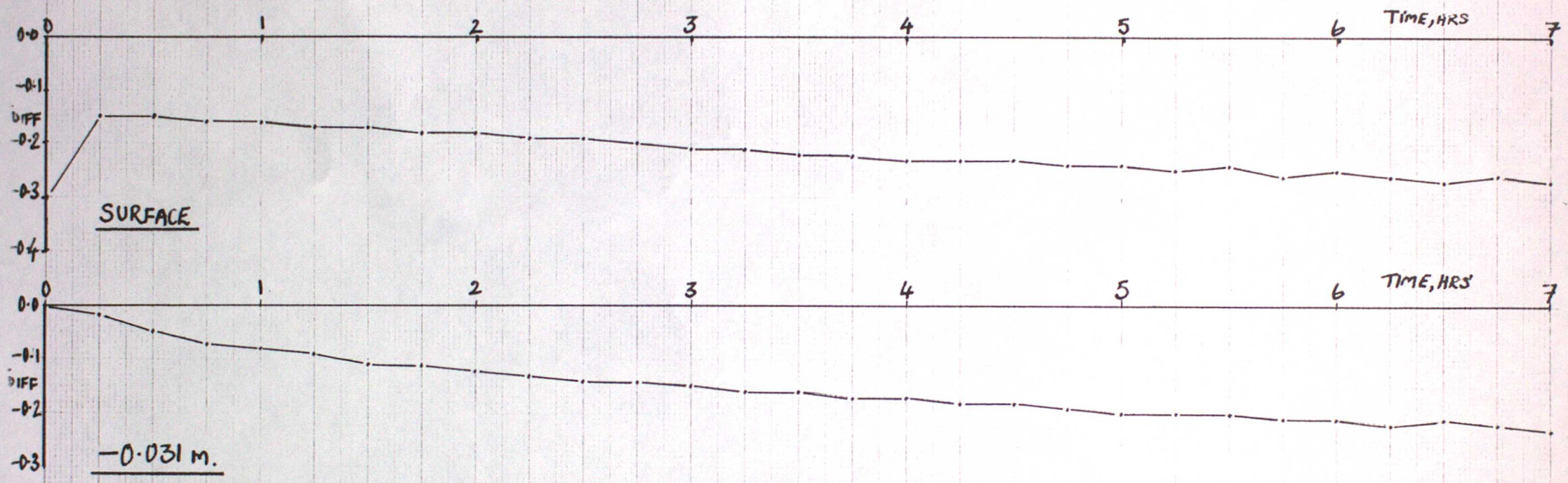

FIGURE 1

Comparsion of Deardorff soil routine and BRUNT ANALYTICAL FORMULA.

T_{DIFF} = Temp. predicted by Deardorff routine — temp. from Brunt formula.

FIGURE 2; DEARDORFF vs. SELLERS ANALYTICAL METHOD.

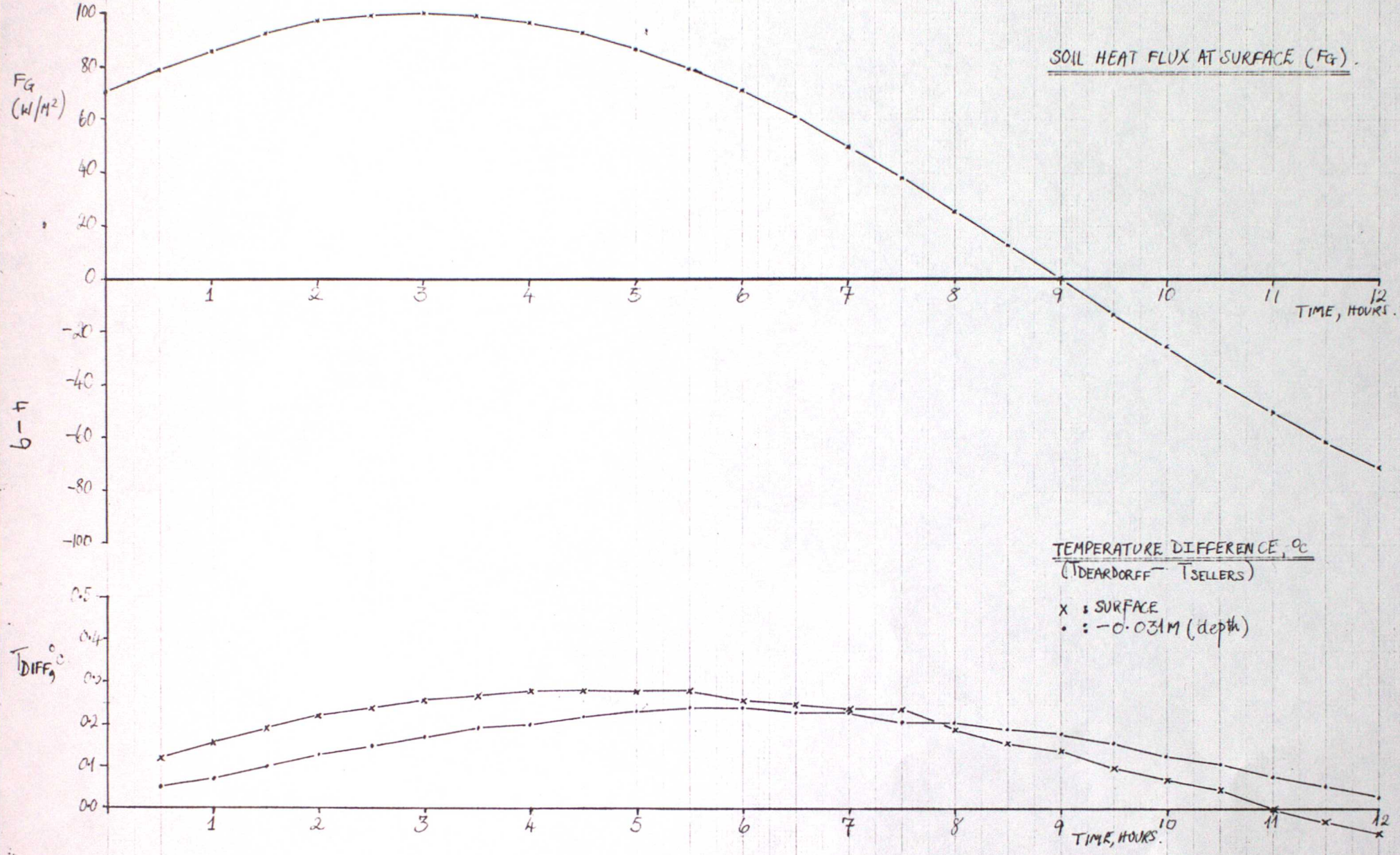

TIME PERIOD = 1 DAY; $F_G = 100 \cdot \sin\left(\frac{2\pi t}{\tau} + \frac{\pi}{4}\right)$

Comparison of Deardorff soil temperature routine and Sellers analytical formula.

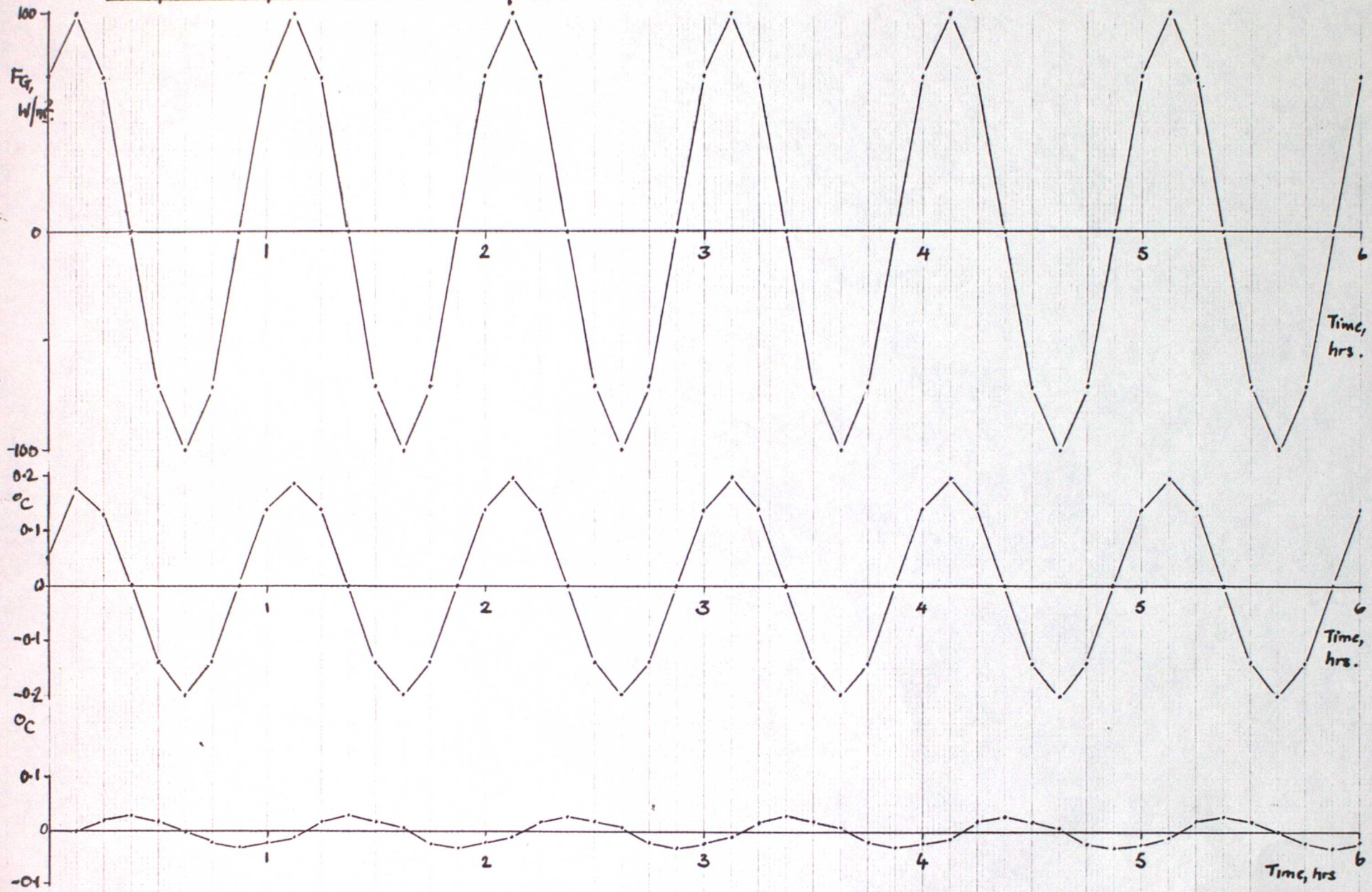

FIGURE 3

(Temp diff = Temp. predicted by Deardorff routine — Temp from Sellers analytic formula)

ANNEX 5

MODIFICATION OF SOIL NUMERICAL SCHEME

The soil temperature numerical scheme has been changed to allow the soil profiles to be varied with depth. By changing the soil exchange coefficient near the surface it was thought that this may promote surface cooling and enhance the screen-soil temperature gradient.

Theory

The basic equation for heat transfer in a soil is

$$\frac{\partial G}{\partial z} = -\frac{\partial}{\partial z}\left(k\,\frac{\partial T}{\partial z}\right) = -\rho c\,\frac{\partial T}{\partial t} \qquad (1)$$

$$\therefore \quad \frac{\partial T}{\partial t} = \frac{1}{\rho c}\,\frac{\partial}{\partial z}\left(k\,\frac{\partial T}{\partial z}\right) \qquad (2)$$

Where k is the soil thermal conductivity ($Wm^{-1}K^{-1}$), ρc is the soil volumetric thermal capacity ($Jm^{-3}\,K^{-1}$) and $\mathcal{K} = \rho c k$ is the soil exchange coefficient ($m^2 s^{-1}$). In the case of a homogeneous soil (2) reduces to

$$\frac{\partial T}{\partial t} = \mathcal{K}\,\frac{\partial^2 T}{\partial z^2} \qquad (3)$$

which is the equation solved by the original soil temperature scheme.

Implicit soil temperature numerical scheme

In the new implicit scheme equation (1) is solved by equating the rate of change of soil temperature to the difference of two fluxes i.e.

$$\frac{\partial T}{\partial t} = \frac{1}{\rho c}\,\frac{\Delta\left(k\,\partial T/\partial z\right)}{\Delta z} \qquad (4)$$

which in finite difference form becomes

$$\frac{T_L^{t+1} - T_L^{t}}{\Delta t} = \frac{1}{(\rho c)_L}\left\{ k_{L+1/2}\,\frac{\left(T_{L+1}^{t+1} - T_L^{t+1}\right)}{\left(z_{L+1} - z_L\right)} - k_{L-1/2}\,\frac{\left(T_L^{t+1} - T_{L-1}^{t+1}\right)}{\left(z_L - z_{L-1}\right)} \right\} \Big/ \left(z_{L+1/2} - z_{L-1/2}\right) \qquad (5)$$

where $L+\frac{1}{2}$ indicates that a staggered grid is used. Equation (5) is then transformed to

$$B\,T_{L+1}^{t+1} + A\,T_{L}^{t+1} + C\,T_{L-1}^{t+1} = -\,T_{L}^{t} - D \qquad (6)$$

and solved implicitly.

The implicit scheme requires a soil grid which is less non-linear than that used previously. The grid has been replaced by a grid which is a reflection of the grid in the air but scaled by a tenth such that the first grid level in the soil is at 3 mm depth. 20 grid levels are used which extend to a depth of 1.85 m.

The implicit scheme requires the specification of the soil properties (k and ρc) at each grid level. The conductivity (k) is then interpolated onto the staggered grid.

Tests of implicit soil temperature numerical scheme

The new soil scheme has been tested against the old scheme and Figure 1 shows results from one such test. This shows that the results are essentially similar using each scheme. Such tests of the new soil scheme for soils with insulating character have shown that a one time-step oscillation of the surface temperature can develop. This oscillation is removed if time smoothing is applied to the surface temperature by

$$T'_{s,t+1} = (1 - K_{TS})\,T_{s,t+1} + K_{TS}\,T_{s,t} \qquad (7)$$

where $K_{TS} = 0.5$. Such smoothing makes no significant difference to the surface temperature in runs where this oscillation was absent, so the smoothing is retained in the scheme.

The new soil scheme has also been checked against the analytic solutions of Brunt and compared to similar tests of the old scheme described in Annex 4. Using the implicit scheme the percentage errors in the

surface temperature and in the 3 cm soil temperature are significantly less than those obtained using the old scheme. These results suggest that the implicit scheme is more accurate than the old scheme for integrations with a homogeneous soil.

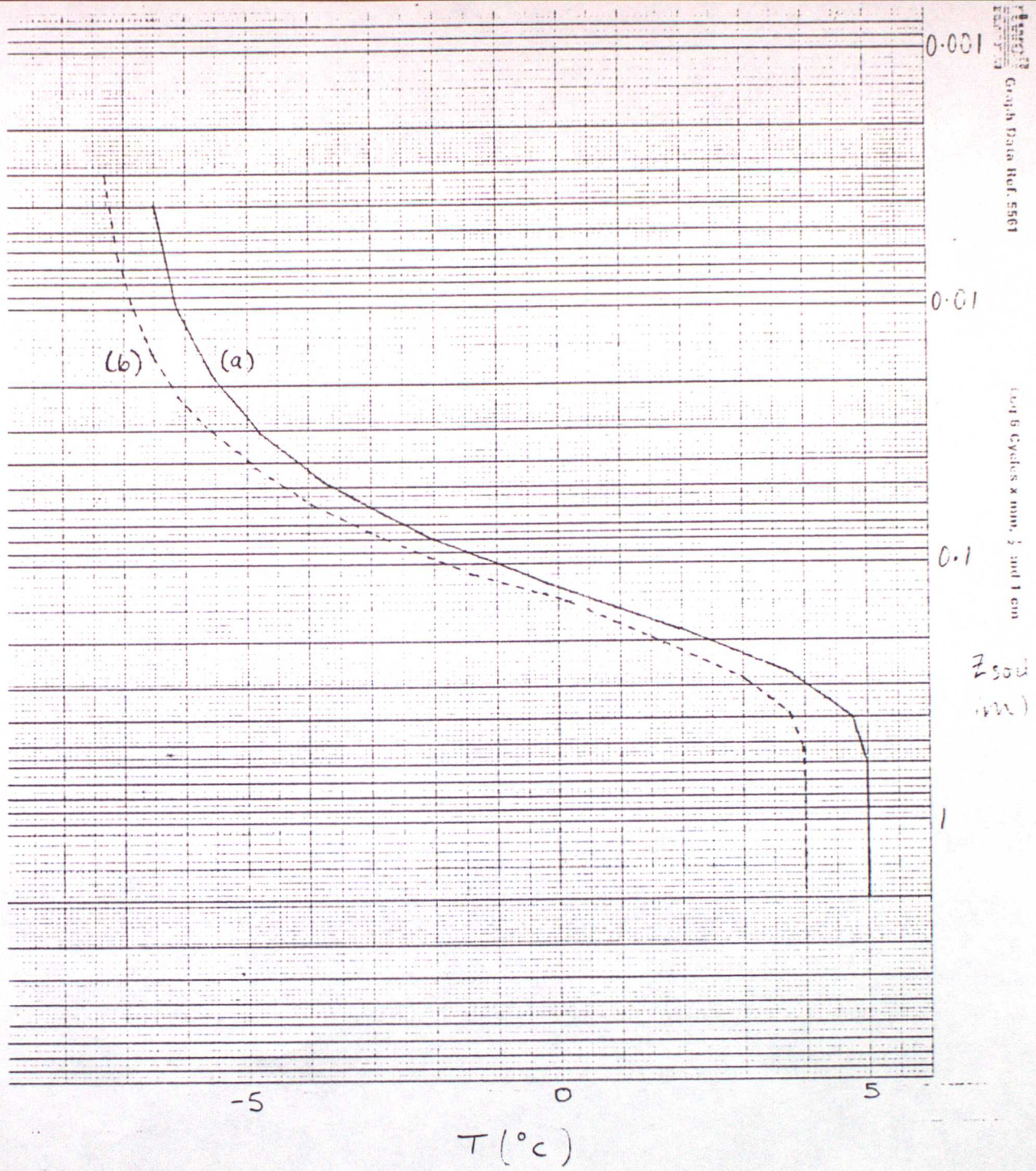

Figure 1. Comparison of soil temps after 14 hours integration (a) original explicit soil diffusion (b) implicit soil diffusion, (b) is shifted 1C to the left of (a) for comparison. Surface temperatures are -6.77 C (a) and -6.51 C (b). Initial temperature profiles at 5 C in soil and air. Soil properties of a sandy-clay soil 15% moisture content.

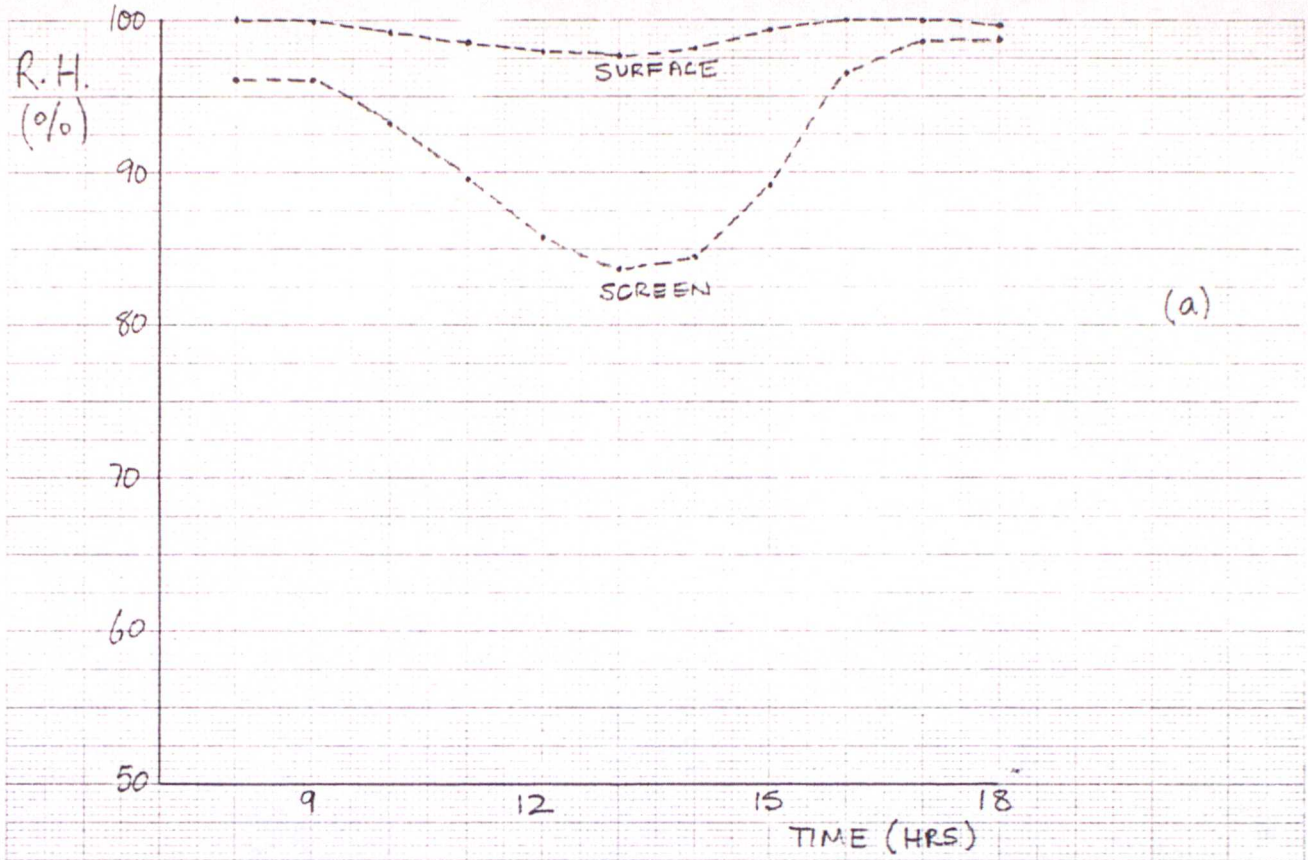

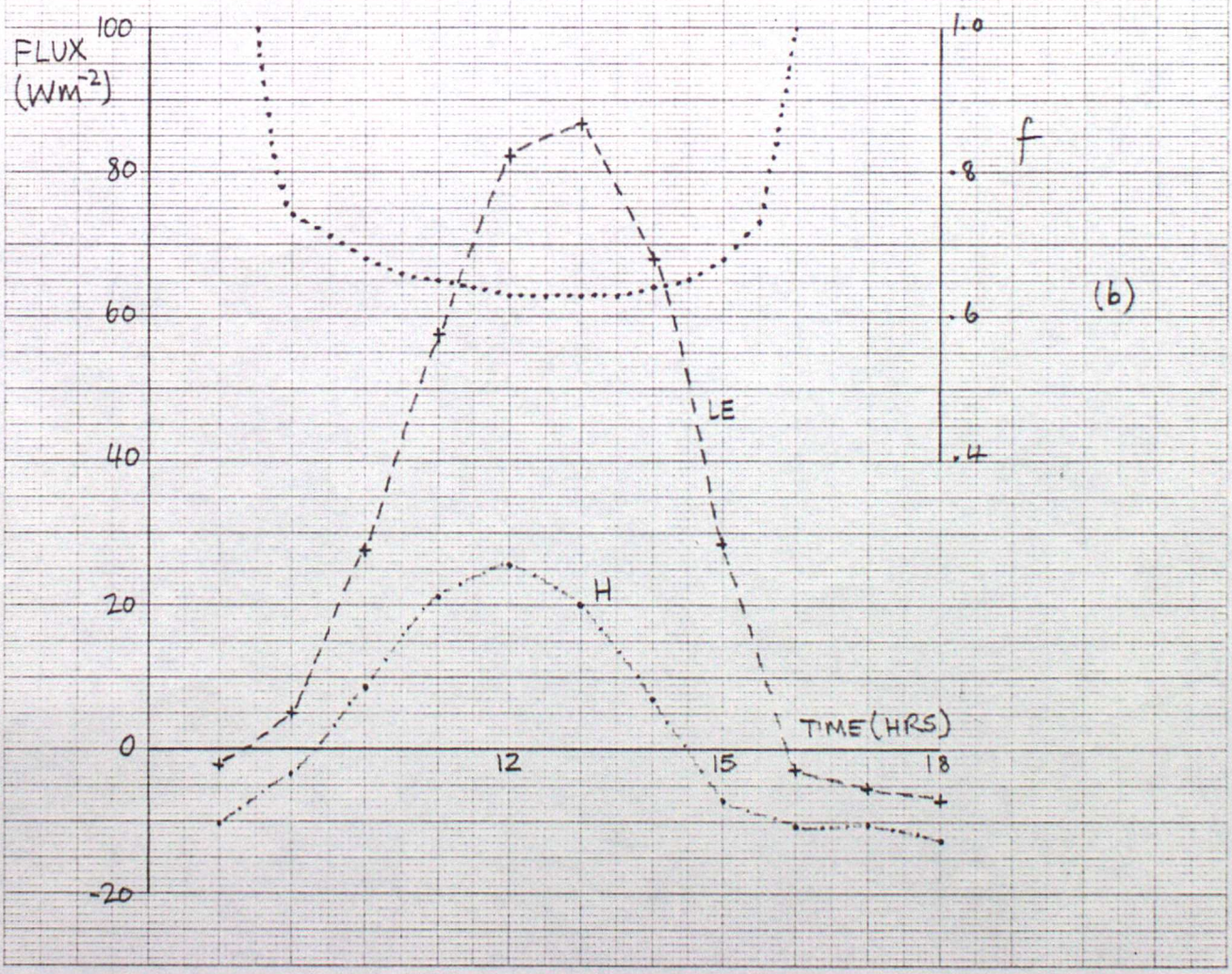

FIG. 1. (a) relative humidity, (b) fluxes for f as shown, calculated from eq. (8), $r_c = 50\ sm^{-1}$.

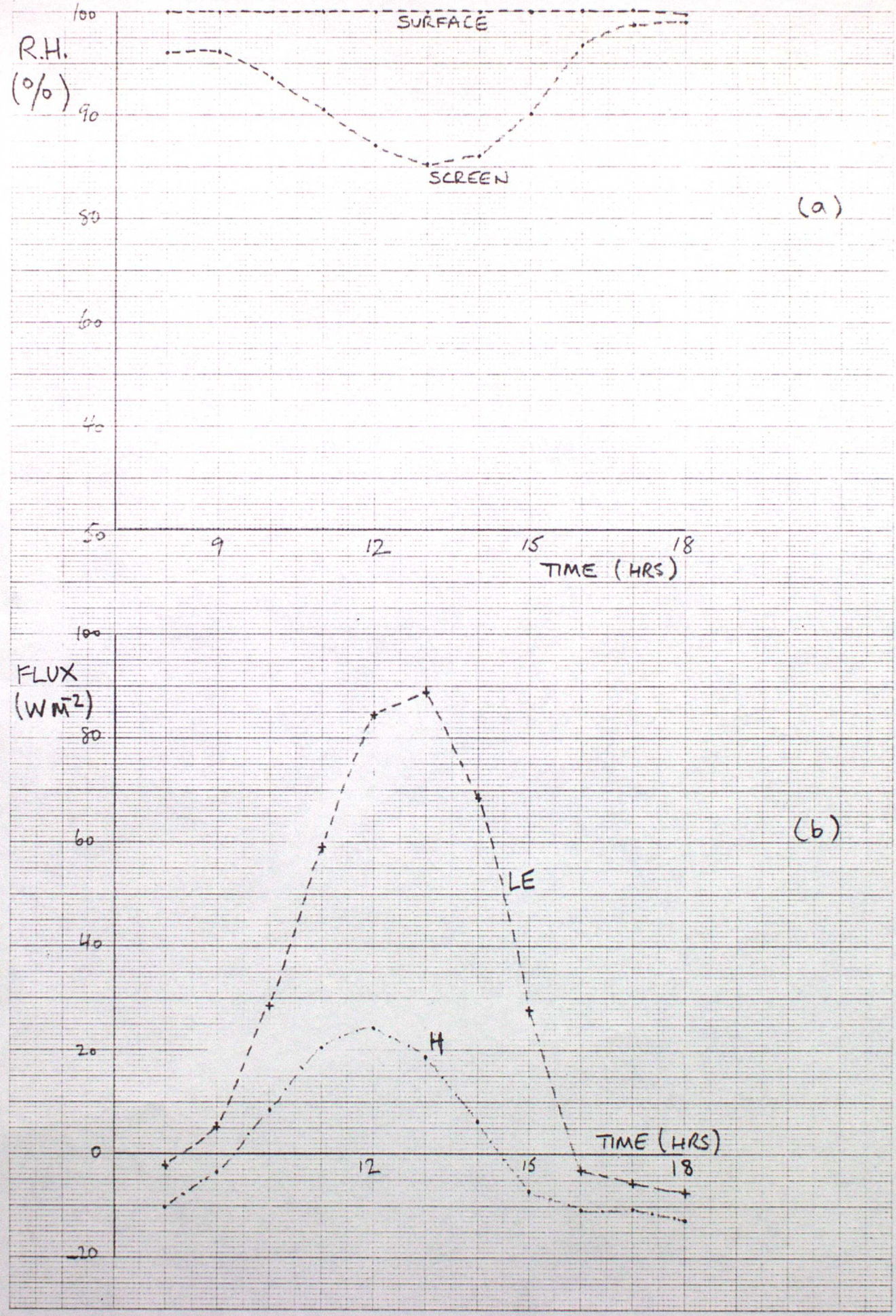

FIG. 2. (a) relative humidity, (b) fluxes for $f = 1$ (potential evaporation).

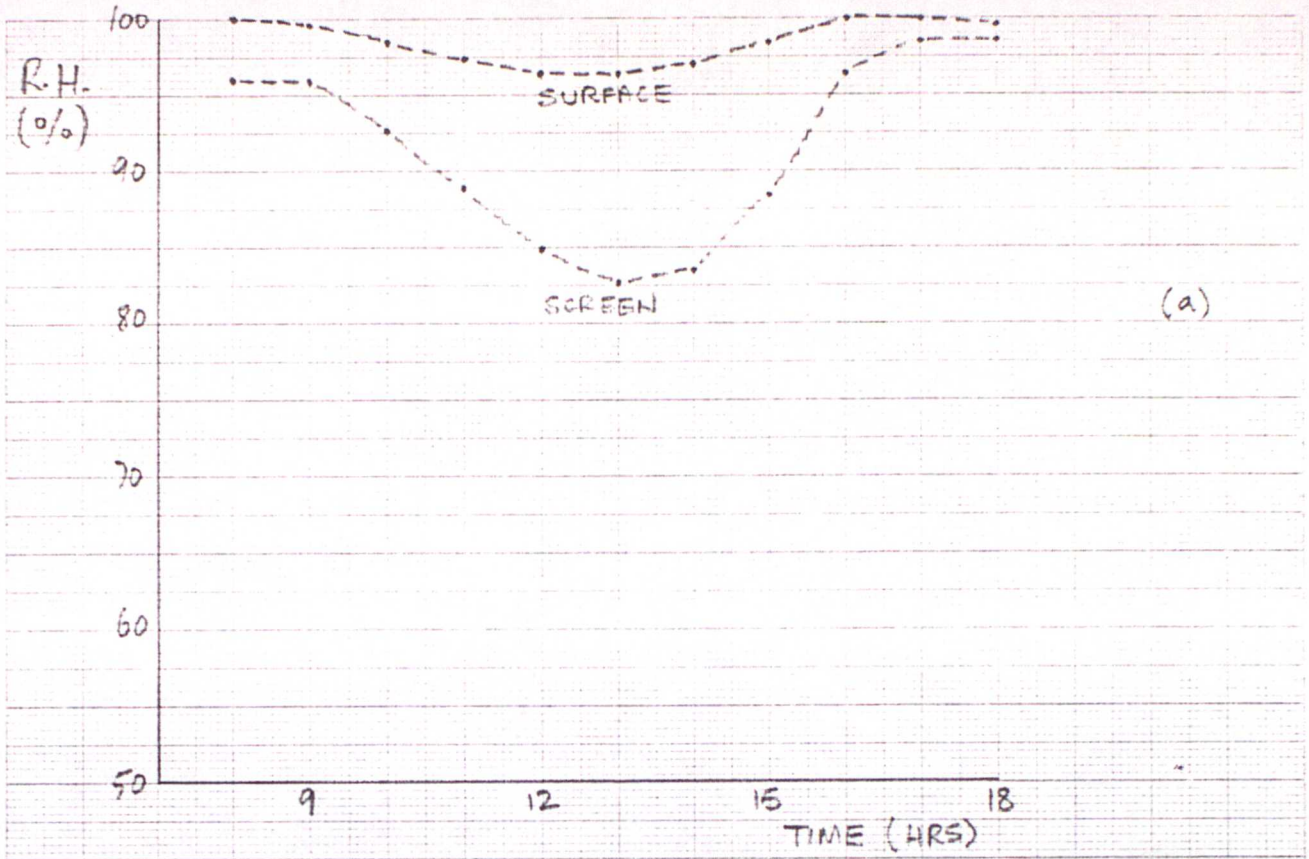

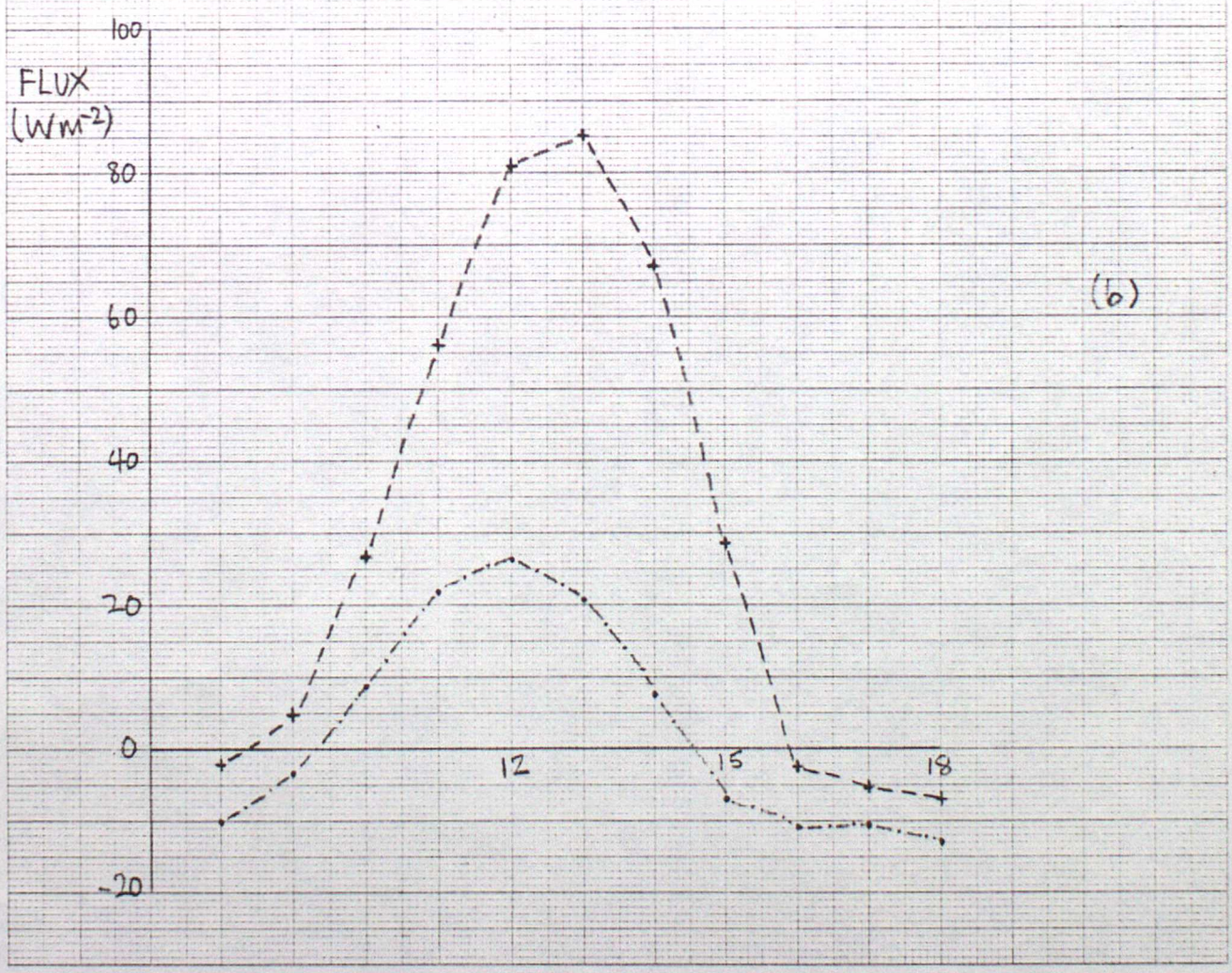

FIG. 3. (a) relative humidity, (b) fluxes for $f = 0.5$, q_2 of eq. (3) equal to 0 at 0.03 m.

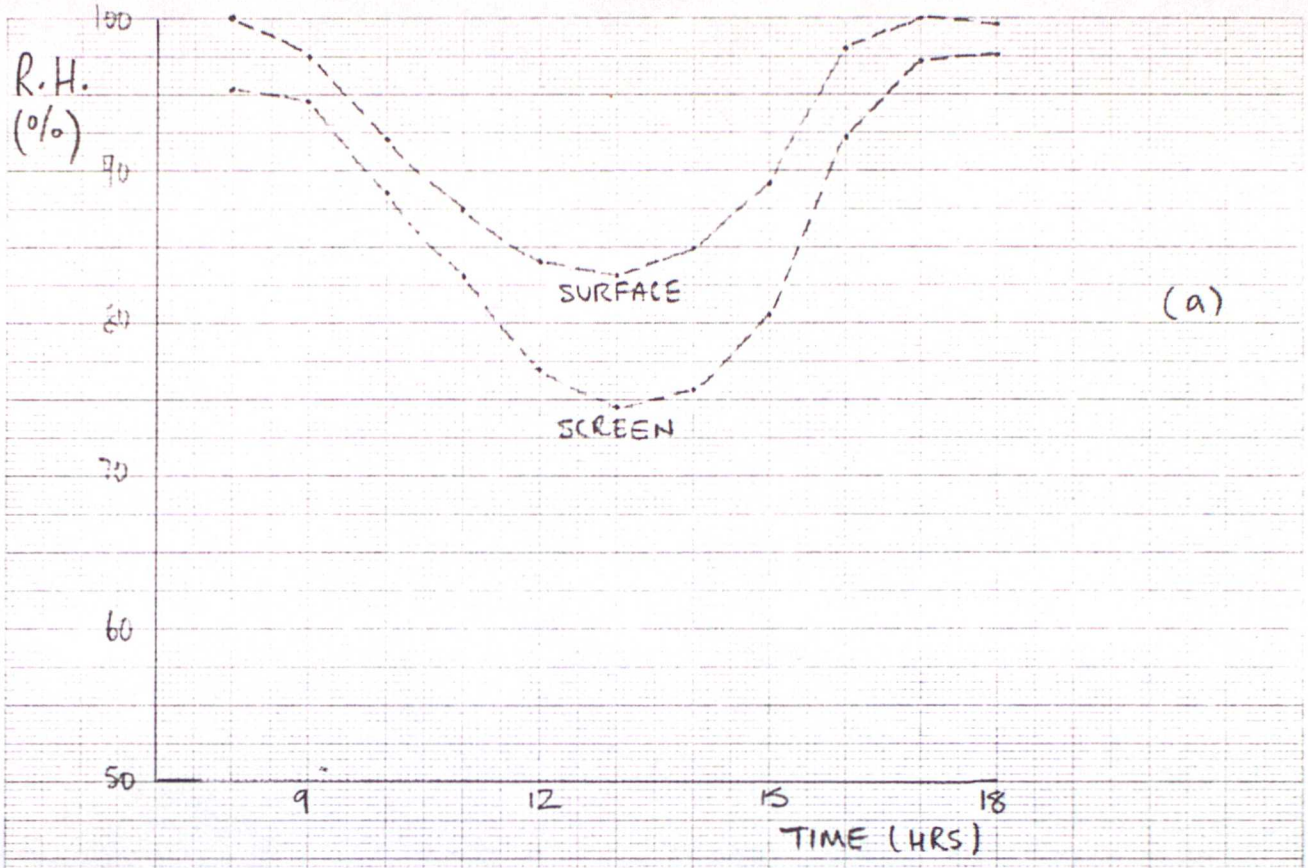

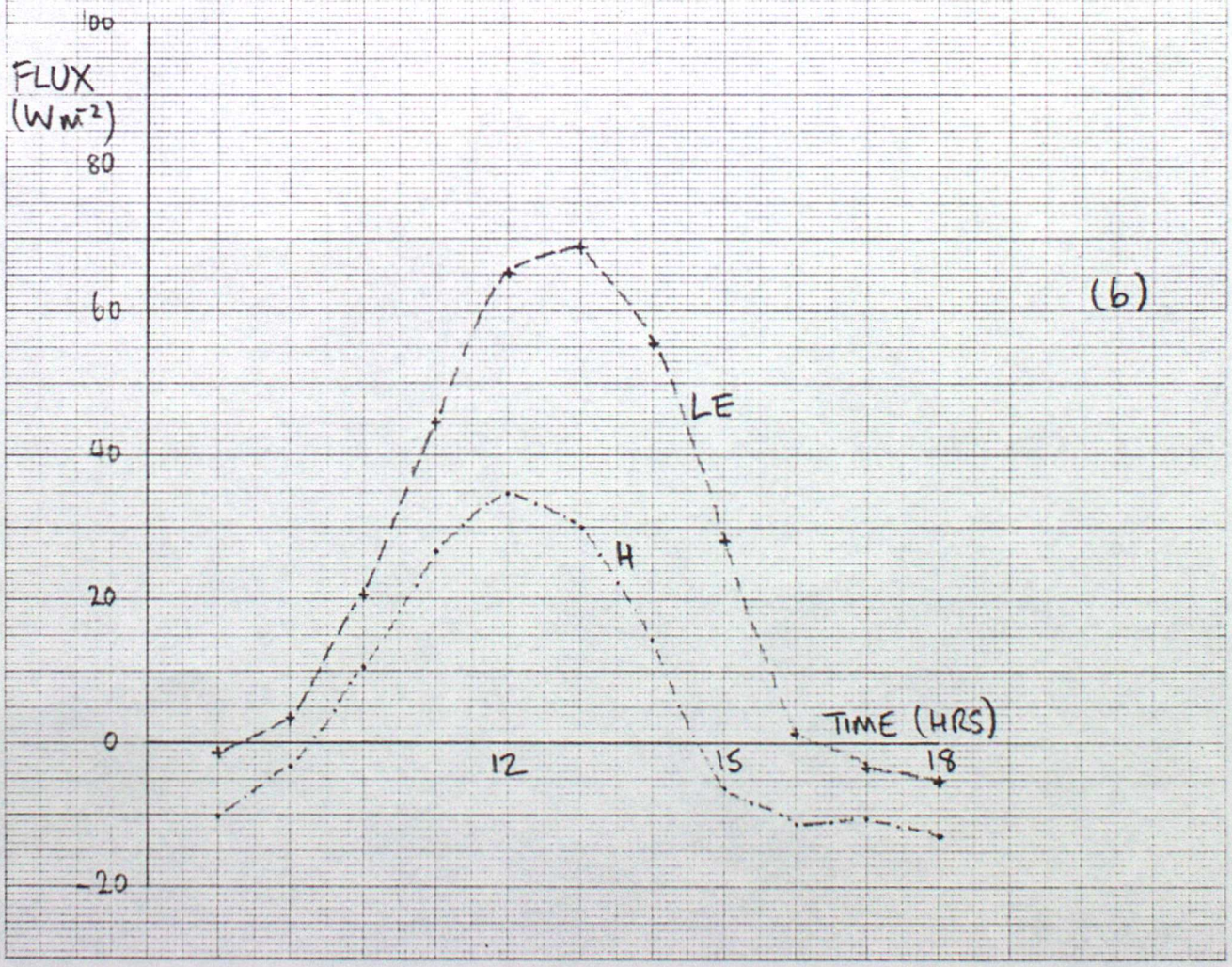

FIG. 4. (a) relative humidity, (b) fluxes for $f = 0.5$, q_2 of eq. (3) equal to q at 9.9 m.

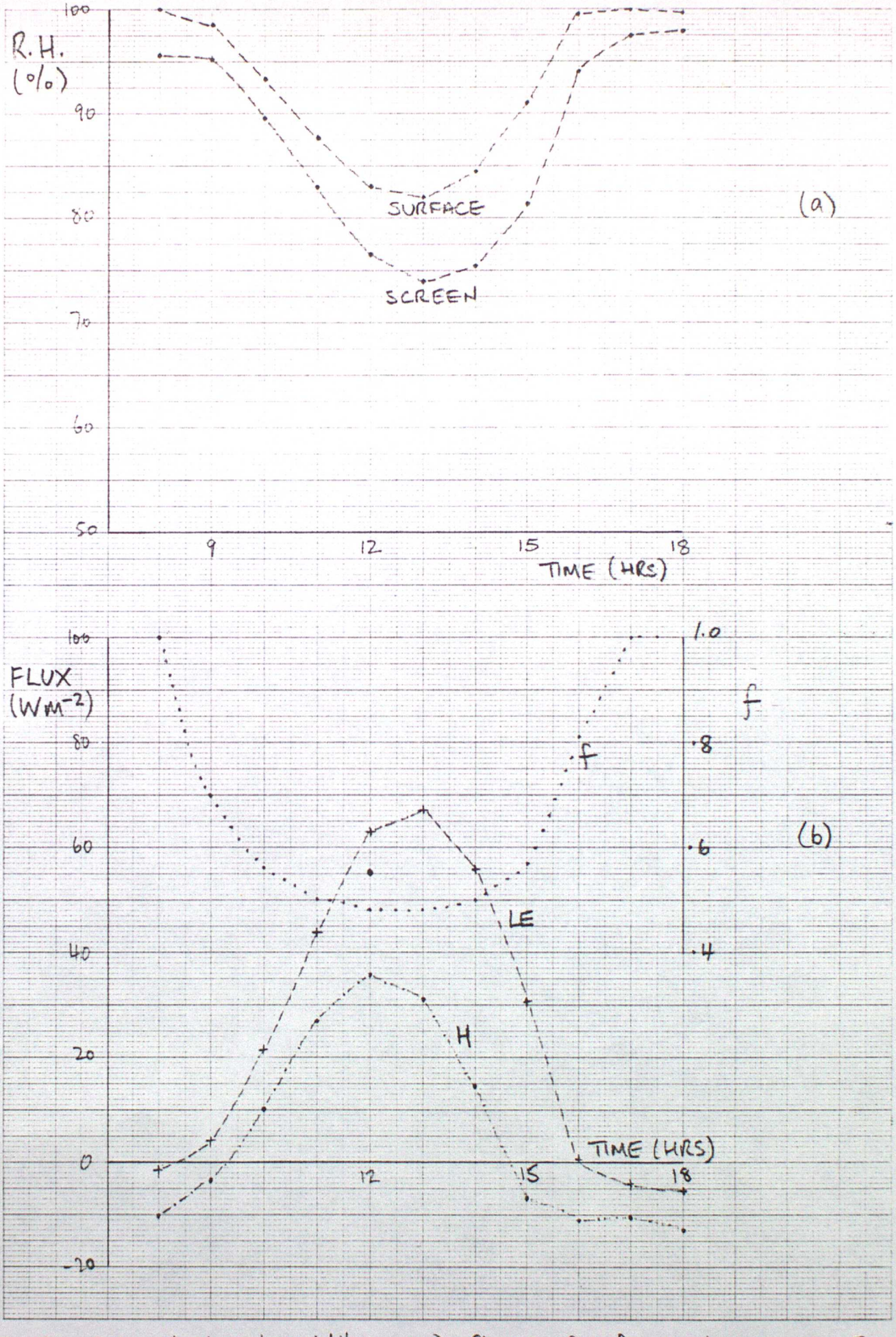

FIG. 5. (a) relative humidity, (b) fluxes for f as shown, $\Gamma_S = 50\ sm^{-1}$.

ANNEX 6

EVAPORATION AND SURFACE MIXING RATIO IN THE FOG MODEL

Comparisons of model integrations and field project case study nights 3-4/11/76 and 17-18/10/77 have identified problems with the model evaporation. The daytime partitioning of model sensible and latent heat fluxes is unrealistic leading to a too high latent heat flux and a too weak sensible heat flux. The consequence of this is the model daytime convective boundary layer becomes too shallow and too moist, producing a tendency in the model towards the formation of radiation fog. It is desirable that integrations should be made starting at midday or earlier to prevent the possibility of fog forming as a result of the initial model fields adjusting into balance and for any possible potential forecasting use. Therefore the model evaporation is a problem that requires study to identify whether or not the scheme is correct.

In the present model version (as at December 1982) evaporation or condensation is driven by the difference between the saturated mixing ratio at the surface $q_s(T_s)$ and the mixing ratio at the first grid point above the surface q_2.

$$LE = f \rho L K_1 (q_s(T_s) - q_2) / z_2 \qquad (1)$$

or

$$LE = \rho L K_1 (q_1 - q_2) / z_2 \qquad (2)$$

For dew deposition $q_s(T_s) < q_2$, f is set to unity. When the surface remains wet then f is unity for evaporation also. The surface mixing ratio is given by:

$$q_1 = f\, q_s(T_s) + (1-f)\, q_2 . \qquad (3)$$

In general circulation models f is often set between 0.6 and 0.8. Deardorff (1978) suggests making f a function of soil moisture content through

$$f = \min (1 , W_2/W_K) \qquad (4)$$

where W_2/W_K is the soil moisture content expressed as a fraction of field capacity. In such models q_{r_2} is at a reference 'anemometer level'. It was previously believed that f was the fraction of potential evaporation, this is now recognised as not being so.

Monteith (1981) writes equation (1) in the form of an analogue of Ohms law.

$$LE = \rho L (q_{r_s}(T_s) - q_{r_2}) / \Gamma_v \qquad (5)$$

where Γ_v is a resistance to evaporation given by

$$\Gamma_v = \int K_q(z)^{-1} \, dz \quad , \qquad (6)$$

Γ_H is a similar resistance to heat transfer given by

$$\Gamma_H = \int K_H(z)^{-1} \, dz \quad , \qquad (7)$$

where Γ_v and Γ_H are calculated to a reference height at which T and q are assumed to be independent of the state of the soil surface. For a wet surface $\Gamma_v = \Gamma_H$. However with a drying soil or vegetation canopy Γ_v may exceed Γ_H by an amount Γ_s, where Γ_s is the surface resistance to vapour transfer (sometimes called the canopy resistance or bulk stomatal resistance). In this case the fraction of potential evaporation may be expressed by (Monteith 1981)

$$F = \frac{(\Delta + \gamma)}{\Delta + \gamma (1 + \Gamma_s/\Gamma_H)} \qquad (8)$$

where $\Delta = \partial q_{r_s}(T)/\partial T$ and $\gamma = c_p / L$. F is then a function of temperature and stability even if Γ_s is constant. The literature on evaporation is generally formulated in terms of Γ_s with typical values for various surfaces. For a well watered arable crop $\Gamma_s \simeq 50 \ sm^{-1}$ (Monteith 1981).

Values of F calculated through equation (8) were used in equation (3) for f and the evaporation calculated from (2). Evaporation calculated by this method was seen to be too high, the reasons for which are discussed later. A series of tests were performed with fog model integrations starting at 0700 (model time) and running through the day. Clear sky solar insolation for a November day was specified. The intital relative humidity profile specified was from 96% at the surface falling to 75% at 10m and constant at 75% above 10m.

Fig 1(a) shows the obtained surface and screen relative humidities and 1(b) shows the sensible and latent heat fluxes and the calculated values of f from equation (8). For comparison a run was made with $f=1$, ie showing potential evaporation. The humidities and fluxes are shown in Figs 2(a) and 2(b). The surface remains saturated and the minimum daytime screen humidity is 85%, compared to 84% in Fig 1(a). The potential evaporation at midday is 85 Wm^{-2} whereas the evaporation calculated previously (Fig 1(b)) is 82 WM^{-2} and the actual fraction of potential evaporation is 0.96 as opposed to the calculated fraction 0.63. This effect is further demonstrated by specifying $f=0.5$ and the resulting humidities and fluxes are shown in Fig 3(a) and 3(b). The actual fraction of potential evaporation at midday is about 0.95 and not 0.5 as specified. The evaporation appears to be fairly insensitive to values of f in the range 0.5 to 1. What happens is that instead of reducing the evaporation by a factor f, the potential evaporation calculated at any time is increased to a value well above that obtained at the same time when $f=1$.

Examination of the method reveals that values of f are calculated to a reference height (1.09m in the model), implying f is representative to that height. The value of f is then used to calculate q_{l1} through equation (3) where q_{l2} is the value at the first grid point above the surface. For consistency q_{l2} ought to be the value at the reference height.

The integration with $f = 0.5$ was repeated with r_H calculated to 9.9 m and with q_{v2} in equation (3) equal to q at 9.9 m. The resulting humidities and fluxes are shown in Figs 4(a) and 4(b). Although the latent heat flux is significantly reduced, the actual fraction of potential evaporation (at midday) is 0.76 still well above the 0.5 specified.

The fundamental problem is that during an integration with $f < 1$ the actual potential evaporation is not known in situ. When the evaporation is less than potential the surface becomes warmer than it otherwise would (if potential evaporation were occurring), consequently $q_{vs}(T_s)$ is higher than it would otherwise be, so $(q_{vs}(T_s) - q)$ is higher. The calculated potential evaporation then becomes larger than the true potential evaporation. Therefore it is not possible to specify a fraction of potential evaporation indicating that the f in equations (1) and (3) is not a fraction of potential evaporation but some other variable.

Returning to the equations in terms of resistances we have after Monteith (1981).

$$LE = \rho L (q_1 - q_n) / r_{Hn} \qquad (9)$$

$$LE = \rho L (q_{vs}(T_s) - q_1) / r_s \qquad (10)$$

where q_n is evaluated at the n th grid level and r_{Hn} is calculated to the n th grid level. Combining (9) and (10) gives

$$LE = \rho L (q_{vs}(T_s) - q_n) / (r_{Hn} + r_s) \qquad (11)$$

where $r_{vn} = r_{Hn} + r_s$. Therefore

$$q_1 = (r_{Hn}\, q_{vs}(T_s) + r_s\, q_n) / (r_{Hn} + r_s) \qquad (12)$$

This is identical to equation (3) with f given by

$$f = r_{Hn} / (r_{Hn} + r_s) \qquad (13)$$

where f is not a fraction of potential evaporation.

Figs 5(a) and 5(b) show the humidities and fluxes obtained following this method. The reference height (z_n) specified was 9.9 m. The results appear similar to those in Figs 4(a) and 4(c) by virtue of values of f calculated around midday being close to 0.5. The values of f calculated by equation (13) are shown in Fig 5(b). Virtually identical results were obtained when $z_n = 0.03$ m (at the first grid point above the surface) as corresponding values for f calculated were much lower. This formulation ($z_n = 0.03 = z_2$) is to be adopted as it allows the lowest grid levels to be changed without recourse to alter the model.

To summarise, the method to be adopted is given by

$$f = (z_2/K_1)/(z_2/K_1 + r_s) \qquad (14)$$

$$q_1 = f\, q_s(T_s) + (1-f)\, q_2 \qquad (15)$$

$$LE = \rho L K_1 (q_1 - q_2)/z_2 \qquad (16)$$

where f is now a function of stability when r_s is constant. Again for dew deposition i.e. $q_s(T_s) < q_2$, f is set to unity so $q_1 = q_s(T_s)$. The method retains the advantage that evaporation is characterised by r_s.

A similar method to this is utilised in the Met. Office meso-scale model (Carpenter 1977) where equations analagous to (9) and (10) in terms of drag coefficients are used. He found that in the mesoscale model the partitioning of energy between sensible and latent heat was most sensitive to the surface resistance. To examine this the adopted model scheme was run with $r_s = 100\ s\,m^{-1}$. The resulting humidities and fluxes are shown in Figs 6(a) and 6(b). The latent heat flux is reduced and the sensible heat flux is increased, a similar result to that of Carpenter (1977).

It is now possible to have daytime evaporation which is significantly less than potential evaporation with a correspondingly stronger sensible heat flux allowing deeper growth of the daytime convective boundary layer. The adopted scheme is sensitive to surface resistance r_s , a parameter which can be adjusted to allow the surface characteristics influence the surface energy balance.

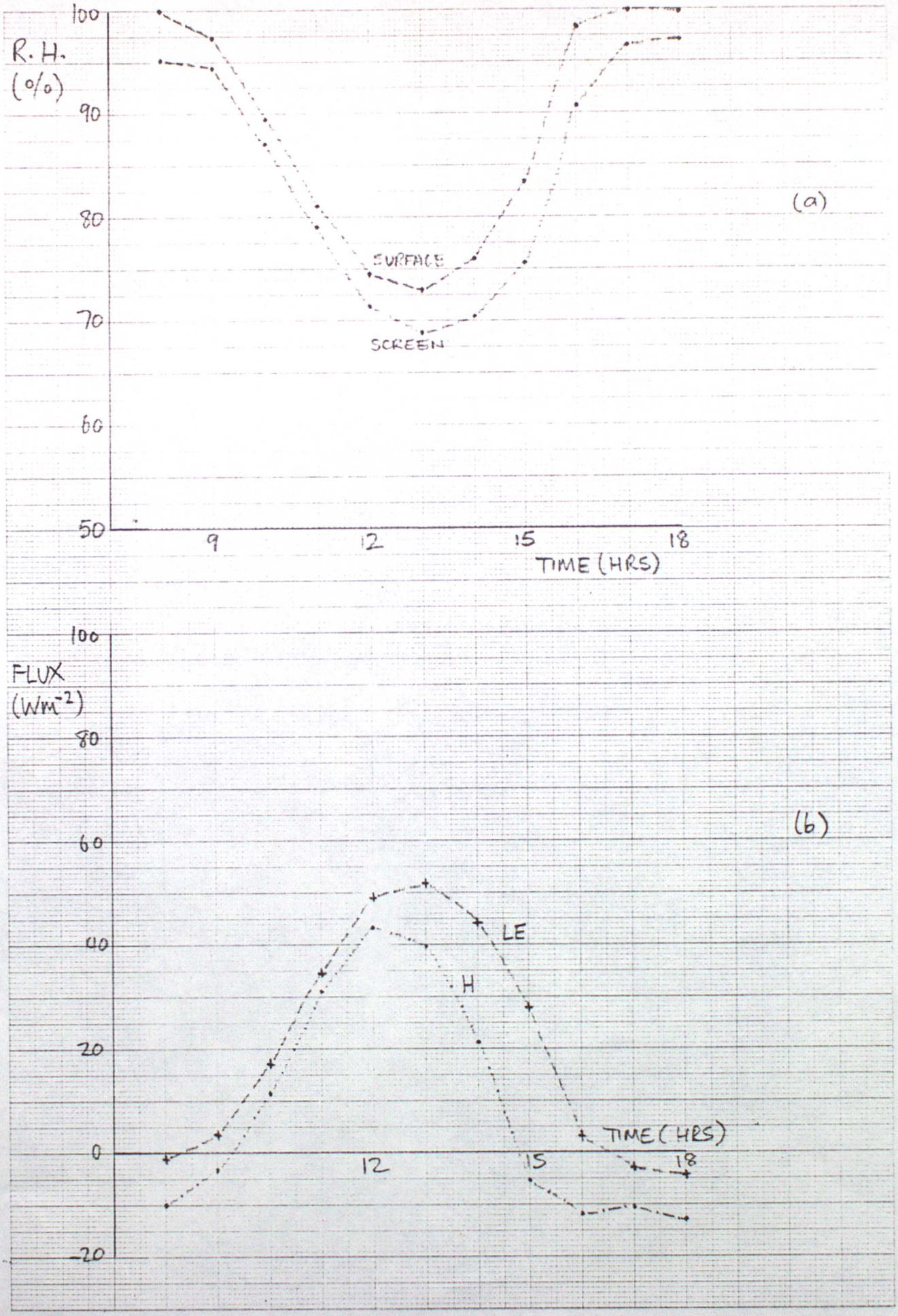

FIG. 6. (a) relative humidity, (b) fluxes, $r_s = 100\ sm^{-1}$.

ANNEX 7

AN ALTERNATIVE METHOD FOR CALCULATING THE MOLECULAR TRANSMISSIVITY IN THE ROACH SLINGO LONGWAVE SCHEME

The method normally employed to calculate molecular transmissivities in a radiative transfer scheme is to use either laboratory or band model data to construct a single curve of transmissivity against absorber amount over a given spectral interval. The curve is then either approximated by an analytic function or look up table. The required transmissivity is then found by scaling the absorber amount to take account of the integration over zenith angle and the dependence of the absorption on pressure and temperature. In the longwave radiation scheme of Roach and Slingo (1976) the random band model of Hunt and Mattingly (1976) is used with the molecular line compilation of McClatchey et al (1973) to construct curves of transmissivity against absorber amount. The curves obtained are approximated by the analytic functions given below.

water vapour, band 1 $$T(u) = \frac{0.02790}{(0.02790 + 1.92u + u^{0.6})}$$

water vapour, band 2 $$T(u) = \frac{0.29250}{(0.29250 + 0.33u + u^{0.6})}$$

water vapour, band 3 $$T(u) = \frac{2.110}{(2.110 + u^{0.6})}$$

water vapour, band 5 $$T(u) = \frac{0.3373}{(0.3373 + u^{0.4})}$$

carbon dioxide, band 3 $$T(u) = \frac{0.1935}{(0.1935 + u^{0.43})}$$

(Note that these analytic functions have been adjusted to take account of the integration over zenith angle).

The fits to the data are very good over the range that the scheme was designed for (pathlengths, $5\ 10^{-4}$ g cm^{-2} < u < $5\ 10^{-1}$ g cm^{-2}). Thus the analytic fits are adequate to a resolution of ~1 mb (~10 m). In some applications (e.g.the fog model) higher resolution may be required. In such cases the analytic fits are still reasonably good except for water vapour in band 5 and carbon dioxide in band 3 (see Fig. 2 of Roach and Slingo (1976)). The underestimation of the transmissivity in these two bands for smaller pathlengths leads to errors in the calculated heating rates at higher resolution.

An alternative method of fitting the transmissivity curves is to use an ESFT (exponential sum fitting of transmissions) technique, in which the band transmissivity is approximated by a set of decaying exponentials. This technique has been used in the shortwave radiation scheme of Slingo and Schrecker (1982). The transmissivity function is then given by

$$T(u) = \sum_{i=1}^{N} a_i \exp(-b_i u) .$$

Each transmissivity function was calculated using the random band model (Hunt and Mattingly (1976)) results over the range 10^{-7} g cm^{-2} to 10^{2} g cm^{-2} and fitting them to twelve terms. The accuracy of the fits to the data are very good over the whole range of pathlengths likely to be

encountered in most applications. The fits to the data and the errors of the fits are given in Tables 1-5 for the water vapour and carbon dioxide bands. (Note that these fits have not been adjusted to take account of the integration over zenith angle).

Fig. 1 shows a comparison of the radiative heating rates obtained from both methods (the analytic functions and the ESFT fits) using data from a fog model integration. The fog model grid, which is non linear with grid spacing increasing from the surface upwards is shown in the figure. The difference between the two methods is apparent below 3 m height where the grid resolution is greatest. The underestimation of the transmissivity by the analytic functions leads to exaggerated cooling just above the surface; in the fog model (which includes the Roach and Slingo scheme) this may have a significant effect on fog formation. The difference between the two curves is due almost entirely to the improved fits for water vapour in band 5 and carbon dioxide in band 3.

The principle drawback of this approach is that the technique is computationally expensive and is not feasible in a time marching model (e.g.the fog model). In order to include the improved fits to the transmissivity curves in the fog model a modified approach was taken. Since the ESFT fits to the transmissivity curves are very accurate the calculated transmissivity functions may be used to define a look up table. This is a once only calculation and thereafter the required transmissivity may be estimated through interpolating values from the table. Look up tables in each of the water vapour and carbon dioxide bands were calculated over 6.5 decades (pathlengths in the range 10^{-6} g cm^{-2} to $10^{0.5}$ g cm^{-2}).

This is sufficient to cover the range of values likely to be encountered in the fog model. 650 calculated values were used to define the look up table over 6.5 decades, the calculated values being logarithmically spaced. A simple linear interpolation for the log of the pathlength was used to estimate the required transmissivity. Radiative heating rates obtained by this method showed no significant difference to those obtained when the ESFT fits were used directly when fog model data (as for Fig. 1) was used. This suggests that this approach is sufficiently accurate and may be used when computation time is an important factor. The method has subsequently been incorporated into the fog model and does not appear to be significantly more expensive computationally than the original analytic functions; whilst producing more realistic cooling rates near the ground where the grid resolution is highest.

The present disposition of the various versions of the Roach-Slingo longwave scheme programs is given in Appendix 1.

TABLE 1

WATER VAPOUR BAND 1 0-400 cm^{-1}

TABLE OF FITS AND ERRORS

U g cm^{-2}	T(u)	T_{fit} (u)	% error
0.10000000D-06	0.99936000D+00	0.99889494D+00	-0.046536
0.31622800D-06	0.99801900D+00	0.99776412D+00	-0.025538
0.10000000D-05	0.99407500D+00	0.99427993D+00	0.020615
0.31622800D-05	0.98339600D+00	0.98410159D+00	0.071750
0.10000000D-04	0.95826500D+00	0.95834834D+00	0.008697
0.31622800D-04	0.90891400D+00	0.90837003D+00	-0.059848
0.10000000D-03	0.82634000D+00	0.82680416D+00	0.056170
0.31622800D-03	0.70358900D+00	0.70324624D+00	-0.048716
0.10000000D-02	0.54146000D+00	0.54172216D+00	0.048418
0.31622800D-02	0.35787200D+00	0.35767820D+00	-0.054154
0.10000000D-01	0.18929300D+00	0.18942348D+00	0.068929
0.31622800D-01	0.71908000D-01	0.71824134D-01	-0.116629
0.10000000D+00	0.16238000D-01	0.16296047D-01	0.357477
0.31622800D+00	0.15500000D-02	0.15023372D-02	-3.075020
0.10000000D+01	0.32000000D-04	0.13968421D-04	-56.348685
0.31622800D+01	0.0	0.10333328D-04	
0.10000000D+02	0.0	0.10333306D-04	
0.31622800D+02	0.0	0.10333306D-04	
0.10000000D+03	0.0	0.10333306D-04	

ESFT coefficients

a_i	b_i
0.10333D-04	0.0
0.37819D-01	0.10447D+02
0.57066D-01	0.11015D+05
0.16684D+00	0.90573D+02
0.16958D+00	0.11066D+04
0.26397D-01	0.10000D+06
0.11401D+00	0.37670D+02
0.13277D+00	0.38107D+04
0.55902D-03	0.53951D+01
0.39811D-01	0.30832D+05
0.25456D+00	0.33266D+03
0.0	0.0

$$T_{fit}(u) = \sum_{i=1}^{12} a_i \exp(-b_i u)$$

TABLE 2

WATER VAPOUR BAND 2 400-560 cm^{-1}

TABLE OF FITS AND ERRORS

U g cm^{-2}	T(u)	T_{fit} (u)	% error
0.10000000D-06	0.99998600D+00	0.99998665D+00	0.000065
0.31622800D-06	0.99995600D+00	0.99995781D+00	0.000181
0.10000000D-05	0.99986400D+00	0.99986674D+00	0.000274
0.31622800D-05	0.99957400D+00	0.99958031D+00	0.000632
0.10000000D-04	0.99867600D+00	0.99868941D+00	0.001343
0.31622800D-04	0.99599600D+00	0.99600531D+00	0.000934
0.10000000D-03	0.98852000D+00	0.98850547D+00	-0.001470
0.31622800D-03	0.97000200D+00	0.97001007D+00	0.000831
0.10000000D-02	0.93116700D+00	0.93116280D+00	-0.000451
0.31622800D-02	0.86274400D+00	0.86274637D+00	0.000274
0.10000000D-01	0.75746300D+00	0.75746169D+00	-0.000173
0.31622800D-01	0.61131100D+00	0.61131167D+00	0.000110
0.10000000D+00	0.43279200D+00	0.43279164D+00	-0.000084
0.31622800D+00	0.25365700D+00	0.25365736D+00	0.000143
0.10000000D+01	0.11593800D+00	0.11593694D+00	-0.000912
0.31622800D+01	0.37704000D-01	0.37709268D-01	0.013972
0.10000000D+02	0.69160000D-02	0.68461091D-02	-1.010569
0.31622800D+02	0.44200000D-03	0.85927235D-03	94.405509
0.10000000D+03	0.40000000D-05	0.20784997D-05	-48.037507

ESFT COEFFICIENTS

a_i	b_i
0.22268D-02	0.82985D+04
0.56778D-03	0.19588D+05
0.13935D-01	0.88105D-01
0.78209D-01	0.93541D+00
0.34373D-01	0.10023D+04
0.11683D+00	0.84723D+02
0.18421D+00	0.73282D+01
0.71038D-01	0.29512D+03
0.19994D+00	0.28708D+01
0.10583D-01	0.30200D+04
0.95705D-01	0.44978D+00
0.19239D+00	0.23878D+02

$$T_{fit}(u) = \sum_{i=1}^{12} a_i \exp(-b_i u)$$

TABLE 3

WATER VAPOUR BAND 3 560-800 cm^{-1}

TABLE OF FITS AND ERRORS

U g cm^{-2}	T(u)	T_{fit} (u)	% error
0.10000000D-06	0.99999800D+00	0.99999884D+00	-0.000084
0.31622800D-06	0.99999600D+00	0.99999633D+00	0.000033
0.10000000D-05	0.99999100D+00	0.99998844D+00	-0.000256
0.31622800D-05	0.99997400D+00	0.99996398D+00	-0.001002
0.10000000D-04	0.99992000D+00	0.99989082D+00	-0.002919
0.31622800D-04	0.99974900D+00	0.99968978D+00	-0.005924
0.10000000D-03	0.99922400D+00	0.99917543D+00	-0.004860
0.31622800D-03	0.99766600D+00	0.99771542D+00	0.004953
0.10000000D-02	0.99336200D+00	0.99347815D+00	0.011692
0.31622800D-02	0.98282900D+00	0.98273021D+00	-0.010051
0.10000000D-01	0.96069500D+00	0.96073287D+00	0.003942
0.31622800D-01	0.92012100D+00	0.92010967D+00	-0.001232
0.10000000D+00	0.85316400D+00	0.85316758D+00	0.000420
0.31622800D+00	0.75229200D+00	0.75229033D+00	-0.000222
0.10000000D+01	0.61461100D+00	0.61461189D+00	0.000145
0.31622800D+01	0.44936400D+00	0.44936363D+00	-0.000083
0.10000000D+02	0.28151500D+00	0.28151513D+00	0.000047
0.31622800D+02	0.14179800D+00	0.14179795D+00	-0.000032
0.10000000D+03	0.51333000D-01	0.51333010D-01	0.000020

ESFT COEFFICIENTS

a_j	b_i
0.35641D-01	0.23442D+02
0.13457D-03	0.34356D+05
0.12041D-01	0.22594D+03
0.88631D-01	0.22646D+00
0.19421D-01	0.11940D+02
0.18539D+00	0.15885D-01
0.25275D-01	0.45082D+02
0.22446D+00	0.55719D+00
0.27216D-02	0.51168D+03
0.23211D+00	0.84333D-01
0.16075D+00	0.32659D+01
0.13421D-01	0.0

$$T_{fit}(u) = \sum_{i=1}^{12} a_i \exp(-b_i u)$$

TABLE 4

WATER VAPOUR BAND 5 1150–2050 cm^{-1}

TABLE OF FITS AND ERRORS

U g cm^{-2}	T (u)	T_{fit} (u)	% error
0.10000000D-06	0.99993300D+00	0.99993473D+00	0.000173
0.31622800D-06	0.99978900D+00	0.99979416D+00	0.000516
0.10000000D-05	0.99933600D+00	0.99935469D+00	0.001871
0.31622800D-05	0.99795300D+00	0.99801125D+00	0.005837
0.10000000D-04	0.99391800D+00	0.99412230D+00	0.020555
0.31622800D-04	0.98317400D+00	0.98372142D+00	0.055679
0.10000000D-03	0.95868300D+00	0.95814755D+00	-0.055853
0.31622800D-03	0.91310300D+00	0.91106668D+00	-0.223011
0.10000000D-02	0.84252800D+00	0.84590792D+00	0.401164
0.31622800D-02	0.74707400D+00	0.74496160D+00	-0.282756
0.10000000D-01	0.63351700D+00	0.63440942D+00	0.140867
0.31622800D-01	0.51662700D+00	0.51619387D+00	-0.083838
0.10000000D+00	0.40982600D+00	0.41016040D+00	0.081596
0.31622800D+00	0.31645700D+00	0.31615263D+00	-0.096180
0.10000000D+01	0.23357100D+00	0.23381762D+00	0.105585
0.31622800D+01	0.15879500D+00	0.15862759D+00	-0.105427
0.10000000D+02	0.93334000D-01	0.93430946D-01	0.103870
0.31622800D+02	0.42525000D-01	0.42479206D-01	-0.107688
0.10000000D+03	0.12441000D-01	0.12454411D-01	0.107794

ESFT COEFFICIENTS

a_i	b_i
0.73636D-01	0.957190+00
0.62283D-01	0.71614D-01
0.84481D-01	0.21627D+03
0.10510D+00	0.12912D+02
0.14514D-02	0.10000D+06
0.67085D-01	0.27990D-01
0.13198D+00	0.63387D+03
0.11891D+00	0.38459D+01
0.62850D-01	0.62806D+04
0.98555D-01	0.32137D+00
0.18534D+00	0.53211D+02
0.83225D-02	0.0

$$T_{fit}(u) = \sum_{i=1}^{12} a_i \exp(-b_i u)$$

TABLE 5

CARBON DIOXIDE BAND 3 560-800 cm^{-1}

TABLE OF FITS AND ERRORS

U g cm^{-2}	T(u)	T_{fit} (u)	% error
0.10000000D-06	0.99989300D+00	0.99988691D+00	-0.000609
0.31622800D-06	0.99966300D+00	0.99964343D+00	-0.001957
0.10000000D-05	0.99894000D+00	0.99888261D+00	-0.005745
0.31622800D-05	0.99671100D+00	0.99656067D+00	-0.015082
0.10000000D-04	0.99010300D+00	0.98987482D+00	-0.023047
0.31622800D-04	0.97209700D+00	0.97227020D+00	0.017817
0.10000000D-03	0.93030600D+00	0.93044699D+00	0.015155
0.31622800D-03	0.85601100D+00	0.85580202D+00	-0.024413
0.10000000D-02	0.75828400D+00	0.75843885D+00	0.020421
0.31622800D-02	0.64848500D+00	0.64838915D+00	-0.014781
0.10000000D-01	0.52638400D+00	0.52643667D+00	0.010007
0.31622800D-01	0.40320200D+00	0.40316782D+00	-0.008477
0.10000000D+00	0.29552900D+00	0.29557486D+00	0.015519
0.31622800D+00	0.20478400D+00	0.20468772D+00	-0.047014
0.10000000D+01	0.12883900D+00	0.12905754D+00	0.169621
0.31622800D+01	0.65754000D-01	0.65320210D-01	-0.659716
0.10000000D+02	0.22547000D-01	0.23146116D-01	2.657186
0.31622800D+02	0.39620000D-02	0.33726903D-02	-14.874046
0.10000000D+03	0.22000000D-03	0.12267898D-03	-44.236825

ESFT COEFFICIENTS

a_i	b_i
0.72833D-01	0.20654D+01
0.25522D-02	0.10000D+06
0.72456D-01	0.32584D+04
0.11008D+00	0.25410D+03
0.59313D-01	0.12190D+00
0.14126D+00	0.22646D+02
0.79094D-02	0.41687D-01
0.12118D+00	0.10280D+04
0.10656D+00	0.62373D+01
0.50023D-01	0.94189D+04
0.10365D+00	0.55463D+00
0.15220D+00	0.87498D+02

$$T_{fit}(u) = \sum_{i=1}^{12} a_i \exp(-b_i u)$$

Appendix 1

Present disposition of Roach Slingo longwave scheme programs

A modified version of the Roach Slingo longwave scheme now exists in which the ESFT fits described in this note (D/Met O 15/12/5B E3) are used to calculate the molecular transmissivity. The current (as at 1.6.83) versions of the scheme are,

i. M15.SOURCLIB(SPROF2#), this is the original version of the scheme with the expanding grid,

ii. M15.SOURCLIB(HIR#), M15.LOADLIB(HRADL), this is the standard version of the scheme,

iii. M15.SOURCLIB(HIR2#), this version is identical to M15.SOURCLIB(HIR#) except that the ESFT fits are used.

FIG. 1

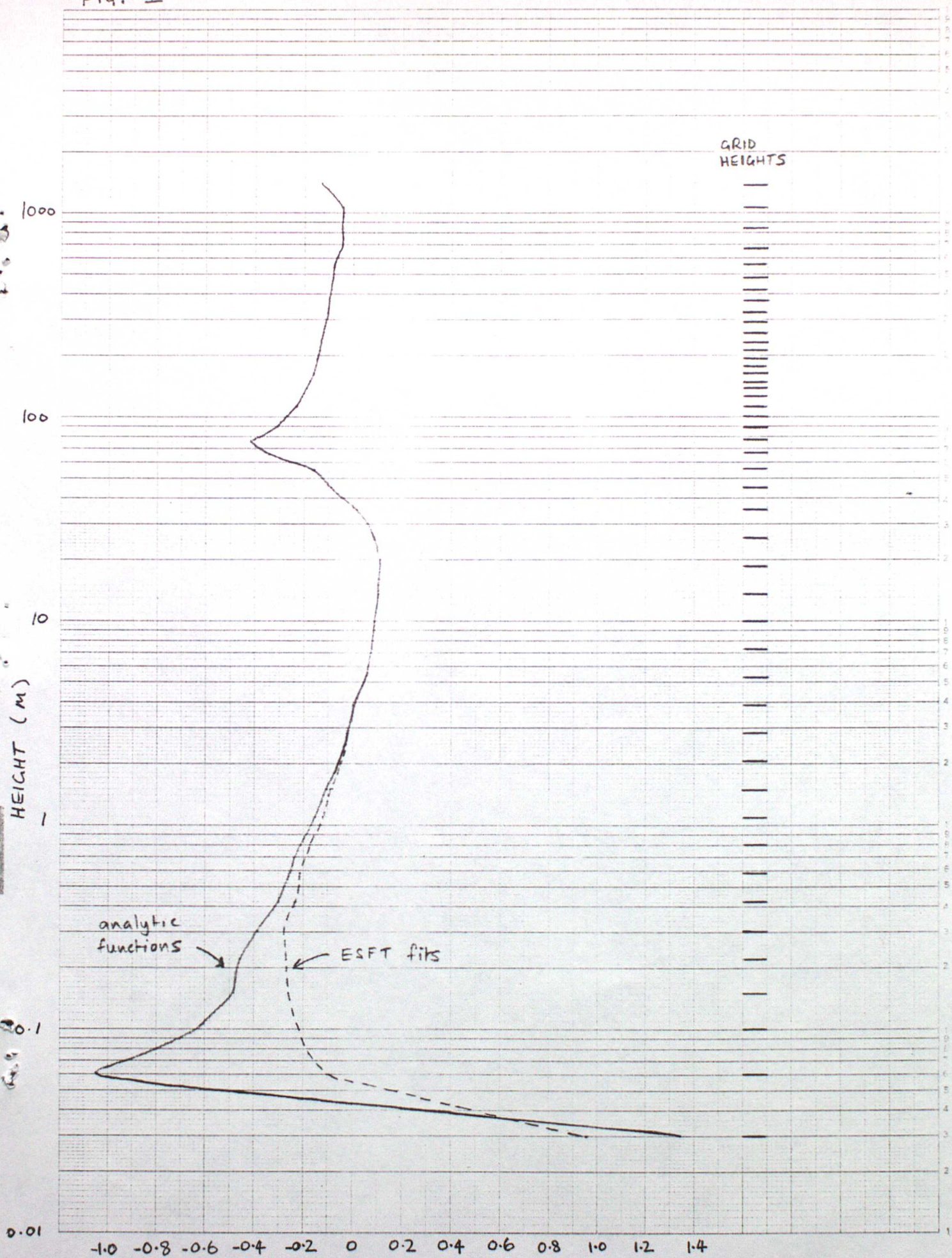
GRID HEIGHTS
1000
100
10
1
0·1
0·01
HEIGHT (M)
analytic functions
ESFT fits
-1·0 -0·8 -0·6 -0·4 -0·2 0 0·2 0·4 0·6 0·8 1·0 1·2 1·4
RADIATIVE HEATING RATE (°C hr⁻¹)

ANNEX 8

A NOTE ON THE SURFACE ADJUSTMENT TO THE EXCHANGE COEFFICIENTS

The model produces logarithmic (neutral) profiles of $\bar{u}$ and θ as $z \to 0$. This implies that $\partial\bar{u}/\partial z$ and $\partial\theta/\partial z$ become infinite at $z = 0$, i.e. at the surface. Since the use of a grid spacing as small as 0.03 m cannot resolve the surface gradients properly, the exchange coefficients at the lowest grid level have been adjusted in a manner similar to Mason. The logarithmic wind profile is given by

$$u(z) = \frac{u_*}{k} \ln \frac{z}{z_0} \qquad (1)$$

As mentioned according to Eq. (1), $\partial\bar{u}/\partial z$ becomes infinite at $z=0$ (at the surface). However in reality this does not occur, motions near a smooth surface (within 1 mm or so) are laminar rather than turbulent, and the same is true of motions close to individual elements of rough surfaces. One result of this is that Eq. (1) which is established for turbulent flow, cannot hold below a certain level, generally somewhat greater than the distance z_0 (the roughness length) from the surface in question.

The adjustment to the exchange coefficient for momentum is as given below, where a and b are two arbitrary heights close to the surface (b > a). The basic equations are the definition of the friction velocity (u_*) and the expression for the stress (τ).

$$u_* = (\tau/\rho)^{1/2} \qquad (2)$$

$$\tau = \rho K_m \partial u/\partial z \qquad (3)$$

$$\therefore \quad u_*^2 = K_m \partial u/\partial z \qquad (4)$$

Near the ground observations and dimensional arguments predict that

$$\partial u/\partial z = u_* / kz \qquad (5)$$

which on integration gives Eq. (1). From Eq. (4) K_{mba} is approximated by

$$K_{mba} \simeq u_*^2 (b-a)/(u_b - u_a) \qquad (6)$$

Integrating Eq. (5) from b to a gives

$$u_b - u_a = \frac{u_*}{k} \ln(b/a) \qquad (7)$$

$$\therefore \quad u_* = k(u_b - u_a) / \ln(b/a) \qquad (8)$$

substituting u_* from (8) into (6) then gives

$$K_{mba} \simeq \frac{k^2 (b-a)(u_b - u_a)}{[\ln(b/a)]^2} \qquad (9)$$

A similar argument follows for the adjustment of the exchange coefficient for heat (water vapour), where c and d are two arbitrary heights close to the surface ($d > c$). The scale value θ_* is defined by

$$H = -\rho c_p u_* \theta_* \qquad (10)$$

Where in terms of a flux gradient relationship H (the sensible heat flux) is given by

$$H = -\rho c_p K_H \partial\theta/\partial z \qquad (11)$$

$$\therefore \quad u_* \theta_* = K_H \partial\theta/\partial z \qquad (12)$$

Near the ground observations and dimensional arguments predict

that $$\partial\theta/\partial z = \theta_* / kz \qquad (13)$$

From Eq. (12) K_{Hdc} is approximated by

$$K_{Hdc} \simeq u_* \theta_* (d-c)/(\theta_d - \theta_c) \qquad (14)$$

Integrating Eq. (13) from d to c gives

$$\theta_d - \theta_c = \frac{\theta_*}{k} \ln(d/c) \qquad (15)$$

$$\therefore \quad \theta_* = k(\theta_d - \theta_c)/\ln(d/c) \qquad (16)$$

From (5)

$$u_* = kz\,\partial u/\partial z = k\,\partial u/\partial \ln z \qquad (17)$$

Therefore u_* is by definition a constant scale quantity in neutral conditions. Substituting u_* from (8) and θ_* from (16) into (14) gives

$$K_{Hdc} \simeq \frac{k^2(u_b - u_a)(d-c)}{\ln(b/a)\ln(d/c)}$$

Eqs. (9) and (18) give the forms of the adjustments to K_M and K_H at the lowest grid level in terms of arbitrary heights a, b, c and d. The exact form of the adjustments depends upon the definition of the heights a, b, c and d.

The logarithmic wind profile is given by Eq. (1)

$$u(z) = \frac{u_*}{k} \ln \frac{z}{z_0} \qquad (1)$$

similarly the logarithmic temperature profile is given by

$$\theta(z) - \theta(0) = \frac{\theta_*}{k} \ln \frac{z}{z_T}$$

where z_T is the equivalent roughness length for temperature. Since momentum unlike heat (and water vapour) may be transferred to the surface (vegetation) by pressure forces as well as molecular diffusion the resistance to momentum transfer from some arbitrary height above the surface is less than the corresponding resistance to heat (and water vapour) transfer. Thom (1975) developed this idea and showed that

$$z_{T,q} \simeq 0.2\, z_0$$

If we follow Mason by defining the arbitrary heights a, b, c and d as below.

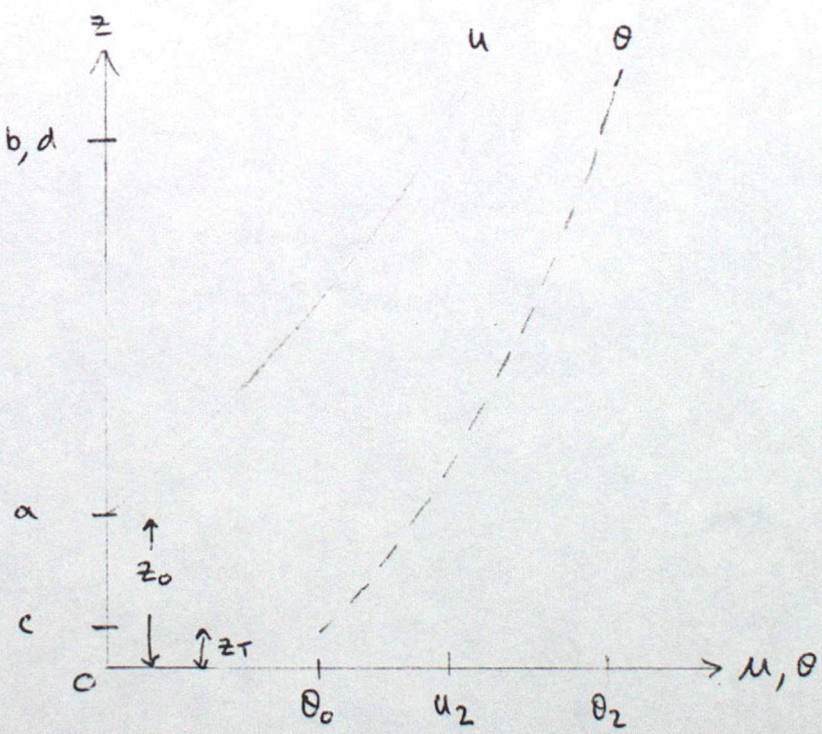

Let z_1 , z_2 the two lowest grid levels be at a and b respectively, where $b \equiv d$

Then for momentum

$$u = 0 \quad \text{at} \quad a = z_o \quad \text{and}$$

$$u = u_2 \quad \text{at} \quad b = (z_2 - z_1) + z_o$$

then (9) gives

$$K_{M12} \simeq \frac{k^2 (z_2 - z_1)\, u_2}{\left[\ln \frac{z_2 - z_1 + z_o}{z_o}\right]^2} \qquad (21)$$

For heat

$$\theta = \theta_o \quad \text{at} \quad c = z_T \quad \text{and}$$

$$\theta = \theta_2 \quad \text{at} \quad d \equiv b \equiv (z_2 - z_1) + z_o$$

then (18) gives

$$K_{H12} \simeq \frac{k^2 (z_2 - z_1 + z_o - z_T)\, u_2}{\ln \frac{z_2 - z_1 + z_o}{z_o} \ln \frac{z_2 - z_1 + z_o}{z_T}} \qquad (22)$$

For momentum Mason defines the lowest grid level $z_1 = 0$ at $z = z_o$, the level at which the wind speed becomes zero. Therefore (21) becomes

$$K_{M12} \simeq \frac{k^2 z_2 u_2}{\left[\ln \frac{z_2 + z_o}{z_o}\right]^2} \qquad (23)$$

and the corresponding equation for heat transfer (22) becomes

$$K_{H12} \simeq \frac{k^2 (z_2 + z_o - z_T)\, u_2}{\left[\ln \frac{z_2 + z_o}{z_o}\right]\left[\ln \frac{z_2 + z_o}{z_T}\right]} \qquad (24)$$

where z_1 is at the same level as for momentum transfer.

Fig. 1 shows typical model profiles of windspeed and temperature near the surface at midnight (model time). The model integrations were started at midday so that the plotted profiles are in balance with the model equations. Also shown in Fig. 1 is the temperature profile obtained when z_T is allowed to equal z_0, in this case the wind profile is virtually unaffected.

The analysis can be repeated using slightly different definitions of the arbitrary heights a, b, c and d. If we define them as below

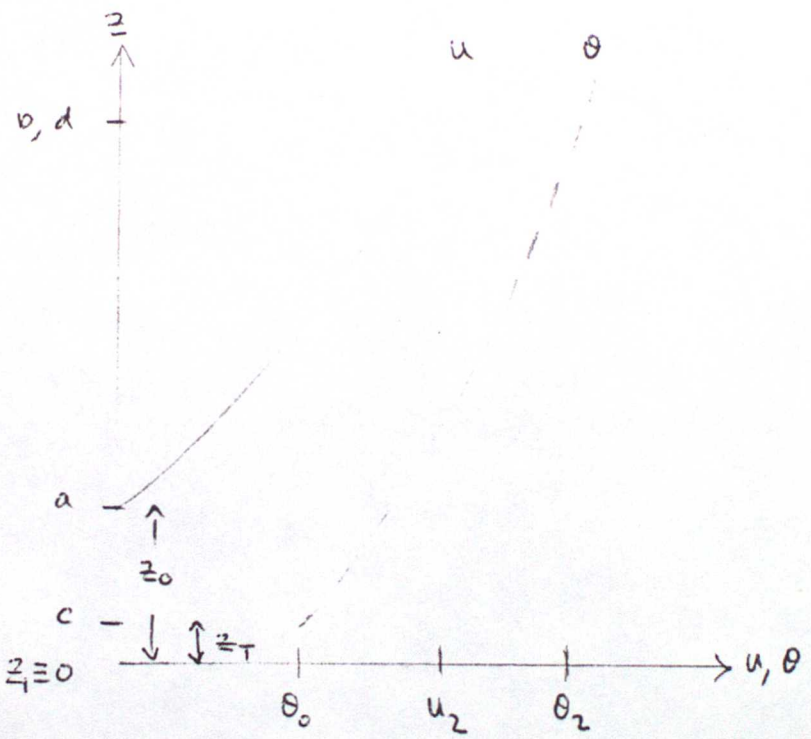

Define $z_1 \equiv 0$ as being at the ground surface so that the logarithmic profiles of windspeed and temperature are terminated above this. Again let z_2 be at b and $b \equiv d$. Then for momentum

$u = 0$ at $a = z_0$ and

$u = u_2$ at $b = z_2$

consistently higher than when K_{M1Z} is adjusted, the gradient (which is given by u_*/k) is not significantly different. Table 1 shows various parameters from the integrations described (at midnight, model time). The tabulated values confirm the initial observations made from comparison of Figs (1), (2) and (3). These results suggest that the adjustment of K_{M1Z} and K_{H1Z} has little effect on the profiles above the first grid point. For the present the adjustments given by Eqs. (25) and (26) will be used in the model since the definition of $z_1 = 0$ at the ground surface is consistent with the air-ground interface being defined by z_1.

However the adjustment at the surface has not helped to make the model profiles of windspeed and temperature more realistic. Two typical observed profiles are shown in Fig. (4) one being from data given by Rider and Robinson (1951), the other from the 16 m mast at Cardington during phase II. The observed profiles show less wind-shear than the model predicts whilst showing a much stronger temperature gradient than the model. The observed temperature gradient from screen height to the surface is typically 4-5°C, whilst the model gradient is always less than 1°C. One reason why the model profiles of temperature and windspeed differ consistently from those observed may be because the model takes no explicit account of the surface vegetation. The only influence of the surface characteristics on the profiles is through the roughness length terms z_o and z_T which appear in Eqs. (1) and (19). Further investigation of the surface vegetation influence is beyond the scope of this note and is not discussed.

Note. The form of the adjustments has recently been changed slightly such that K_{M12} and K_{H12} are now given by

$$K_{M12} \simeq \frac{k^2 z_2 u_2}{[\ln z_2/z_0]^2} \qquad (27)$$

$$K_{H12} \simeq \frac{k^2 z_2 u_2}{\ln z_2/z_0 \ln z_2/z_T}$$

Again this change has made little difference to the results. Eqns (27) and (28) are used in the final published results.

$u_{9.9m}$ (ms^{-1})	u_* (ms^{-1})	K_{M12} (m^2s^{-1})	$T_{1.49m}$ (C)	T_o (C)	ΔT (C)	H (Wm^{-2})	K_{H12} (m^2s^{-1})		
2.82	0.140	1.6E-3	1.70	0.94	0.76	-10.0	9.1E-4	$K_{M12} \neq K_{H12}$	) Mason $z_1 \equiv 0$ at z_o
2.83	0.139	1.6E-3	1.62	0.96	0.66	-10.1	1.6E-3	$K_{M12} = K_{H12}$	)
2.77	0.141	2.2E-3	1.68	0.96	0.72	-10.1	1.1E-3	$K_{M12} \neq K_{H12}$	) $z_1 \equiv 0$ at $z = 0$
2.77	0.140	2.1E-3	1.61	0.98	0.63	-10.3	2.1E-3	$K_{M12} = K_{H12}$	)
3.09	0.133	7.1E-4	1.62	0.87	0.75	-9.5	8.9E-4	No adjustment	

Table 1

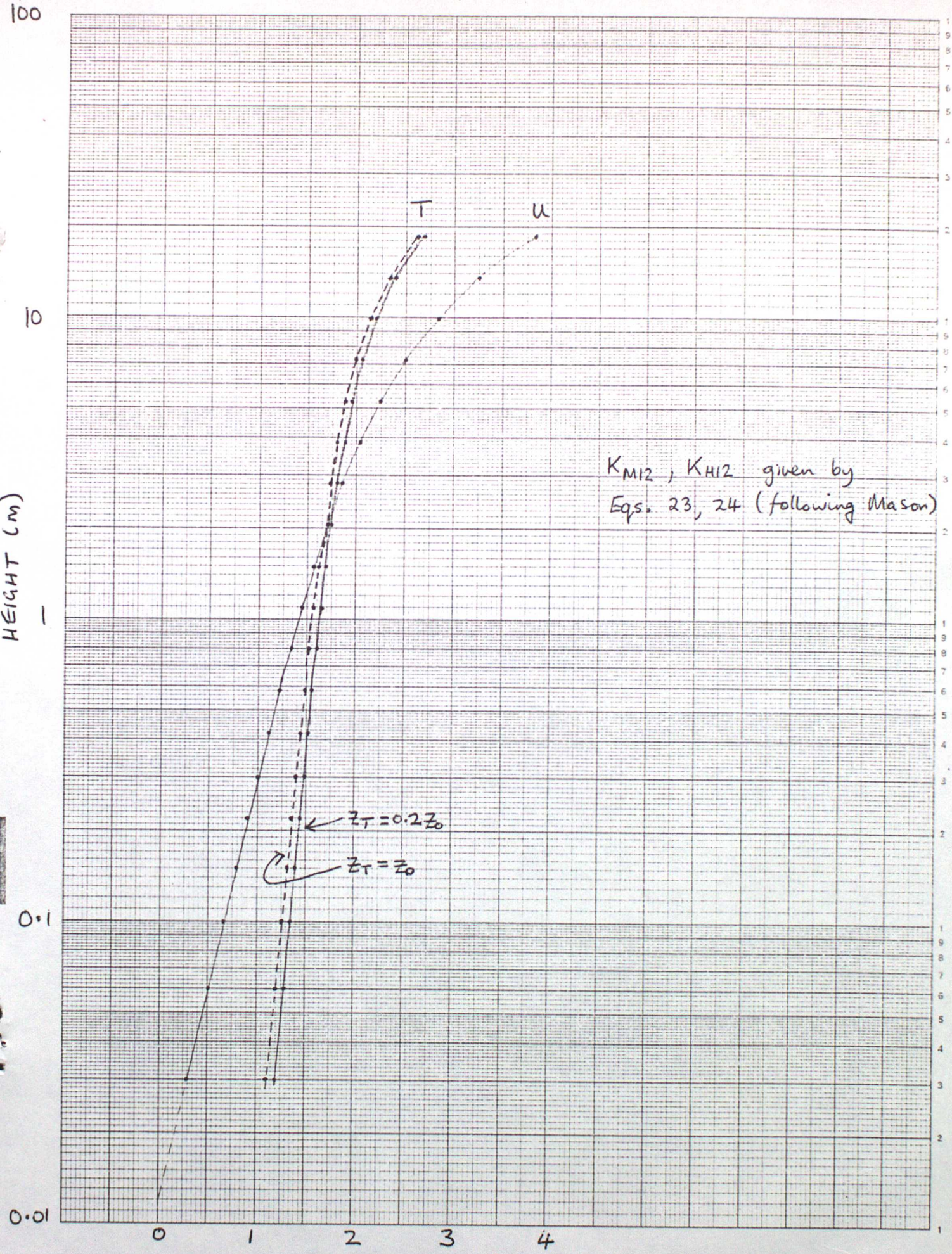
100
10
1
0.1
0.01
HEIGHT (m)
T
u
K_{M12}, K_{H12} given by
Eqs. 23, 24 (following Mason)
$z_T = 0.2 z_0$
$z_T = z_0$
0
1
2
3
4
WINDSPEED u (ms^{-1})
TEMPERATURE T (°C)

FIG. 1

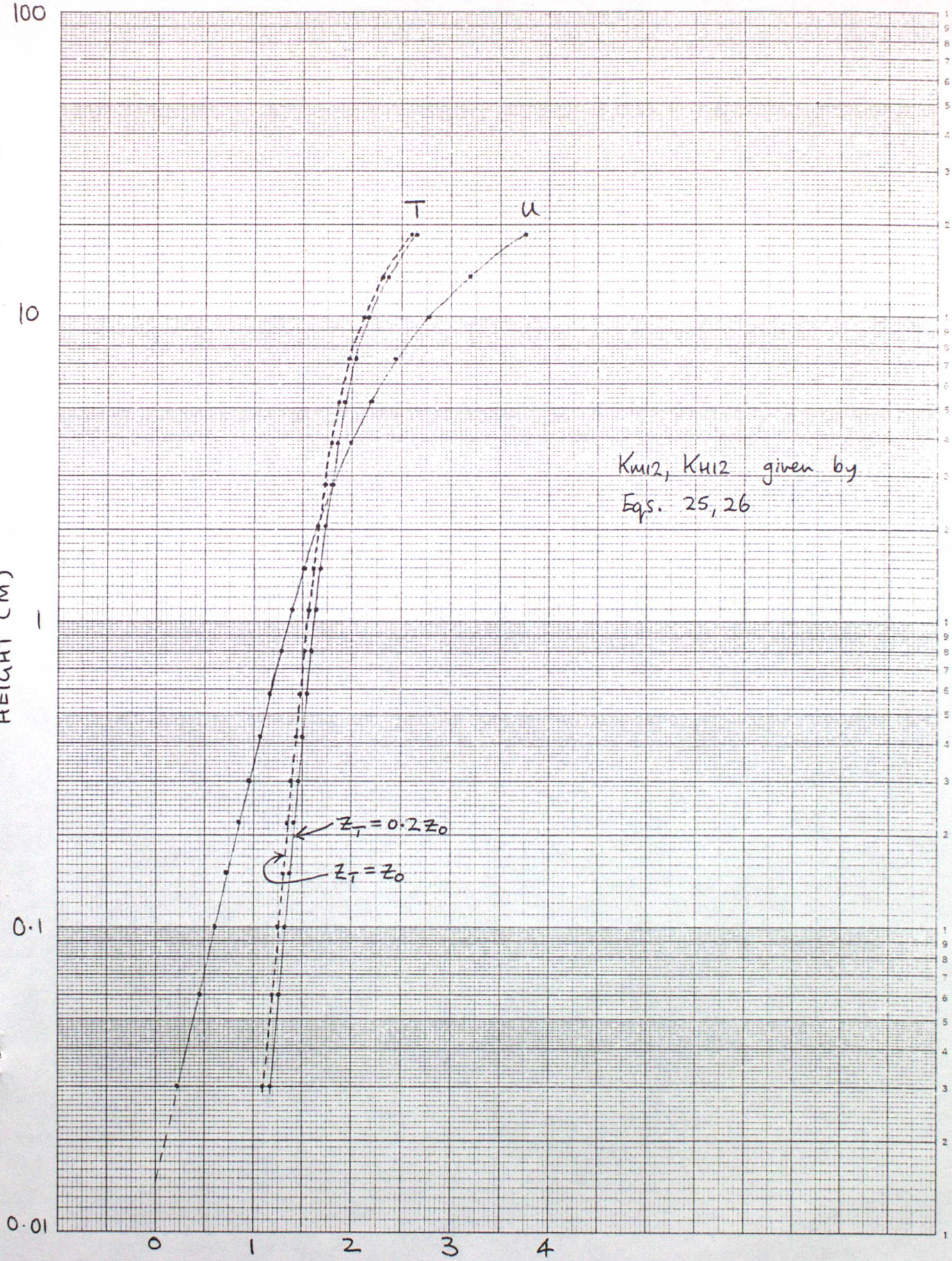
100
10
1
0.1
0.01
HEIGHT (M)
0
1
2
3
4
WINDSPEED u (ms⁻¹)
TEMPERATURE T (°C)
T
u
K_{M12}, K_{H12} given by
Eqs. 25, 26
$z_T = 0.2 z_0$
$z_T = z_0$
Log 4 Cycles x mm, ½ and 1 cm
Graph Data Ref. 5541

FIG. 2

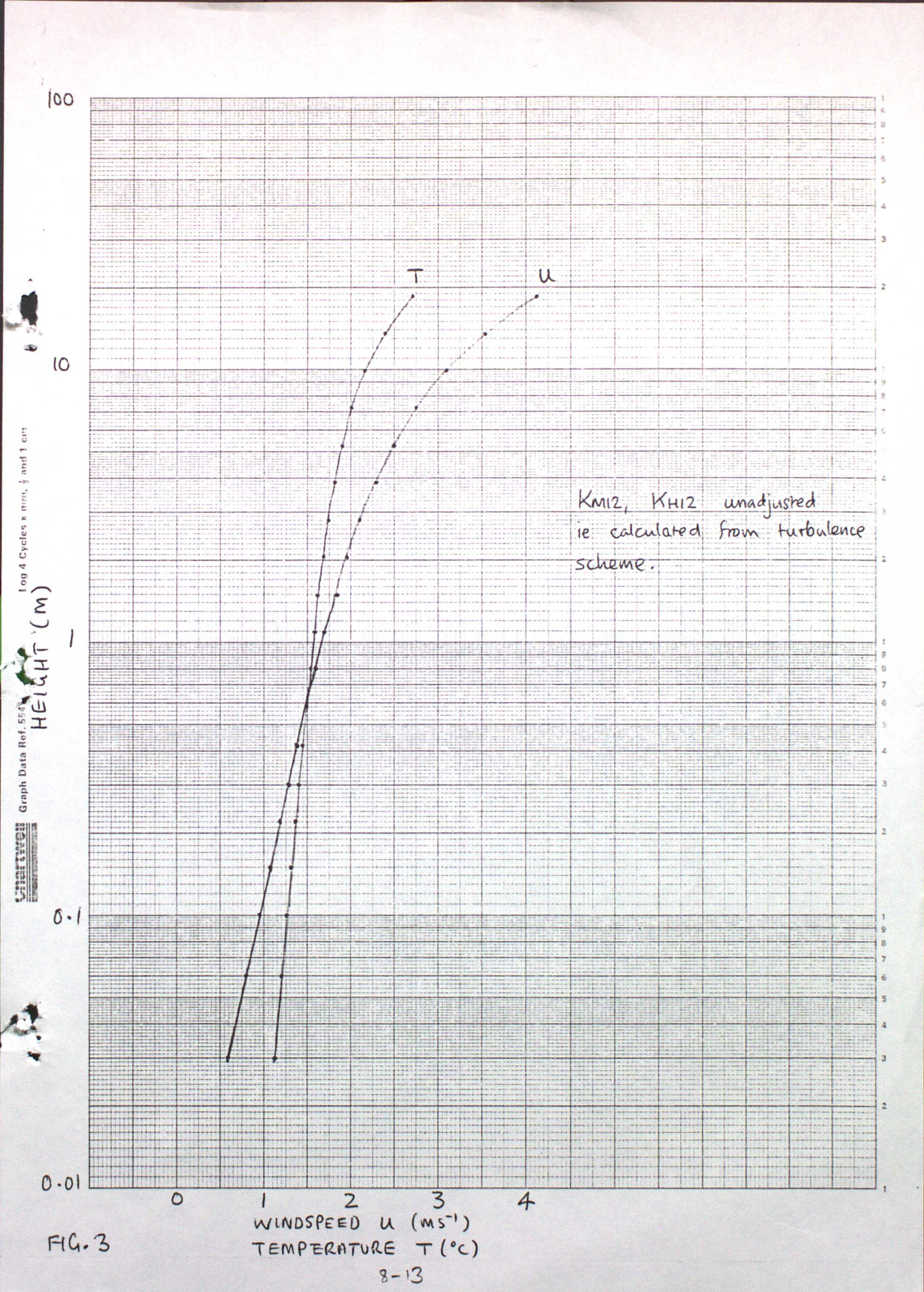
100
10
1
0.1
0.01
HEIGHT (M)
T
u
K_{M12}, K_{H12} unadjusted
ie calculated from turbulence
scheme.
0
1
2
3
4
WINDSPEED u (ms^{-1})
TEMPERATURE T (°C)
Graph Data Ref. 5540
Log 4 Cycles x mm, ½ and 1 cm

FIG. 3

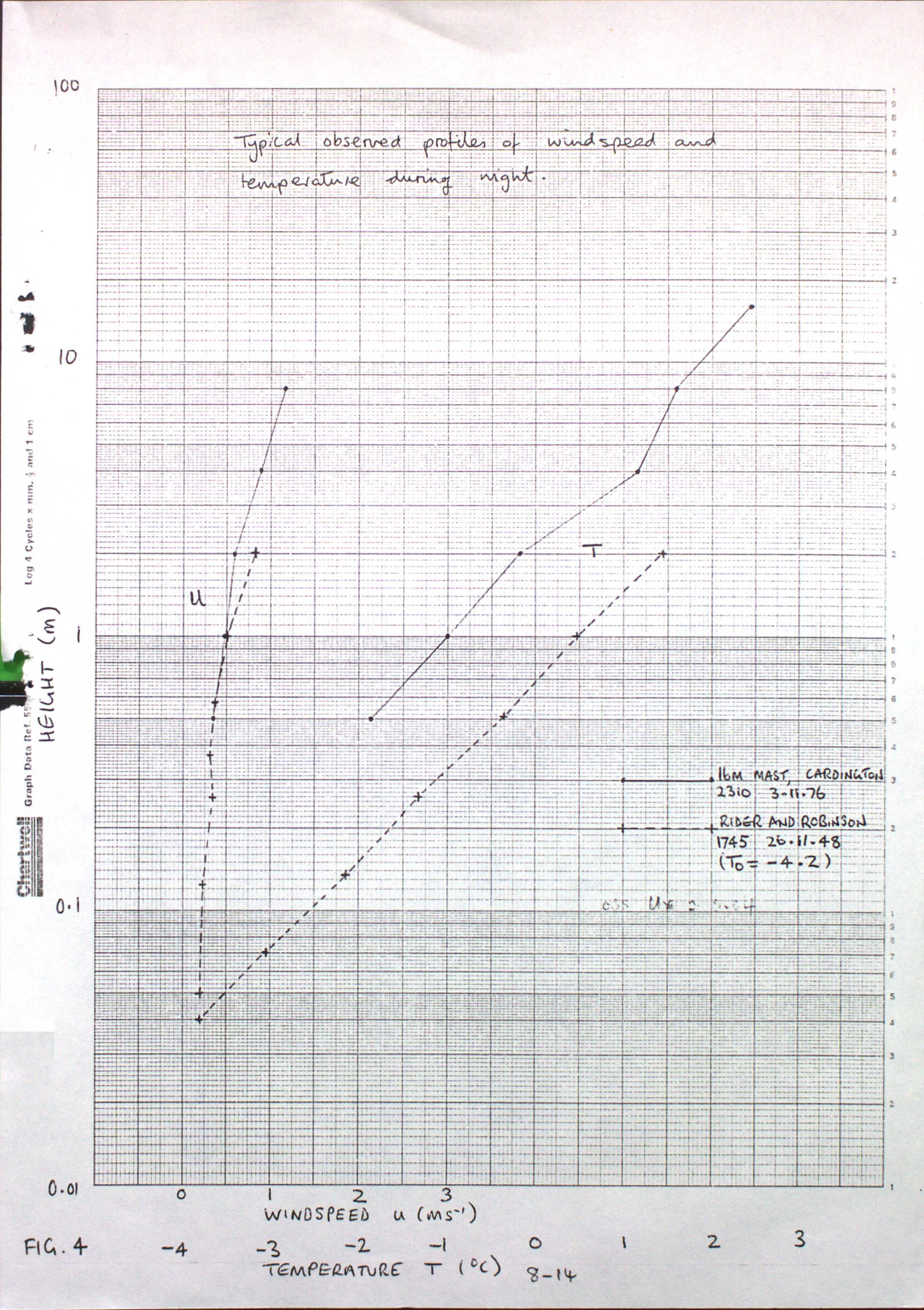
Typical observed profiles of windspeed and temperature during night.
100
10
1
0.1
0.01
HEIGHT (m)
u
T
16M MAST, CARDINGTON
2310 3-11-76
RIDER AND ROBINSON
1745 26-11-48
(T0 = -4.2)
0
1
2
3
WINDSPEED u (ms⁻¹)
-4
-3
-2
-1
0
1
2
3
TEMPERATURE T (°C)
Log 4 Cycles x min. ½ and 1 cm
Graph Data Ref. 55
Chartwell

FIG. 4

8-14